

POLITECNICO DI TORINO

Master degree course in Electronic Engineering

Master Degree Thesis

**Single-Molecule Electret: a
long-sought-after nanoscale
component**



Supervisor:

Prof. Mariagrazia Graziano

Correlatori:

Prof. Gianluca Piccinini

Ph.D Chiara Elfi Spano

Candidate

Chiara PECILE
s277486

ANNO ACCADEMICO 2020-2021

*First, think.
Second, believe.
Third, dream.
And finally, dare.
Walt Disney*

Summary

The miniaturization of modern electronic devices has been approaching the nanoscale. This trend has led researchers to study and develop of single-molecule devices (SMDs), where molecules are employed as active components. Among these molecules, fullerenes and their derivatives distinguish for their distinctive cage-like structures. A single-molecule electret (SME) is a long-desired nanoscale component since it can conduct us to new small storage device with the feature of non-volatile memory. Its main attribute is the switching between two different states by means of an external electric field. Recent studies report a single-molecule electret device based on an endohedral metallofullerene, demonstrating memory capabilities. The existence of two distinguishable energetic stable states of the Gadolinium (Gd) encapsulated into the C82 fullerene plays a vital role in exploiting Gd@C82 as a memory component. They correspond to two different spatial arrangement of the Gd atom inside the C82. This master thesis starts with the creation of the Gd@C82 molecule with the purpose to test its behavior considering the changes on the different properties with the encapsulation of the Gd atom in the cage C82. This has been done analyzing two different stable positions, taking into account the considerations made in literature. These steps are realized with the use of ATK tool and the tool ORCA for the optimization of the geometry. The second part focuses on the device level. Three different devices are analyzed and compared. The Gd@C82 molecule in the two different configurations (namely I and IV) corresponding to different Gd atom spatial sites are placed between two bulky gold electrode. Their electron structure and transport properties are studied and compared to the reference configuration constituted by the empty C82 cage placed between gold electrodes. With these steps, it could be possible to understand how the presence of the Gd atom perturbs the C82 cage and how its position changes the behavior of the entire device including the resulting transmission spectra and IV curves. In conclusion, the differences in the current magnitude monitored at the electrodes in the two different configurations (I and IV) reveal two different stable logical states, demonstrating the single-molecule electret as promising candidate for future technology for storage applications.

Acknowledgements

I would like to thank Ph.D student C. E. Spano for her expertise that was invaluable in answering all my questions and her kind availability in all these months. I would like also to thank the Professors G. Piccinini and M. Graziano who taught me not to limit my curiosity, but to enhance it by carrying out this wonderful work.

Thanks to my parents and my brother who have always believed in me and in my dreams. Thank you for giving me all the love and sustain I could ever hoped for. You made all this possible.

Last but not least, thanks to Felice. Thank you for your love and patience, for teaching me that everything can be achieved, just believe it, just do it. You always manage to value the best part of me.

Contents

Summary	v
Acknowledgements	vii
1 Introduction	1
1.1 A bit of history	1
1.2 Electronics: then and now	2
1.3 Small, smaller and smallest devices	5
1.3.1 Predictions on the future of integrated circuits: Moore's law	7
1.3.2 Moore's law and scaling: challenges	8
1.3.3 Industry and economic implications of Moore's Law	9
1.4 Single-molecule devices (SMDs)	10
1.5 In this thesis: goals and outline	10
2 Theoretical background	11
2.1 What is an electret?	11
2.1.1 History	12
2.1.2 Similarities: magnets and capacitors	12
2.2 Fullerenes: a unique cage-like structure	13
2.2.1 Historical facts	14
2.2.2 Types and characteristics	15
2.2.3 Insights	17
2.3 Endohedral fullerenes	18
2.3.1 The encapsulated clusters	19
2.3.2 Effects: size and shape	19
2.4 How it is possible to trap atoms or molecules into fullerene cages?	20
2.4.1 A practical example	21
2.5 Single-Molecule electret	22
2.5.1 Single-electron transport in Gd@C82 transistor	23
2.5.2 Theoretical modelling revealing the SME physics	25

2.5.3	Other SME	27
2.5.4	To sum up	28
3	Methodology	29
3.1	From theory to practice	29
3.2	A small recap on conduction at nanoscale	30
3.2.1	Transport regimes: classical transport vs quantum transport	34
3.3	ATK	36
3.4	Further theory	37
3.4.1	Potential Energy Surface	37
3.4.2	Molecular structures	38
3.5	Geometrical optimization	39
3.5.1	Local minima: how to find them	41
3.5.2	The problem of the global minimum and characterization of the PES	45
3.5.3	Vibrational frequencies: how to calculate them	46
3.6	ORCA	47
3.6.1	Hartree-Fock method and basis set	48
3.6.2	Density Functional Theory (DFT)	50
3.7	The structure: choices	51
3.7.1	The cage	51
3.7.2	The encapsulated atom	54
3.7.3	Electrodes and the final structure	55
3.8	Optimization results	57
4	Results	61
4.1	Cage C82 and the two stable configurations	61
4.2	Mulliken population	61
4.2.1	What is electronegativity	61
4.2.2	Mulliken Electronegativity	62
4.2.3	Mulliken Populations analysis	63
4.2.4	Settings	66
4.2.5	Results	69
4.3	Molecular Energy Spectrum	70
4.3.1	Molecular energy spectrum of the three cases	71
4.4	The device	71
4.4.1	A general overview	71
4.5	The empty C82 cage	72
4.5.1	Transmission spectrum at the equilibrium	73
4.5.2	Density of state	74
4.5.3	Molecular energy spectrum vs DDOS	76
4.5.4	IV characteristic	77

4.6	Improvements	80
4.6.1	Chemical Adsorption	81
4.6.2	The new device: empty C82 cage	83
4.6.3	Transmission spectrum at the equilibrium	84
4.6.4	Density of state	86
4.6.5	Molecular energy spectrum vs DDOS	87
4.6.6	IV characteristic	88
4.6.7	IV curve: old vs new device	89
4.7	Gd@C82 - I	90
4.7.1	Transmission spectrum at the equilibrium	91
4.7.2	Density of state	93
4.7.3	Molecular energy spectrum vs DDOS	96
4.7.4	IV characteristic	96
4.8	Improvements	99
4.8.1	The new device: Gd@C82 - I	99
4.8.2	Transmission spectrum at the equilibrium	100
4.8.3	Density of state	101
4.8.4	Molecular energy spectrum vs DDOS	102
4.8.5	IV characteristic	103
4.8.6	IV curve: old vs new device	104
4.9	Gd@C82 - IV	106
4.9.1	Transmission spectrum at the equilibrium	106
4.9.2	Density of state	108
4.9.3	Molecular energy spectrum vs DDOS	110
4.10	Improvements	111
4.10.1	The new device: Gd@C82 - IV	111
4.10.2	Transmission spectrum at the equilibrium	112
4.10.3	Density of state	113
4.10.4	Molecular energy spectrum vs DDOS	116
4.10.5	IV characteristic	116
4.11	Nudged Elastic Band (NEB)	118
4.11.1	NEB tools in ATK and a bit of useful theory	119
4.11.2	NEB performed on the created structures	121
4.11.3	Results and observations	123
5	Conclusions	131
5.1	Comments and final application	132
5.2	Future works	134
6	Appendix	137
	Bibliography	147

List of Tables

1.1	A list of events that happened in the evolution of the field of electronics [1].	4
1.2	Formulas related to scaling.	8
2.1	Relative total energies and the heights of the adsorbed Gd atom at different sites shown in Figure 2.8 [4].	26
2.2	Relative total energies and the heights of the adsorbed Gd atom at the sites shown in Fig. 2.8 [4].	26
3.1	The algorithms for minimizing nonlinear functions with many variables can be grouped into this three broad categories.	41
4.1	The population matrix.	65
4.2	Equilibrium transmission spectrum analysis settings.	73
4.3	Device DOS analysis settings.	75
4.4	IV curve report - case1: empty C82 cage.	79
4.5	IV curve report - case1, new device: empty C82 cage.	90
4.6	Transmission spectrum analysis settings - Gd@C82-I.	91
4.7	Device DOS analysis settings - Gd@C82-I.	94
4.8	IV curve report - case2: Gd@C82 - I.	98
4.9	IV curve report - case2, new device: Gd@C82-I.	105
4.10	Transmission spectrum analysis settings - Gd@C82-IV.	107
4.11	Device DOS analysis settings - Gd@C82-IV.	109
4.12	IV curve report - case3, new device: Gd@C82-IV.	117

List of Figures

1.1	John Bardeen, William Shockley, and Walter Brattain in Brattain's laboratory in 1948 [1].	2
1.2	The first Germanium bipolar transistor [1].	3
1.3	From left: Vacuum tube, individual transistor and integrated circuit in dual-in-line package (DIP) [3].	6
1.4	Transistor count per die [29].	7
2.1	Structural illustration of a Fullerene [19].	13
2.2	Allotropes of carbon: diamond, graphite and fullerene [27].	14
2.3	Four equivalent ways of representing the structural formula of benzene [23].	16
2.4	The major isomers of fullerenes: structures and their symmetry [22].	17
2.5	A replica of the graph obtained by the authors of the paper: I_{DS} as a function of the gate voltage. V_{DS} is fixed at 2mV.	23
2.6	A replica of the I_{DS} vs V_g (with V_{DS} fixed at 2 mV). The gate voltage was moved backward and forward. It can be easily seen that two states are accessed: <i>State 1</i> and <i>State 2</i>	24
2.7	A different representation of the switching process. The gate voltage (V_g) switches the device between <i>State 1</i> and <i>State 2</i>	24
2.8	The first seven adsorption sites of a single Gd atom that have been considered [4].	25
2.9	The six inequivalent cases. In the figures you can easily see which is the face considered for the adsorption of the Gd atom in each case.	26
3.1	Any device simulation program performs an iterative self-consistent solution of a transport equation and a Poisson-like equation.	31
3.2	Surface model of potential energy with indicated minima, transition structures, second order saddle points and reaction paths [38].	39
3.3	One-dimensional potential energy surface with two minima.	45
3.4	STO-nG basis set, that is, n Gaussian functions fitting for the STO orbital.	50

3.5	Some of the C82 fullerene provided by ATK tool, from left: named No.2 (82 atoms, symmetry group Cs), named No.4 (82 atoms, symmetry group Cs), named No.7 (82 atoms, symmetry group C3v) and named No.8 (82 atoms, symmetry group C3v).	53
3.6	The C82 cage chosen. In the tool it is named No.5 (82 atoms, symmetry group C2).	53
3.7	On the left it is shown the configuration I, on the right configuration IV. The C82 cage is represented in grey, the Gd atom is light blue. The figure on the left follows the coordinate system reported in fig. 3.8, the other on the right has been rotated a bit in order to better see the position of the Gd atom.	55
3.8	This is the coordinate system used with the atk tool. It is remarkable that the z of atk corresponds to the x in the images of the paper. .	55
3.9	The final devices. In the first on the top you can see the one with the empty C82 cage, the second one exploits the I configuration and the third one the IV. In yellow are represented the gold electrodes.	57
3.10	Geometrical optimization, input file, structure Gd@C82-I: first try.	59
3.11	Geometrical optimization, input file, structure Gd@C82-I: second try.	59
3.12	Screenshot of the timing at the end of the second try of geometrical optimization: it did not convert after 35 days and 500 cycles. . . .	60
3.13	A warning presented at the end of the output file: they wavefunction did not convert, but there are signs of convergence.	60
3.14	It has not been reached any convergence after 500 cycles. In the picture are shown the values of the 499th iteration.	60
4.1	Script generator: molecule on the right and the selected simulations.	66
4.2	LCAO calculator: basis sets.	67
4.3	LCAO calculator: Poisson solver.	67
4.4	LCAO calculator: iterations.	68
4.5	Final settings before running.	69
4.6	The first studied device: empty C82 cage and the electrodes. . . .	73
4.7	Transmission spectrum of the first device: empty C82 cage.	74
4.8	Device Density of States of the single C82 molecule (part of the first device).	76
4.9	Picture of the DOS analyzer, on the right it is possible to see the selection of the C82 molecule done in order to realize the graph 4.8, on the top you can see the possible selection of the s, p, d and f orbitals.	77
4.10	Device Density of States of the single electrodes, respectively right and left, reading from the top side (part of the first device in exam).	78
4.11	Device Density of States of the first device in exam.	79
4.12	Device density of States vs Molecular energy spectrum - case 1: empty C82 cage.	80

4.13	Plot of the IV curve - case 1: empty C82 cage, old device (higher distance between molecule and electrodes).	81
4.14	Example of the distances of the previous configuration, between the left electrode and the C82 molecule.	83
4.15	Final distances set in the new device. In these pictures you can see the lower ones; In particular you can also see the references of the atoms considered to calculate the distance (in the small white note).	83
4.16	The new device - case 1: empty C82 cage.	84
4.17	Settings: Transmission Analyzer of the new device - case 1: empty C82 cage.	84
4.18	Transmission spectrum of the new device - case 1: empty C82 cage.	85
4.19	Device density of States of the molecule of the new device - case 1: empty C82 cage.	87
4.20	Device density of States of the entire new device - case 1: empty C82 cage.	88
4.21	Device Density of States of the single electrodes, respectively right and left, reading from the top side - case 1: empty C82 cage.. . . .	89
4.22	Device density of States vs Molecular energy spectrum - case 1: empty C82 cage.	90
4.23	Plot of the IV curve - case 1: empty C82 cage, new device.	91
4.24	Plot of the IV curve - case 1: empty C82 cage, old vs new device. Linear scale.	92
4.25	Plot of the IV curve - case 1: empty C82 cage, old vs new device. Semilogarithmic scale (y).	93
4.26	The second studied device: C82 cage with the encapsulated Gd atom and the electrodes.	93
4.27	Transmission spectrum of the second device: Gd@C82 - I.	94
4.28	Device Density of States of the single Gd@C82 molecule - configuration I (part of the second device).	95
4.29	Picture of the DOS analyzer, on the top you can see the possible selection of the s, p, d and f orbitals and on the left the representation given by the ATK tool of the DDOS of this system (both contributions of spin).	96
4.30	Device Density of States of the single electrodes, respectively left and right, reading from the top side (part of the second device in exam).	97
4.31	Device Density of States of the second device in exam.	98
4.32	Device density of States vs Molecular energy spectrum - case 2: Gd@C82-I.	99
4.33	Plot of the IV curve - case 2: Gd@C82-I, old device.	100
4.34	The new device - case 2: Gd@C82 - I.	100
4.35	Transmission spectrum of the new device - case 2: Gd@C82-I.	101

4.36	Device density of States of the Gd@C82 molecule of the new device - case 2: Gd@C82-I.	102
4.37	Device density of States of the entire new device - case 2: Gd@C82-I.	103
4.38	Device Density of States of the single electrodes, respectively right and left, reading from the top side - case 2: Gd@C82-I.	104
4.39	Device density of States vs Molecular energy spectrum - case 2: Gd@C82-I.	105
4.40	Plot of the IV curve - case 2: Gd@C82-I, new device.	106
4.41	Plot of the IV curve - case 2: Gd@C82-I, old vs new device. Linear scale.	107
4.42	Plot of the IV curve - case 2: Gd@C82-I, old vs new device. Semilogarithmic scale (y).	108
4.43	The third studied device: C82 cage with the encapsulated Gd atom and the electrodes.	108
4.44	Transmission spectrum of the third device: Gd@C82 - IV.	109
4.45	Transmission Analyzer in ATK: example for the third device Gd@C82 - IV.	110
4.46	Device Density of States of the single Gd@C82 molecule - configuration IV (part of the third device).	111
4.47	Device Density of States of the single electrodes, respectively left and right, reading from the top side (part of the third device in exam).	112
4.48	Device Density of States of the second device in exam.	113
4.49	Device density of States vs Molecular energy spectrum - case 3: Gd@C82-IV.	114
4.50	The new device - case 3: Gd@C82 - IV.	114
4.51	Transmission spectrum of the new device - case 3: Gd@C82-IV.	115
4.52	Device density of States of the Gd@C82 molecule of the new device - case 2: Gd@C82-I.	116
4.53	Device density of States of the entire new device - case 2: Gd@C82-I.	117
4.54	Device Density of States of the single electrodes, respectively right and left, reading from the top side - case 2: Gd@C82-I.	118
4.55	Device density of States vs Molecular energy spectrum - case 3: Gd@C82-IV.	119
4.56	Plot of the IV curve - case 3: Gd@C82-IV, new device.	120
4.57	A practical example of the reaction path computed with NEB.	121
4.58	Creation of the NEB analysis. Since the NEB consist of the initial and final configurations, the tool requires them. In this case you can see the initial state Gd@C82-I and the final one Gd@C82-IV. The selected interpolation method is the linear one.	122

4.59	First sequence of states given by ATK, after the creation for the NEB analysis. In the first image Gd@C82-I, in the second one Gd@C82-IV. Below are shown the additional images.	123
4.60	<i>Script Generator</i> of the NEB simulation.	124
4.61	<i>Optimize Geometry</i> window of the NEB simulation.	124
4.62	<i>Potential Editor</i> window of the NEB simulation (Forced Field calculator).	125
4.63	Needed energy to move from configuration I to IV (and viceversa) according to the analysis of the paper [4].	125
4.64	Needed energy to move from configuration I to IV (and viceversa) according to the analysis on the structures created in this work.	126
4.65	Needed energy to move from configuration I to IV, according to the analysis on the structures created in this work. In this picture, the Gd atom is in the starting position (Gd@C82-I).	126
4.66	Needed energy to move from configuration I to IV, according to the analysis on the structures created in this work. In this picture, the Gd atom is in a "middle" position respect to the initial and final ones.	127
4.67	Needed energy to move from configuration I to IV, according to the analysis on the structures created in this work. In this picture, the Gd atom is in the final position (Gd@C82-IV).	127
4.68	Needed energy to move from configuration IV to I, according to the analysis on the structures created in this work. In this picture, the Gd atom is in the starting position (Gd@C82-I).	128
4.69	Needed energy to move from configuration IV to I, according to the analysis on the structures created in this work. In this picture, the Gd atom is in a "middle" position respect to the initial and final ones.	128
4.70	Needed energy to move from configuration IV to I, according to the analysis on the structures created in this work. In this picture, the Gd atom is in the final position (Gd@C82-I).	129
5.1	$I_{DS}(V_{DS})$ - Gd@C82-I vs Gd@C82-IV - new device. In blue Gd@C82-I and in green Gd@C82-IV.	133

Chapter 1

Introduction

This chapter provides a historical perspective on the field of electronics and its impact on the global economy.

In our everyday life, we face electronics everytime. We meet it in our mobilephones, televisions, and also in all home appliances [1]. Electronics is always present also in the industries, in particular because this world uses systems based on data processing in order to easily manage its operations.

1.1 A bit of history

November 2017 was the 70th anniversary of the discovery of the bipolar transistor by John Bardeen and Walter Brattain at Bell Laboratories, a seminal event that marked the beginning of the semiconductor age. The discovery of the transistor and the following expansion of microelectronics have form our era more than any other event [1].

The term transistor finds its origin in the association of two words: "transfer" and "resistor". This can be explained by the fact that, by definition, it is centered on the voltage-controlled resistance of the characteristics of the MOS transistor [1]. In figure 1.2 is shown the first Germanium bipolar transistor.

In general, microelectronics have influenced the controlling of the business, the design and fabrication of machines, the methodology that is used to interact and share information, etc. [1]. Only in 1956, Bardeen, Brattain and Shockley obtained the Nobel prize in physics, for the invention of the transistor [1]. In figure 1.1 are shown, starting from the left, John Bardeen, William Shockley, and Walter Brattain in Brattain's laboratory in 1948.

Coming back to the late 40s, the researcher Gordon Teal made the first silicon transistors and promoted the first radio composed entirely. By transistors. The other first proprietor of the transistor was Tokyo Tsushin Kogyo. It then became the Sony Company in 1955 and supported the idea that everyone could have its own private radio [1].



Figure 1.1. John Bardeen, William Shockley, and Walter Brattain in Brattain's laboratory in 1948 [1].

1.2 Electronics: then and now

Because most of us have grown up with electronic products all around us, we often lose perspective of how far the industry has come in a relatively short time [1].

At the beginning of the twentieth century, there were no commercial electron devices and transistors were not invented until the late 1940s [1]. Explosive growth



Figure 1.2. The first Germanium bipolar transistor [1].

was triggered by first the commercial availability of the bipolar transistor in the late 1950s and then the realization of the integrated circuit (IC) in 1961. Since that time, signal processing using electron devices and electronic technology has become a pervasive force in our lives [1].

Table 1.1 gives a list of a number of important milestones in the evolution of the field of electronics. It can be seen that the Age of Electronics began in the early 1900s with the invention of the first electronic two-terminal devices, called diodes [1]. The vacuum diode, or diode vacuum tube, was invented by Fleming in 1904; in 1906 Pickard created a diode by forming a point contact to a silicon crystal [1].

The invention of the three-element vacuum tube known as the triode was an extremely important milestone. The addition of a third element to a diode enabled

Year	Event
1874	The solid-state rectifier was invented by Ferdinand Braun.
1895	The creation of the first radio transmissions, made by Marconi.
1904	Invention of the diode vacuum tube, by Fleming. Here, the age of Electronics finally begins.
1906	Creation of the solid-state diode.
1906	Creation of the triode vacuum tube.
1907 ÷ 1927	From diodes and triodes, the first radio circuits have been developed.
1920	Important invention of the super heterodyne receiver, by Armstrong. Then in 1933, he invented the FM modulation.
1940	World War II: new radar developed. The Television was introduced, but with some limitations in the usage.
1947	The bipolar transistors was invented by Bardeen, Brattain, and Shockley. They have the obtained the Nobel prize for their invention in 1956.
1950	Finally, colors in the TV.
1952	Production of silicon bipolar transistors. In the same year, the junction field-effect transistor was demonstrated.
1961	First availability of digital IC in commerce.
1967	First discussion of the semiconductor RAM (64 bits).
1968	First IC operational amplifier (the uA709) available in commerce.
1971	Intel introduced the first 4004 microprocessor.
1972	Intel introduced the first 8-bit microprocessor: the 8008.
1978	Intel developed the first 16-bit microprocessor.
1984	First introcution of the megabit memory chip. Ten years later, the experimental gigabit memory chip was presented.

Table 1.1. A list of events that happened in the evolution of the field of electronics [1].

electronic amplification to take place with good isolation between the input and output ports of the device [1].

Silicon-based three-element devices now form the basis of virtually all electronic systems. Fabrication of tubes that could be used reliably in circuits followed the invention of the triode by a few years and enabled rapid circuit innovation [1]. Amplifiers and oscillators were developed that significantly improved radio transmission and reception. Armstrong invented the super heterodyne receiver in 1920 and FM modulation in 1933 [1]. Electronics developed rapidly during World War II, with great advances in the field of radio communications and the development of radar. Although first demonstrated in 1930, television did not begin to come into widespread use until the 1950s [1].

An important event in electronics occurred in 1947, when John Bardeen, Walter Brattain, and William Shockley at Bell Telephone Laboratories invented the bipolar transistor [1]. Although field-effect devices had actually been conceived by Lilienfeld in 1925, Heil in 1935, and Shockley in 1952, the technology to produce such devices on a commercial basis did not yet exist. Bipolar devices, however, were rapidly commercialized. Then in 1958, the nearly simultaneous invention of the integrated circuit (IC) by Kilby at Texas Instruments and Noyce and Moore at Fairchild Semiconductor [1] produced a new technology that would profoundly change our lives.

The miniaturization achievable through IC technology made available complex electronic functions with high performance at low cost. The attendant characteristics of high reliability, low power and small physical size and weight were additional important advantages [1].

In 2000, Jack St. Clair Kilby received a share of the Nobel prize for the invention of the integrated circuit [1]. In the mind of the authors, this was an exceptional event as it represented one of the first awards to an electronic technologist [1].

Most of us have had some experience with personal computers, and nowhere is the impact of the integrated circuit more evident than in the area of digital electronics. For example, 4-gigabit (Gb) dynamic memory chips contain more than 4 billion transistors [1]. Creating this much memory using individual vacuum tubes or even discrete transistors would be an almost inconceivable feat. [1] In figure 1.3 are reported, from left, the vacuum tube, a transistor and integrated circuit in dual-in-line package (DIP).

1.3 Small, smaller and smallest devices

The semiconductor industry will continue to be a significant driver in the modern global economy as society becomes increasingly dependent on mobile devices, the Internet of Things (IoT) emerges, massive quantities of data generated need to be stored and analyzed, and high-performance computing develops to support vital national interests in science, medicine, engineering, technology and industry [1] [2].

As previously said, these applications will be enabled, in part, with ever increasing miniaturization of semiconductor based information processing and memory devices. Continuing to shrink device dimensions is important in order to further improve chip and system performance and reduce manufacturing cost per bit [1] [2]. As the physical length scales of devices approach atomic dimensions, continued miniaturization is limited by the fundamental physics of current approaches.

Innovation in nanoelectronics will carry complementary metal-oxide semiconductor (CMOS) technology to its physical limits and provide new methods and architectures to store and manipulate information into the future [1] [2].

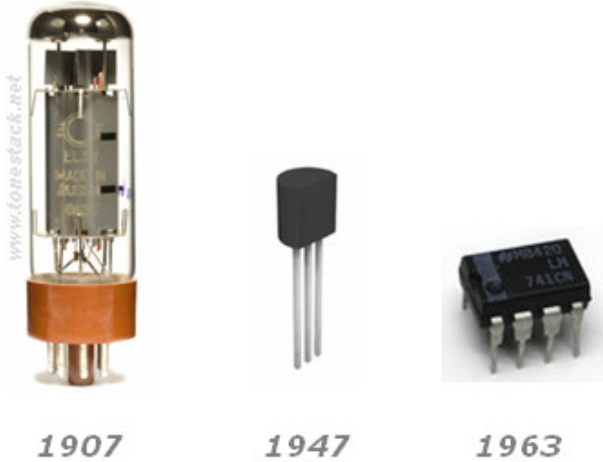


Figure 1.3. From left: Vacuum tube, individual transistor and integrated circuit in dual-in-line package (DIP) [3].

The complexities of memory chips and microprocessors have grown exponentially with time. Over the last four decades, for example, the number of transistors on a microprocessor chip has increased by a factor of one million.

The various levels of integration is commonly described by some abbreviations that can be summarized as below:

- The first ICs, with less than 10 components, were distinguished as Small Scale Integration, or SSI [1];
- As density improved, circuits were considered as Medium Scale Integration or MSI (from 10 to 100 components/chip) [1];
- Then we have the Large Scale Integration, or LSI (from 10 to 10000 components/chip) [1];
- Very Large Scale of Integration, or VLSI (from 10000 to 100000 components/chip) [1];
- Nowadays, we consider Ultra Large Scale of Integration, or ULSI and Giga Scale of Integration, or GSI (above 1000000 components/chip) [1].

of the size. In the 80s, minimum were about 3 μ m, while nowadays we talk about 3nm. This means like four orders of growth in density of each device. Certainly, supply voltages had a reduction from 5 to 1V, which is for sure made in an effort to reduce power consumption [28].

1.3.2 Moore’s law and scaling: challenges

Considering the previous facts, it has to be added that in the 90s, it became obvious that scaling was facing a number of issues. For example it has to be mentioned the increasing of power consumption of the interconnections [28]. This has encouraged the researchers to find new material systems and subsequently, also related processes to support this drastic growth in transistor amounts. This definitely was offering an increase from the performance and functionality point of view.

A possible example of technology revolution was the introduction of copper interconnects. This material is important in order to replace the interconnects based on aluminum. A remarkable problem to be mentioned is the reduction in the thickness of the gate oxide to few nm. In fact, this has implied the upsurge of the gate leakage currents. This problem could be solved by including new materials for the gate with a higher dielectric constant (e.g. Hafnium oxide). [28].

Starting from the law cited before it is possible to derive other laws as it can be seen from table 1.2.

Scaling	Formula
The channel length reduces 50% approximately every 6 years	$L(t) \simeq L(t_0) \times 2^{-\frac{(t-t_0)}{6}}$
The area of an IC increases of 50% every 3 years	$A(t) \simeq A(t_0) \times 1.5^{\frac{(t-t_0)}{3}}$
The area of a transistor reduces of 50% every 3 years	$A(t) \simeq A(t_0) \times 2^{-\frac{(t-t_0)}{3}}$
The number of transistors/IC doubles every 1.5 years	$N(t) \simeq N(t_0) \times \sqrt{3}^{\frac{(t-t_0)}{1.5}}$
The clock frequency increases of 50% every 3 years	$Clk(t) \simeq Clk(t_0) \times 1.5^{\frac{(t-t_0)}{3}}$

Table 1.2. Formulas related to scaling.

Clock frequency is not a primary parameter of the technology because doesn’t depend directly on the process but depend on the design and on many choices that the designer performs. In old technology, clock frequency was related on the device speed: for example by doubling device speed, we double the clock frequency, today it is no longer true due to the interconnection.

It has to be said that, the more we reduce the transistor size, the more it becomes difficult to manufacture functional transistors. Below a certain size (10

nm) becomes impossible to achieve a transistor with the traditional lithographic process, where then the need for a new technology of manufacturing that involves unsustainable costs. So we are arrived at a situation in which the reduction of the transistor size no longer implies the reduction of the cost per unit. This constraint on the sized transistor is pushing us towards the end of Moore's law [28] [37].

So the game is to ship large unit volumes, which implies large number of customers. Chip makers will probably turn to the same methods they have used in the past improving other system aspects such as I/O and memory adding other system-level features and attempting to market their way out of a tough product sell. In conclusion, as scaling features become more difficult it will be necessary for advances in design, architectures, 3D packaging etc. [37] to play an increased role in cost reduction. Parallel fabrication to decrease manufacturing costs per unit transistor needs to be emphasized, e.g. by increasing wafer size, continuous innovation, rigorous planning and technology execution. Even though it is getting more expensive to build wafers, improvements in density can provide real cost reduction at the most fundamental level and this economical benefit drives the ability to continue investing in Moore's law. As long as there is a cost benefit and rich options for future innovation there is no reason to predict an early end [37].

1.3.3 Industry and economic implications of Moore's Law

In 1965, Moore's law was first published.

The importance of this law becomes immediately evident. In fact, the industry of semiconductor production has created a guideline that gives a prediction on almost five decades, from the 70s through 2020. This set of documents is titled "The International Technology Roadmap for Semiconductors" [37]. This guideline was established by different regions that represent all chip manufacturers. Therefore, all decisions made about future product are based on the Moore's law.

For these reasons, there are a lot of economic impacts. One for sure is that computing devices continue to exhibit an exponential growth their complexity, but a severe reduction in terms of costs [37]. The latter together with the higher reliability on the new technology have lead to a considerable improvement in terms of profits in the field of the semiconductor industry and so also in electronics in general. For example, it is interesting to know that Social Media Technologies give the greatest demand for more and more components on a single chip. For this reason, in this field it is possible to see a great implication of Moore's law. Moreover, the considerable influence of this law guided the electronic field to a new industry segment: nanoelectronics. This certainly opened the doors to new different areas, in particular nanomaterials. Even if nowadays many researches stated that this law is stalling, it continues to be an important guiding maxim of

the industry [37].

1.4 Single-molecule devices (SMDs)

The miniaturization of modern electrical devices has been approaching the single molecular scale. This has guided researchers into the study and development of single-molecule devices (SMDs), molecules are used individually as normal active components [31].

Though, this led to different problems: first of all, the studying and controlling charge transport at molecular level, secondly, the exploitation of these new devices. It is curious to know that between these molecules, fullerenes and their derivatives attract attention due to their inimitable cage-like structures. As we will see later, C60-based SMDs have shown several physical properties [31].

To conclude, it is necessary to say that the novel limit presented on the reduction of new devices is for sure the usage of single molecules in electronics. This certainly guides us to the trend of continue downscaling of silicon-based electronic devices, resulting also on the exploitation of different new functionalities.

1.5 In this thesis: goals and outline

In this thesis we will go through a new class of memory device: the single molecule electret. This document, a part from the introduction and conclusion parts, is divided in three main chapters:

- Theoretical background (2) which will give the theoretical aspects fundamental to better understand this work. After some general historical aspects and the definition of the electret, it will focus on some basics related to particular structures such as Fullerenes and then Endohedral Fullerenes which play a vital role in the creation of the Single Molecule Electret (SME).
- Methodology (3) will provide the steps necessary to pass from the theory to the practice and so realize the SME structure. Moreover, in this chapter some important theoretical aspects related to the different used tools will be analyzed including the different factors that support the choices made in order to create the final structure.
- Results (4) where you can find the obtained results and the path followed in order to reveal the SME behaviour.

Chapter 2

Theoretical background

In this chapter, it will be discussed what is an electret in general from a theoretical point of view and some pieces of historical information will be given.

Then I will focus on the single-molecule electrets and on their related properties in order to consider a prediction of possible new applications.

It will be also given a bit of theory of Endohedral Fullerenes and their unique cage-like structure that has been useful during this work.

2.1 What is an electret?

In general, an electret can be defined as a dielectric material that exhibits a quasi-permanent charge: positive on one surface and negative in the other. The term "quasi-permanent" is used since the amount of charges retained in the material, in any case, decays very slowly. However, it has to be said that the decay time is usually much longer than the lifetime of the electret. In addition, it is interesting to know that an electret works as a battery but also that as a permanent magnet. For this reason it could be said that it is its electrical counterpart. Then, also a general poled ferroelectric material could be considered an electret.

Furthermore, it is interesting to notice that the word "electret" is an association of the terms "electricity" and "magnet". In fact, the material used in electrets is a particular dielectric with the ability to retain a significant amount of electric field where it was immersed at the time of its manufacture [25].

2.1.1 History

The existence of electrets was first discussed by Michael Faraday in his "Experimental Researches in Electricity" in 1839. Then in 1892, the scientist Oliver Heaviside, from Britain, was the first to propose the term electret and also to consider its properties.

Next, in 1919, the researcher Mototaro Eguchi, from Japan, was the first to practically realize an electret. This has been done by melting equal parts of Carnauba wax and resin, then lowering the temperature, the mixture solidified [25] [26]. This method of fabrication allowed the electrets to maintain their polarization for many years. Moreover, these electrets created by Eguchi are called the thermo-electrets, because they are constituted mainly by a thermal process. Currently, there are even more materials that could be used to fabricate the Eguchi-electrets. For example it is possible to use organic materials (e.g. ebonite and polymethylmethacrylate) but also inorganic materials (e.g. quartz and glasses) [26].

Of course, there are also other ways to create polarization, so immediately after Eguchi, other types of electrets were discovered. As an example, there are the electro-electrets. These are formed by applying a severe electric field in the dielectric material, placed between two metallic electrodes. This method offers the wanted polarization [25] [26].

Another example are the magneto-electrets, which are produced by warming up the dielectric by means of a severe magnetic field. Then they are brought back to normal room temperature [25] [26]. Thanks to the magnetic anisotropy of molecules, this process drives the dielectric material to be polarized. Besides, other electrets can be created by a thermal process without the implication of either electric or magnetic fields.

Otherwise, some electrets can be created by applying a mechanical pressure to the dielectric material. So, in this case, surface charges can be acquired simply by contact electrification, deformation, or friction without the application of an electric field [25] [26].

2.1.2 Similarities: magnets and capacitors

Electrets demonstrate an intense electrostatic polarization.

This propose that the preserved potential is comparable to the magnetic polarization of the common permanent magnets. The only difference between an electret and a permanent magnet is the fact that the latter holds a permanent magnetic field, whereas an electret has a permanent electric field [26].

In addition to this, it can be seen also a similarity between the dielectric layer used in capacitors and an electret. The first has an induced polarisation that is only transient and it is strongly dependent on the potential applied on it, while dielectrics with electret properties exhibit quasi-permanent charge storage.

Moreover, some materials also exhibit ferroelectricity which is the capability to have a natural electric polarization that can be managed by the application of an external electric field.

Thanks to their thermodynamic equilibrium, ferroelectrics can maintain their polarisation continually, and for this reason they are used in ferroelectric capacitors. An interesting example is the electret microphone which is a type of condenser microphone [37]. It uses a permanently charged material and so it eliminates the need for a polarisation voltage from the power supply [37].

2.2 Fullerenes: a unique cage-like structure

Fullerenes are spheroidal carbon cages with a molecular formula of C_{2n} with $n = 30 \div 41$ and a diameter of about 1 nm [21]. Thanks to their strong chemical stability, fullerenes can resist any potential metabolic cage-opening process and also avoid degradation [21].

An interesting fact is that fullerenes contain hollow interiors and for this reason they can hold atoms or ions as payloads for many different implementations. For instance, Gd atoms or the Gd_3N (trimetallic nitride) can be imprisoned inside the cage to form endohedral metallofullerenes denoted as $Gd@C_{2n}$ or $Gd_3N@C_{2n}$. It is important to say that the symbol "@" refers to the encapsulated nature of the Gd or Gd_3N [21].



Figure 2.1. Structural illustration of a Fullerene [19].

2.2.1 Historical facts

The first fullerene was discovered in 1985 by Sir Harold W. Kroto of the United Kingdom and by Richard E. Smalley and Robert F. Curl, Jr., of the United States [21].

These chemists attained cage-like molecules composed of 60 carbon atoms joined together by single and double bonds. For this reason, these molecules have been named "C60" molecules or "the buckyballs" and form a hollow sphere with 12 pentagonal and 20 hexagonal faces [21]. As it can be seen from the figure 2.1, their construction reminds a soccer ball. This result has been obtained using a laser to vaporize graphite rods in an atmosphere of helium gas.

In 1996, these chemists were conferred the Nobel Prize for their work.

The fullerenes, particularly the highly symmetrical C60 sphere, have a beauty and elegance that excites the imagination of scientists and nonscientists alike, as they bridge aesthetic gaps between the sciences, architecture, mathematics, engineering and the visual arts [16].

It has to be said that before their discovery, there were known only two allotropes of carbon: diamond and graphite, which are composed respectively of a 3D crystalline array of carbon atoms and of piled up sheets of 2D hexagonal arrays of carbon atoms [21]. This can be easily seen in the figure 2.2. For this reason, fullerenes constituted a new very important form and for many scientists, it is remarkable that the existence of fullerenes was not discovered until almost the end of the 20th century.

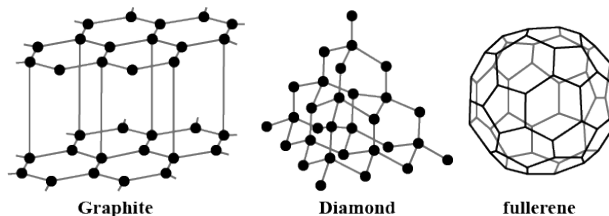


Figure 2.2. Allotropes of carbon: diamond, graphite and fullerene [27].

In addition to this, their discovery has opened a totally new chapter of nanotechnology which includes a new chemistry of complex systems at the atomic scale, very important to exhibit advanced materials behaviour [16].

2.2.2 Types and characteristics

As said before, Fullerenes are spheroidal carbon cages and have such high temperature stability and electrical conductivity to be utilized in nanocompounds [21].

In order to understand their nomenclature, it is useful to know that fullerenes are composed of several numbers of polygones and so their name changes according to the number of carbon atoms present in their structure [21]. In particular, fullerene molecule holds sp^2 and sp^3 hybridized carbon atoms and the angle strain in these molecules is due to sp^2 carbon atoms in structure.

The letter 'C' associated with fullerene denotes the atom of carbon and the number '60', for instance, denotes the numbers of atoms present in a single molecule.

To give an example, in C60 cage each carbon atom is connected to other three atoms using sp^2 orbitals with an electron in each orbital. Moreover, the fourth valence electron of each carbon would be in an orbital p perpendicular to the spherical surface. Thus, the orbitals superimpose creating a variety of orbitals with p electrons inside and outside the sphere. This is verified as in the case of Benzene with the six p electrons that give it the aromatic character [15] [18] [21].

This propose that fullerenes can be considered as aromatic and stable spheres.

Aromatic and stable compounds

An aromatic molecule or compound is one that has special stability and properties due to a closed loop of electrons. Not all molecules with ring/closed structures are aromatic [23]. Aromatic molecules are sometimes referred to simply as aromatics and molecules that are not aromatic are named aliphatic [23]. Moreover, if a molecule contains an aromatic sub-unit, this is often called an aryl group [23].

A prototypical aromatic compound is benzene C_6H_6 , so in general it is common to think of an aromatic compound as something that has a ring structure like that of benzene [23]. In figure 2.3 are shown four equivalent ways of representing the structural formula of benzene [23] where C corresponds to a carbon atom, H refers to a hydrogen atom and a line is a chemical bond.

An introductory organic chemistry definition of an aromatic compound is one that has a planar ring with $4n + 2$ π -electrons, where n is a non-negative integer (Huckel's Rule) [23]. In first and third drawings of Fig. 2.3, the double lines and so the bonds between carbon atoms each have 2 π -electrons. There are 3 double bonds in these drawings, and therefore six π -electrons. Systems with six π -electrons in a planar ring are aromatic according to Huckel's Rule where $n = 1$, i.e. $4(1) + 2 = 6$ [23].

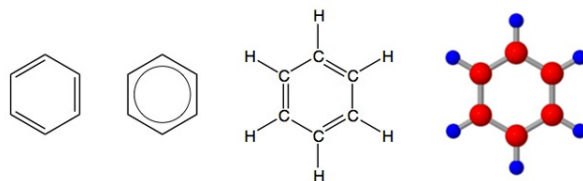


Figure 2.3. Four equivalent ways of representing the structural formula of benzene [23].

Hence, aromatic compounds, originally named because of their aromatic properties, are unsaturated hydrocarbon ring structures that expose peculiar properties. These attributes include for sure the stability that is mainly due to their aromaticity [24]. These compounds are commonly represented as resonance structures (they also contain single and double bonds). However, the bonding is superior than the predicted one for a conjugated structure [24].

In more depth, aromatic compounds are cyclic structures and each ring atom is a contributor in a π bond. This has an effect in the delocalization of π electron density on both sides of the ring. Due to this connected network of π bonds, the rings are planar, unlike the table structures typical of cycloalkanes [24]. Typically, aromatic compounds are nonpolar and non-mixable with water. By definition a nonpolar compound is the one that possess a symmetric distribution of charge, so that no positive or negative poles exist, and that are not ionizable in solution [20]. As they are generally unreactive, they are useful as solvents for other nonpolar compounds [24].

Characteristics of Fullerenes

As anticipated in the previous section, the structure of the C60 is similar to that of a soccer ball. It can be said that it is configured as a truncated icosahedron with 60 vertices and in each of them there is a carbon atom. Furthermore, the structure of the C60 has thirty two faces: twelve pentagons and twenty hexagons. Additionally, each pentagon is surrounded by five hexagons, so for this reason two pentagons cannot be next to each other. Instead, the six bonds of each hexagon are alternately fused to three pentagons and three hexagons [15] [18] [21].

Considering what anticipated before, regarding the chemical behavior of this type of compounds, it can be said that they experiment double bond addition reactions, even if they are not aromatic in the sense of benzene [21]. In other words, they cannot experience substitution reactions since they do not have hydrogens.

It is very important to keep in mind that the C60 carbons are equivalent but

not the bonds. In fact, the C60 has two types of links: the one shared by adjacent hexagons and the other shared by a pentagon and a hexagon. On one hand, the first ones are shorter, about 1.39 Å. On the other hand, the latter, about 1.43 Å are more similar to the double bonds [21].

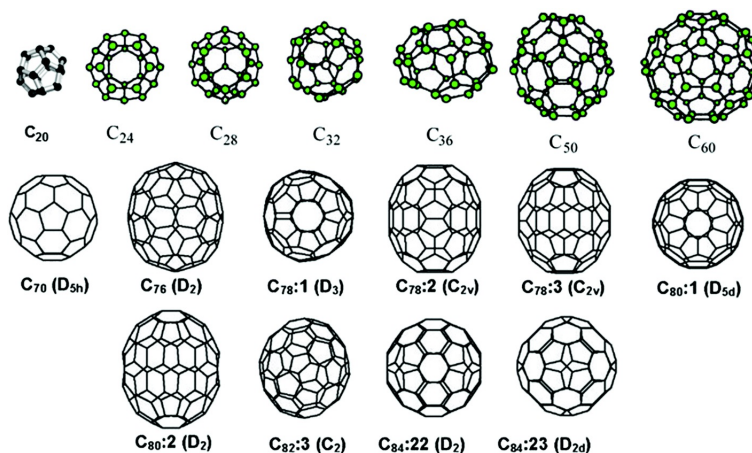


Figure 2.4. The major isomers of fullerenes: structures and their symmetry [22].

To give another example, the C70 fullerene is the last of the three allotropic forms of Carbon, after diamond and graphite [21]. This molecule consists of 70 atoms of carbon and it can be said that remind us of a rugby ball. This structure is interlinked with twelve pentagons and twenty five hexagons. As before, an atom of carbon is present at each pentagon or hexagon's vertices, with a bond at each edge [21].

Moreover, a single atom of Carbon is connected to the other three Carbon atoms placed next to it, bonded in this way with single s and two p orbitals; in other words: sp^2 hybridization. It has to be said that this fact makes them enhanced than the original ones, providing even stronger bonds [21]. In addition, these molecules can sustain a huge amount of chemical reactions simply by accepting or donating an electron instantaneously.

In figure 2.4 are shown the the major isomers of fullerenes. There can be easily noted the different structures and their symmetry, starting with the smallest one named C20 going to the biggest one C84.

2.2.3 Insights

The relevance of the discovery of fullerene molecules can be understood by analyzing the huge amount of new fields of possible applications. Firstly the introduction

of novel types of polymers and superconductors, secondly structures with metals or other different type of atoms trapped within these carbon clusters, that met with great success in new industrial applications [21].

One of the most exciting applications of C60 fullerene is for sure the electronic battery, created with a basis of lithium cathodes [21]. However, remarkable usages of fullerenes may also be found in the pharmacy field for the creation of new pharmaceuticals or they can also find a use as additives in fire retardant paint [21].

On the other hand, C70 fullerenes for example are very often employed as organic photovoltaics. Furthermore, they are very powerful and intense antioxidants, thus they react immediately and at a great rate with free radicals, that are mainly the reason for death or cell damages [21]. In addition to this, they are also assigned as catalysts in several chemical reactions, starting from the purification of water, going through the production of portable power and in the field of medical and vehicles [21].

It is interesting to know that the smallest fullerene is the C20, so the one that contains 20 pentagons and no hexagons. Nevertheless, since the shape of each carbon molecule is firmly non-planar, this type of molecule has robust internal tensions. There are many other achievable fullerenes, for example: C28, C32, C44, C50, C58, C70, C76, C84, C240, C540, C960 [21]. It has to be said, as previously announced, that the most frequently used are C60 and C70, while the others are very unusual.

2.3 Endohedral fullerenes

Magnetic properties of fullerene molecules can be explored and studied through the encapsulation of atoms inside the cage. This is named endohedral fullerene.

Endohedral fullerenes belong to a new class of compounds which are experimentally and theoretically important due to their singular structures and related properties [6] [7].

As previously stated, in 1985, it was first suggested that fullerenes could imprison atoms in their closed-cage structure. In fact, it was demonstrated that different types of reactive atoms can be encapsulated inside the fullerene molecule.

Since then, metal-containing endohedral fullerenes have attracted special attention as a new class of technologically relevant materials due to their combined fullerene-like and metallic properties [6].

Moreover, it is remarkable that in most endohedral fullerenes, the insertion

of metal atoms into the cages produces an increase from the electron affinity (this concept will be explained in section 4.2.2) point of view respect to the corresponding empty cages [6]. Endohedral metallofullerenes have generated great interest for optoelectronic applications. Indeed, changing the encapsulated metal cluster, it can be seen a variation of the related optical and electronic properties. This alteration of the properties happens without the modification of the structural nature of the carbon cage.

The studies on endohedral fullerenes have shed light on the effect of encapsulation on the carbon cage, including two most important aspects: the location of the encapsulated atoms and also the type of interaction between the encapsulated specie and the the carbon cage [6] [7]. These interesting aspects will be studied more deeply in the following section 2.3.1.

As previously announced, Moore's law promoted the miniaturization of the recent electronic devices and so, in the last years, this led to consider the atomic or molecular scale. Thus the research has concentrated the investigations on single molecular devices, in particular to fabricate them and design functional devices which are assumed to be the building blocks of future molecular computers.

Obviously, fullerenes stand out due to their unique cage-like structures that provides versatility in the design of single molecular devices.

2.3.1 The encapsulated clusters

Foreign atoms can be inserted into fullerene cages to cast new physics.

Cage-cluster complementarity is of crucial importance in determining the sizes and structures, as well as the properties of endohedral fullerenes [8]. The encapsulated atoms or clusters, which are typically in a positively charged state, in a irreversible way, mechanically and electrostatically trapped inside the typically negatively charged cages. These rather exotic compounds exhibit complementary properties between their components [8].

It is interesting to know that considerable experimental and theoretical efforts have been devoted to explore this endohedral family, to account for their unusual stabilities, and to explain their structural and electronic properties. For more you can see [8].

2.3.2 Effects: size and shape

The discovery and increased interest of trapping and studying atoms and clusters inside the carbon cages began almost immediately after the initial discovery of the fullerenes in 1985, with the detection of La@C60 by Smalley et al., the first reported endohedral fullerene [8].

Since then, a wide variety of endohedral systems have been prepared and characterized from compounds encapsulating neutral atom species such as noble gases

and diatomic and triatomic molecules (H_2 and H_2O) to those with trapped metals and multiatomic clusters inside [8].

Size and shape effects are factors that are closely correlated and contribute simultaneously to determine the observed structures. A lot has been said about cluster size effects in determining the size of the corresponding cages, as well as their specific geometries.

As an example, C82 has a deformed cage with lower symmetry and X@C82 (X = La, Gd, Tb, Dy, Ho, Er) have been prepared with the aim of extremely small and stable storage units, where the SMD of Ce@C82 has ever accessed an additional state [8]. Such continuous molecular optimization efforts finally lead to non-superimposable charge center and structural center, which may form stabilized electric dipoles in the molecule.

Eventually, this can enable the long desired single molecular electret (SME), a system exhibiting electric polarization switching above room temperature [8], raising expectations regarding the development and practical applications of single-molecule memory devices.

2.4 How it is possible to trap atoms or molecules into fullerene cages?

The development of Endohedral fullerenes applications has been disadvantaged by a constraint in their production. In fact, they can be created only involving physical methods. The most known ones are the co-vaporization of carbon and high pressure or temperature treatment with the usage of noble gases. It can be easily said that these processes are difficult to control and at the end of many painful developments, it can be reached a very small quantity of product.

So, it is very interesting to know that, with the encapsulation of an atom or a molecule, it is possible to observe a change in the different properties of the single fullerene cage. But how can we trap an atom or a molecule inside these cages, in an effective way without involving such a great effort for a little result?

The solution has been proposed in these last years and consist on the realization of endohedral fullerenes by the use of organic reactions. This is also called *Molecular Surgery method* [9] and consists on these steps:

- *Incision* of the fullerene cage: this step is done in order to form an opening on the surface. The "hole" is very small and can host a molecule or an atom.
- *Suture* of the opening: this step involves a sequence of chemical reactions that are exploited to "stitch" the cavity to restructure the original cage with the atom or molecule inside it.

2.4.1 A practical example

The best way to understand a process is to give a practical example. Here after I will refer to the encapsulation of a molecular hydrogen inside the C60 fullerene cage. The steps described are the ones followed for the Molecular Surgical method. Many thermal reactions with phthalazine caused the creation of cage-opened C60 derivatives. These obtained structures have an eight-membered opening in a ring. So it can be said that the different methods for the creation of an opening follow a simple procedure that involves a thermal reaction of the C60 fullerene cage with 5,6-diphenyl-3-(2-pyridyl)-1,2,4-triazine [11].

1,2,4-Triazines are renowned compounds and in literature you can easily find different synthetic methods for the creation of their derivatives. It is interesting to know that compounds that contain the 1,2,4-triazine can be found in natural materials [10]. This reaction lasts about 17 hours in order to obtain an opened cage. This process must be experienced through a preliminary cycloaddition of 5,6-diphenyl-3-(2-pyridyl)-1,2,4-triazine with C60.

Afterwards, an intramolecular reaction at high temperature and following retro-reaction provide a final opening in the eight-membered ring. With the usage of X-rays, it is possible to observe that this final structure has the C=C double bonds significantly distorted, at the edge of the opening [11].

After the opening, as an example, it can be selected the smallest molecule to be encapsulated: H_2 . This is the most simple example, for other cases refer to the book [11]. In order to realize the trapping of the selected molecule, the structure with the opening has to be treated with high-pressure H_2 gas. We are talking of about 800 atm, at a temperature of 200 C for 8 hours in an autoclave. Subsequently, we have the inclusion of the entire H_2 molecule inside the cage.

Lastly, it is performed a technique to suture the opening of the fullerene cage. Although, the H_2 molecule is held inside the cage, in fact this is the final step to finish the Molecular Surgery process. This is done by removing all the organic addends that have been left on the fullerene cage during the previous steps. This can be achieved by just heating a powder in a glass tube under vacuum. This performance is done in an electric furnace at a temperature of 340 C for 2 hours.

It must be said that the given explanation of the process is just a basic summary that can give a practical idea on the procedure for Electronic Engineers. Indeed, the steps are more complicated and need a more specific chemical background to be understood into deep [11].

A further example that can be mentioned is for sure the encapsulation of Hydrogen Fluoride inside C60 ($HF@C60$) [12]. This is also done by using the Molecular Surgery method explained above, however it involves different agents respect to the case of H_2 . The researchers, in fact, found the internal cavity of the C60 cage an exceptional environment for the study of different isolated atoms and molecules.

In the paper [12] you can find more information on the procedure followed and a complete analysis on the properties obtained.

2.5 Single-Molecule electret

As said before, electrets are dielectrics that present an almost permanent dipole polarization. A single-molecule electret (SME) is a long desired nanoscale component since it can conduct us to new very small storage device with the feature of non-volatile memory [4]. Its main attribute is the switching between two different states by means of an external electric field. Due to their poor electrical stability considering single molecules, the presence of this type of electrets has been contentious in the last years [4] [5].

Recent studies report an endohedral metallofullerene (Gd@C82) single molecule electret device, demonstrating its non volatile memory capabilities. SME behaviours can be observed in a molecule containing an internal cavity, in which a trapped ion shuttles between two or more energetically stable sites [5].

The direction of the electric polarization switches with the ion position. At a temperature range where the thermal energy is adequately lower than the energy barrier between the stable ion sites, suppression of ionic inter-site movement occurs, thereby resulting in semi-permanent molecular polarization [4] [5]. However, applying an electric field to the SME within this temperature range can alter individual ion site energy, thus inducing inter-site ion transfer with polarization reversal. Consequently, SMEs exhibit ferroelectric characteristic, for example, polarization hysteresis and spontaneous polarization, without long-range dipole ordering (a mechanism pertinent to Single molecule magnets) [4] [5]. In addition to this, researchers reveal the SME nature of the Gd@C82 molecule by indicating the existence of two Gd stable sites inside C82 through theoretical calculations and observing the dielectric relaxation process between them (Full explanation will be given in section 2.5.2).

It has to be said that the physics of a SME differs from that of ferroelectricity in solids, where the system is stabilized by the exchange coupling between a large number of dipoles in a large domain. Instead, it is more alike to the physics of a single-molecule magnet, where spin polarization is stabilized by the anisotropy energy of individual molecules. Such a SME is free of any inter-dipole coupling and has been anticipated by recent theories and experimentally tested in long-range ordered crystals, where, however, the inter-dipole coupling is still possible. The position of the single Gd atom inside the C82 cage forms the memory storage information unit and may thus lead to miniaturized storage devices in future electronics

[4] [5].

2.5.1 Single-electron transport in Gd@C82 transistor

Let's have now a deeper look into the considerations made in the previous section. In order to better understand the topic, it is useful to start analyzing some relevant observations found in literature that involve the Gd@C82 transistor. As it is explained in some recent articles, the single Gd@C82 molecular transistor is prepared by setting a Gd@C82 molecule into a pair of Au electrodes [4].

It has been observed that a back gate of 7-10V can modulate the I-V curve and there is a current blockade area at low voltage. So, the gate voltage can decrease or increase the blockade voltage range, indicating change in the electrochemical potential [4]. As observed by the researchers, changing the gate voltage will tune the chemical potential of the molecule. When the electrochemical potential is aligned with the Fermi energy of the source and drain electrodes, the conductance gap will decrease to zero and reach a degeneracy point, indicating the successful preparation of a single-electron transistor with a Gd@C82 SMD [4]. In figure 2.5, which is a replica of the graph showed in the article, you can easily see that multiple peaks are present and indicate that the wanted SMD could access a series of redox states and degeneracy points. These points are related to the molecular energy levels [4].

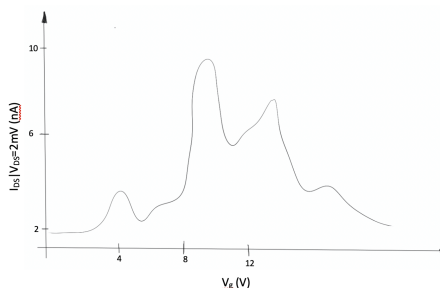


Figure 2.5. A replica of the graph obtained by the authors of the paper: I_{DS} as a function of the gate voltage. V_{DS} is fixed at 2mV.

Gate-controlled switching between two electronic states, and its hysteresis loop

Proceeding with this analysis, an interesting switching between two molecular states is observed. The authors of the experiment carefully measured the current I_{DS} as a function of the gate voltage V_g when the V_{DS} is fixed at 2 mV. A

replica of the graph shown in the paper is given in Fig. 2.6. The gate voltage was moved backward and forward. It can be easily seen that two states are accessed: *State 1* and *State 2* [4].

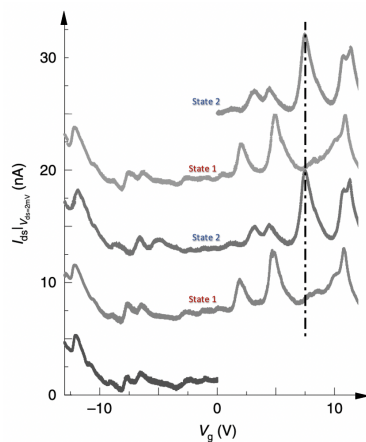


Figure 2.6. A replica of the I_{DS} vs V_g (with V_{DS} fixed at 2 mV). The gate voltage was moved backward and forward. It can be easily seen that two states are accessed: *State 1* and *State 2*.

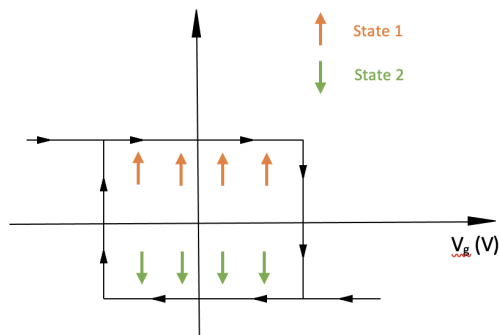


Figure 2.7. A different representation of the switching process. The gate voltage (V_g) switches the device between *State 1* and *State 2*.

Furthermore, the authors add that the oscillation peaks can be related to the molecular orbitals. Hence, they speculate that the two sets of oscillation peaks means that Gd@C82 may present two stable states [4]. This observation suggests that the structure of the molecule can be controlled and switched by an external

electric field [4]. In figure 2.7 you can see a scheme that represents this behaviour. The device maintains the current state until a certain V_g is applied and so it changes its state. And so on. In more depth, it is remarkable that the starting state is initially set to *State 1* when the gate voltage is 0V. The device maintains *State 1* even if we decrease the gate voltage to -10 V [4]. The authors then changed the gate voltage direction. When the gate voltage is increased positively to over 10.5 V, the device was found to switch to *State 2*. The state can be set back to *State 1* when a large enough negative gate voltage is applied [4]. The authors underlined that this behaviour is stable and so it is highly repeatable, reproducible and stable for more than one month, indicating that the gate voltage changes the internal structure of the molecule [4].

Moreover, the figure 2.7 shows an hysteresis loop, which is typical in ferroelectricity operations at the single-molecular level. This is basically the evidence of a SME [4].

2.5.2 Theoretical modelling revealing the SME physics

Finally, Density Functional Theory (DFT - Theory can be found in section 3.6.2) calculations were performed to demonstrate the corresponding atomic configurations of the two switchable states [4]. For this purpose, tens of Gd adsorption configurations were considered. Besides, two of them denoted configurations Gd-I and Gd-IV, were discovered to be considerably more stable than the others [4]. Hereafter we will refer to Figs. 2.8, 2.9 and Tables 2.1 and 2.2.

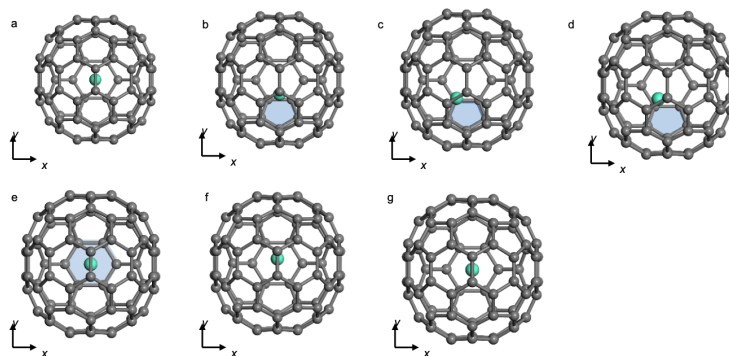


Figure 2.8. The first seven adsorption sites of a single Gd atom that have been considered [4].

Researchers observed that, since the molecule stochastically drops into the gap at a random position, the electrical field cannot always flip the dipole of the molecule once the electric polarization is perpendicular to the gate electrical field

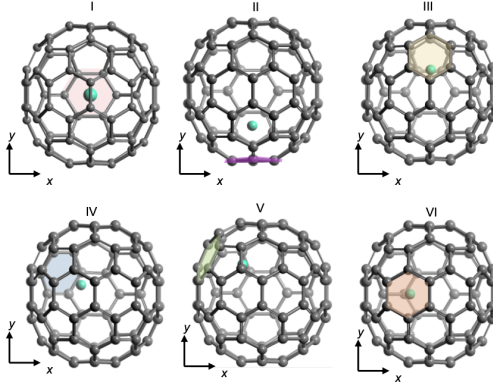


Figure 2.9. The six inequivalent cases. In the figures you can easily see which is the face considered for the adsorption of the Gd atom in each case.

Adsorption site	$\Delta E(meV)$	d_{C-Gd} (Å)
C82-center	6C-Hol	-
C5-Hol	6C-Gol	-
C5-C-top	6C-Hol	-
C5-bond-top	6C-Hol	-
C6-Hol-I	0.0	2.45
C6-C-top	6C-Hol	-
C6-bond-top	1969.4	2.34

Table 2.1. Relative total energies and the heights of the adsorbed Gd atom at different sites shown in Figure 2.8 [4].

[4]. Although with this experiment it is achieved the reproducibility of the reversible switch [4].

Adsorption site	$\Delta E(meV)$	d_{C-Gd} (Å)
C6-Hol-I	0.0	2.45
C6-Hol-II	474.9	2.38
C6-Hol-III	1439.4	2.35
C6-Hol-IV	22.4	2.35
C6-Hol-V	609.1	2.31
C6-Hol-VI	1248.3	2.34

Table 2.2. Relative total energies and the heights of the adsorbed Gd atom at the sites shown in Fig. 2.8 [4].

2.5.3 Other SME

It is very difficult to find in literature articles mentioning the discover of the single molecule electret.

The very few reliable expose, in a very detailed way, only the case of the encapsulation of the Gadolinium in the C82 cage, considering it the revelation of the SME and so a miniaturized non-volatile memory storage device. There is only a mention in some articles of X@C82 species ($X = \text{La, Gd, Tb, Dy, Ho, Er}$) that have been analyzed as small and stable memory storage units [8], but there are not given more information.

By definition, as previously stated, SME behaviour can be monitored in a molecule that holds an internal cavity, in which can be encapsulated an ion that shuttles between different energetically stable sites [5]. Moreover, the behavior of single-electron transport in the case of Gd@C82 changes according to the position of the Gd ion respect to the cage. All the location are different and it has to be said that the site where the single Gd atom is placed inside the C82 cage produces the storage information.

It is important to note that every position is different because of the geometrical organization of the C82 cage (see details in subsection 3.7.1). Besides, this asymmetry plays a vital role on the utilization of Gd@C82 molecules as memory components. To be more precise, on one hand the information can be preserved as the location of the Gd ion respect to the cage (monitored by the gate voltage). On the other hand, the known site of the Gd ion can be read as the stored information (the position of the ion can be achieved from I_{DS} calculation).

In any case, even if we do not have more cases and articles revealing other SME devices, there are many experiments that involve the encapsulation of different species in more dissimilar cages. Considering the observations made above and what is reported in the articles [4] and [5], it can be expected that other species, encapsulated in fullerene cages that exploits asymmetry, can reach the wanted SME behaviour. In addition, if we consider smaller cages, we would have a lower computational time and so save time during the practical simulations.

In the article [13], for example, is underlined that the Buckminsterfullerene C60 is only one member of a large family of carbon cage molecules, so it is important to distinguish and organize all fullerenes by categorizing them by the type of their symmetries. The huge amount of structures provides us the opportunity to be creative and maybe find other cages that will replace the much discussed C82 cage.

However, this is just my humble thought and would be a good hint for an

interesting deepening on this topic in the future.

2.5.4 To sum up

Going through this topic, researchers found that it is possible to notice that the physics of a SME differs from that of ferroelectricity in solids, where the system is stabilized by the exchange coupling between a large number of dipoles in a large domain. Instead, they said it is more alike to the physics of a single-molecule magnet, where spin polarization is stabilized by the anisotropy energy of individual molecules [4].

It has to be said that such a SME is free of any inter-dipole coupling, and has been anticipated by recent theories and experimentally tested in long-range ordered crystals, where, however, the inter-dipole coupling is still possible. Recent experiment demonstrates that the SME at the single-molecule level and thus excludes any inter-dipole coupling, providing convincing evidence of a SME [4].

The position of the single Gd atom inside the C82 cage forms the memory storage information unit and may thus lead to miniaturized storage devices in future electronics [4].

Finally, with these considerations, we can start with the practical section of this Master Thesis work. In particular, after some useful theory, I have tried to create the Gd@C82 molecule and test its behaviour considering the changes on the different properties with the encapsulation of the Gd atom in the cage C82, testing two different stable positions, tanking into account the considerations made in literature reported in the section 2.5.2.

Chapter 3

Methodology

3.1 From theory to practice

As announced before, the Single-molecule electret device is a new memory device in which the electric dipole, rather than the magnetic dipole, stores information at the single-molecule level [4] [5].

It would be interesting to analyze deeply the Endohedral metallofullerene Gd@C82 single-molecule electret device, demonstrating its non-volatile memory capabilities. As reported in the previous chapter, the behavior of single-electron transport in Gd@C82 varies depending on the location of the Gd ion because all the different sites are non-equivalent [4]. This asymmetry is central to the employment of Gd@C82 molecules as memory elements. As suggested from the reference articles there are two stable Gd@C82 sites, but in order to proceed with the simulation it is necessary to do an optimization of the geometry of the molecule [4] [5]. In the section 3.5 you can find the explanation on what consist the geometrical optimization and why it is useful.

In the present chapter are reported the main steps followed and the needed theory used to study the molecule and reach the proof that the Gd@C82 molecule acts as an electret. In section 3.2, I will expose a bit of helpful theory on conduction a nanoscale, focusing on the main important aspects. The following section 3.3 will provide information about ATK, which is one of the tool used for the objective of the thesis. After that, you can find the section 3.6 about ORCA, another tool that is very useful for the geometrical optimization of the molecule.

Finally you can find the section describing the created device (section 3.7).

3.2 A small recap on conduction at nanoscale

In order to describe carrier transport in nanoscale devices, we have to think about charge carriers as quantum mechanical entities, rather than as classical particles.

In the recent years, it has become fundamental to model and understand the quantum physics that governs the properties of these extraordinarily small devices.

The typical methods used on the investigation of the behavior of molecular devices are:

- The Non-Equilibrium Green's Function (NEGF) formalism;
- The Density Functional Theory (DFT);
- Semi-Empirical methods (for example using the Extended-Huckel theory (EHT)).

Non-Equilibrium Green's Function (NEGF): an elementary introduction

The non-equilibrium Green's function (NEGF) formalism provides a sound conceptual basis for the development of quantitative models for quantum transport. The purpose of this subsection is to present an understandable description of the NEGF equations illustrating the basic physics [32].

Firstly, it has to be said that any device simulation program performs a self-consistent solution of a transport equation and a "Poisson" equation. The transport equation calculates the electron density $n(r)$ and the current I for a given potential profile $U(r)$, while the "Poisson" equation calculates the effective potential $U(r)$ that an electron feels due to the presence of the other electrons [32]. The two calculations are iterated till $n(r)$ and $U(r)$ converge to a self-consistent value (Fig. 3.1). A quantum transport simulator also performs a similar iterative solution of a transport equation and a Poisson-like equation [32].

Transport equation First of all, consider a really small device with just one energy level E in the energy range of interest, connected to a source and a drain contact [32].

What is the number of electrons N in our device? The answer is clear if everything is in equilibrium, with a Fermi energy E_f set by the work function of the source and drain contacts. However, once we apply a drain bias V , the Fermi energies in the source and drain contacts, denoted by μ_1 and μ_2 will separate as follows [32]:

$$\mu_1 = E_f + (qV/2) \tag{3.1}$$

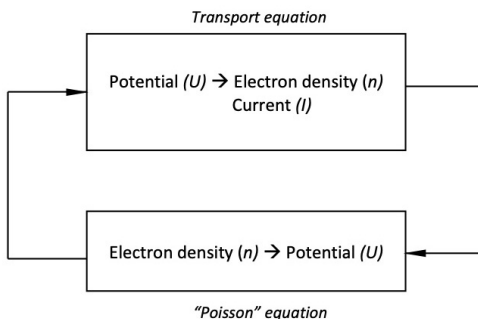


Figure 3.1. Any device simulation program performs an iterative self-consistent solution of a transport equation and a Poisson-like equation.

$$\mu_2 = E_f - (qV/2) \quad (3.2)$$

giving rise to two distinct Fermi functions for the two contacts [32]. If the device were in equilibrium with the source, the number of electrons would equal f_2 . However, if the device were in equilibrium with the drain, the number of electrons would equal f_1 , where [32]:

$$f_{1,2}(\epsilon) = \frac{1}{\exp[(\epsilon - \mu_{1,2})/k_B T]} \quad (3.3)$$

The actual number of electrons N will clearly be intermediate between f_1 and f_2 and can be determined by writing simple rate equations for the currents $I_{1,2}$ crossing the source and drain interfaces [32]:

$$I_1 = \frac{q\gamma_1}{h}(f_1 - N) \quad (3.4)$$

$$I_2 = \frac{q\gamma_2}{h}(N - f_2) \quad (3.5)$$

where the constants (γ_1/h) and (γ_2/h) represent the rates (per second) at which an electron inside the device will escape into the source and drain respectively [32]. Setting $I_1 = I_2 \equiv I$, we obtain the steady-state number of electrons N and the current I [32]:

$$N = \frac{\gamma_1}{\gamma_1 + \gamma_2} f_1(\epsilon) + \frac{\gamma_2}{\gamma_1 + \gamma_2} f_2(\epsilon) \quad (3.6)$$

$$I = \frac{q}{h} \frac{\gamma_1 \gamma_2}{\gamma_1 + \gamma_2} [f_1(\epsilon) - f_2(\epsilon)] \quad (3.7)$$

This simple derivation exhibits the physics of current flow through a small conductor attached to two reservoirs that try to maintain it at two different levels of occupation f_1 and f_2 [32]. It can be said that the actual occupation is intermediate between the two (Eq. 3.6) and one reservoir keeps pumping in electrons trying to increase the number while the other keeps emptying it trying to lower the number [32]. The overall effect is a continuous flow of electrons from one reservoir to the other, leading to a net current in the external circuit, described by Eq.3.7 [32].

The coupling to the Source and Drain contacts broadens the discrete level into a distribution:

$$D(E) = \frac{\gamma/2\pi}{(E - \epsilon - \Delta)^2 + (\gamma/2)^2} \quad (3.8)$$

having a linewidth of γ along with a possible shift in the level from ϵ to *epsilon*+ Δ , where $\gamma = \gamma_1 + \gamma_2$, $\Delta = \Delta_1 + \Delta_2$. It is possible to account for this broadening by modifying Eqs.3.6, 3.7 to include an integral over all energies, weighted by the distribution $D(E)$ [32]:

$$N = \int_{-\infty}^{+\infty} dE D(E) \left[\frac{\gamma_1}{\gamma_1 + \gamma_2} f_1(E) + \frac{\gamma_2}{\gamma_1 + \gamma_2} f_2(E) \right] \quad (3.9)$$

$$I = \int_{-\infty}^{+\infty} dE D(E) \frac{q}{h} \frac{\gamma_1 \gamma_2}{\gamma_1 + \gamma_2} [f_1(E) - f_2(E)] \quad (3.10)$$

Using elementary algebra, Eqs.3.9 and 3.10 can be rewritten as [32]:

$$N = \int_{-\infty}^{+\infty} \frac{dE}{2\pi} D(E) [A_1(E) f_1(E) + A_2(E) f_2(E)] \quad (3.11)$$

$$I = \frac{q}{h} \int_{-\infty}^{+\infty} dE \bar{T}(E) [f_1(E) - f_2(E)] \quad (3.12)$$

Where $A_1 = G\gamma_1 G^+$, $A_2 = G\gamma_2 G^+$, $\bar{T} = \gamma_1 G\gamma_2 G^+$, $G = [E - \epsilon - \sigma_1 - \sigma_2]^{-1}$, $\sigma_{1,2} \equiv \Delta - 1, 2 - i\gamma_{1,2}/2$.

So far we have assumed that the device has just one energy level with energy E . In general real devices have multiple energy levels in the energy range of interest. So any device is described by a Hamiltonian matrix $[H]$ whose eigenvalues advise us the allowed energy levels. As an example, if we describe the device using an effective mass Hamiltonian $H = -\hbar^2/2m^* \nabla^2 + U(r)$ [32]. We could represent it with a $N \times N$ matrix by choosing a discrete lattice with N points and using the method of finite differences. This corresponds to using a (discretized) real space basis [32]. More generally we could use valence atomic orbitals like $sp^3 s^*$ as a basis and write down a semi-empirical Hamiltonian, or go further and include the core atomic orbitals as well, with an ab initio approach. If you are interested in a more

theoretical point of view or you just want more details, please refer to [32].

Similarly, once we have chosen a basis or a representation, we can define self-energy matrices $[\sum_{1,2}]$ that describe the broadening and shift of the energy levels due to the coupling to the source and drain. The appropriate NEGF equations are obtained from Eqs. 3.11 and 3.12 simply by replacing the scalar quantities like ϵ and $\sigma_{1,2}$ with the corresponding matrices $[H]$ and $[\sum_{1,2}]$ [32]. This yields: $G = [EI - H - \sum_1 - \sum_2]^{-1}$, $\Gamma_{1,2} = i[\sum_{1,2} - \sum_{1,2}^+]$:

$$A_1(E) = G\Gamma_1G^+ \quad (3.13)$$

The same for A_2 , where I is an identity matrix of the same size as the rest [32]. The number of electrons N (Eq. 3.11) is replaced by the density matrix given by an analogous quantity:

$$[\rho] = \int_{-\infty}^{+\infty} \frac{dE}{2\pi} [A_1(E)]f_1(E) + [A_2(E)]f_2(E) \quad (3.14)$$

The current is still given by Eq.3.12, but if we define the transmission as the trace of the analogous matrix quantity [32]:

$$\bar{T}(E) = Trace[\Gamma_1G\Gamma_2G^+] \quad (3.15)$$

We cannot say that what we have done here represents a "derivation" of the NEGF equations. In fact, what we have obtained is the one-level scalar version (Eqs. from 3.8 to 3.12). The multi-level matrix version (Eqs. from 3.12 to 3.15)) follows from it only if all the matrices are diagonal [32]. But in general one cannot diagonalize both the Hamiltonian $[H]$ and the self-energy matrices $[\sum_{1,2}]$ simultaneously and a more careful treatment is called for: $A_1 = G\gamma_1G^+$, $A_2 = G\gamma_2G^+$, $\bar{T} = \gamma_1G\gamma_2G^+$. It is useful to say that the real value of this discussion is that gives us an intuitive opinion for the meanings of the quantities of the NEGF equations [32].

It is remarkable that the NEGF equations presented here do not reflect the effect of incoherent scattering processes (such as electron-phonon interaction) inside the device which become increasingly important as the device gets longer [32]. In an approximate qualitative sense, scattering processes are like additional floating contacts that extract electrons from the device. However, unlike the source and drain contacts, they reinject the electrons so as not to draw any net current [32].

Scattering processes can be included in the NEGF formalism by defining additional self-energy matrices like the ones we have defined for the source and drain contacts but the details are more complicated [32].

Density Functional Theory (DFT)

Density Functional Theory (DFT) is a ground-state theory in which focuses on the importance of the charge density [33]. DFT has demonstrated to be extremely effective in describing structural and electronic properties in a massive class of materials, including atoms and molecules but also complicated systems. Moreover DFT is computationally simple [33].

For these reasons DFT has become a common tool in first-principles calculations. It is useful for sure to define but also to predict properties [33]. If you are interested in a more specific explanation on this theory, you can find a good theoretical lesson on [33]. Moreover, in the section 3.6.2 a more practical use will be explained.

Semi-Empirical methods: an idea on the extended Huckel method (EHT)

The first think to take in mind is that semi-empirical methods reduce the computational cost by reducing the number of integrals.

The extended Huckel method (EHT) is a semi-empirical LCAO method, which exploits all valence orbitals of the atoms as the basis functions. Contrarily to the original Huckel method, the extended one takes into account not only π -orbitals but also σ ones [34].

This approach requires only a fraction of the computational effort needed by the more elaborated ab initio methods and often provides reasonably accurate quantitative results that give insight into the essential physics [34].

Remarks

It is important to say that the design of molecular devices is only possible after having a complete theoretical model, with which we can explain and predict the charge transport behavior through molecular devices. This is why before starting with the examined case of the Gd@C82 molecule, I have decided to give a bit of theoretical background on how to model conduction at nanoscale.

3.2.1 Transport regimes: classical transport vs quantum transport

Hereafter I will give some useful pieces of theory on the classical and quantum transport regimes. It is important to underline that this subsection explains the topic in a very simplistic way, indeed it gives just few ideas on this matter, focusing on the most helpful points for this Master Thesis work.

If we consider bulk-systems and so 3D-systems, electrons are managed as classical particles that flow through a channel under the influence of an electric field. Besides, they can arbitrarily introduce different scattering events inside the crystal lattice. If these assumptions are true, the drift-diffusion model is acceptable. On the other hand, if we consider nanostructures, both of these suppositions loose of authenticity. This is why it becomes necessary to include quantum mechanical facts. In addition, by decreasing the dimensions of the channel, carriers are more confined and so it must be considered also their quantum nature of wave-particles.

Furthermore, it is remarkable that in the direction of confinement the potential cannot be considered periodic (to simplify), therefore quantities such as resistance or current indicated through the average measures loose their significance.

Types of nanoscale systems

So what are the different types of nanoscale systems? The first to be considered are the 2D ones, also called *Quantum wells*. In general they include all the structures made of different layers assembled in a nanoscaled way.

The thickness of the channel is of the order of few nanometers and certainly, downscaling one dimension towards nanosizes leads to the confinement of the carriers in one direction. The direction of confinement is x (thickness of the channel), so there are only two degrees of freedom that correspond to y and z directions.

The second type are the 1D-systems, also known as *Quantum wires*. They are systems where two dimensions are of the order of few nanometers. Surely, downscaling two dimensions towards nanosizes leads to the confinement of the carriers in two direction. These two directions of confinement are x and y (thickness and width of the channel), so the only two degree of freedom is along z direction.

Lastly, 0D-systems, also called *Quantum dots* are obtained by scaling the three dimensions (x, y, z). They are systems like molecules involve a total quantum confinement of carriers.

As we will see in this work (in the following chapters, mostly on the 4.4), in 0D-systems the quality of the interfaces plays a vital role and influences a lot the conduction. In fact, depending on the coupling strengths of the dot between the electrodes there will be completely different type of conduction and this for sure gives also rise to different type of devices.

It is interesting to note that according to the time interval during which the electron stays confined in the dot (*escape time*) defined as $\tau = \frac{\hbar}{\gamma}$ where γ is the so called *coupling factor*, there are three remarkable types of coupling:

- $\tau \rightarrow \infty$: there is **no coupling** between the reservoirs and the channel (i.e.

S/D and the dot). The dot is considered a closed system, in fact there is no exchange of matter with the external world. For sure this is a not truthful case.

- $\tau \simeq f_s$: the system is in the so called **strong coupling** where the eigenvalues of the system and so the allowed discrete energy levels of the dot, are broadened due to the strong influence of the electrodes. The transfer of electrons is easier and there is exchange of matter with the external world. Moreover, the dot is considered an open system.
- $\tau \simeq n_s$: the system is in the so called **weak coupling** where the discrete energy levels of the dot are no more broadened due to the very weak influence of the electrodes. No broadening occurs and electrons are more confined in the dot and it is more difficult for them to escape.

It is important to take in mind that the more is the coupling strength, the higher is the broadening of the energy levels and at the end the smaller is the escape time.

Tips

In order to model conduction in any structure, it is necessary firstly to know its Density Of States (DOS) $N(E)$. By definition, the Density Of States is the one of the allowed energy states of the system which, if are occupied by carriers, may contribute to the conduction.

They are basically determined by the geometry of the system and once they are known, the density of carriers available for conduction $\rho(E)$ can be obtained as:

$$N(E)f_{FD}(E) = \rho(E) \quad (3.16)$$

with $f_{FD}(E)$, Fermi-Dirac function which tells the probability distribution of electrons as function of energy. After the determination of $\rho(E)$ then the current distribution can be easily determined.

3.3 ATK

I have decided to use the ATK tool in order to realize the different structures used in the practical experience.

QuantumATK package is a powerful set of tools for calculating properties of nano-scale systems. These atomic-scale calculators are based on density functional theory, semi-empirical tight binding, and classical potentials [39].

The non-equilibrium Green’s function method is a unique feature of QuantumATK; it allows simulations on nano-scale devices and interfaces, including support for non-zero bias between the electrode leads and device components such as electrostatic gates and dielectrics [39].

This tool has been very useful since it allowed me to build different structures and realize all the simulations that have been helpful to reach the objective of this thesis. However, it is remarkable that I have found some difficulties and issues on the 2021 version, in a certain extend. I have started using the 2020 version in March/April, then I moved to the 2021 one. During the months I have met some issues in the results: presented in a disordered manner and some of them lost. So in September I moved back to the previous version (i.e. 2020). As I will expose in the section 4.4, the provided results of the I/V analysis are given by the 2020 version of the ATK tool.

In addition, it has to be said that these structures are made by hand and for sure need a geometrical optimization (refer to section 3.5 to find out what is the geometrical optimization and why it is useful). For more information about the tool itself and all its possible usages, please refer to the ATK manual [39].

Before going through the practical part of this work, I will give some helpful theory, touching different topics that have been used during the various tasks.

3.4 Further theory

Before analyzing the realized structure it is useful to analyze another important aspect to take into account: geometrical optimization and so what is it and why it is useful. To do this, it is necessary to study what is a Potential Energy Surface (PES) and the characterization of the molecular structures.

3.4.1 Potential Energy Surface

The potential energy surface (PES) describes the energy of a molecule as a function of the position of the nucleus:

$$E_{PES} = E(X), X \equiv (x_1, y_1, z_1; x_2, y_2, z_2; \dots; x_N, y_N, z_N) \quad (3.17)$$

where x_i , y_i and z_i are the Cartesian coordinates of the i -th atom.

The concept of potential energy surface originates naturally from the Born-Oppenheimer approximation that separates the motion of electrons from that of nuclei.

Within this approximation, a potential energy surface is obtained by calculating the energy of the molecule for a series of fixed nuclear positions. Energy can be obtained indifferently with classical or quantum methods and this is usually quite satisfactory for most molecules in their fundamental state.

PES is a $3N-6$ dimensional hypersurface, where N is the number of atoms in the molecule. In the expression 3.17, the set of coordinates X refers to an arbitrary origin. If the origin is fixed, for example in the center of mass, three dimensions corresponding to the translational degrees of freedom are removed. Three other dimensions, associated with the rotational degrees of freedom, can be eliminated by aligning the principal moments of inertia of the molecule with the x , y and z axes.

A different way of imagining PES is to consider it dependent on internal coordinates, that is, a function of bond distances, bond angles and dihedral angles. The choice of coordinate system determines the shape of the surface, although a one-to-one correspondence remains between the different coordinate systems.

Since molecules can contain many atoms and the molecular structure is described by many coordinates, it is difficult to calculate or represent the entire surface of potential energy. A simplified two-dimensional potential energy surface can be visualized as a mountainous landscape with valleys representing reactants, intermediates and products, while the transition states correspond to the steps connecting the valleys. Figure 3.2 shows a simple two-dimensional potential energy surface and illustrates some of its characteristics.

3.4.2 Molecular structures

Through the concept of potential energy surface it is possible to discuss molecular structures.

The equilibrium geometry of a molecule corresponds to a minimum on the surface of potential energy. There can be different minima, which represent different conformers and isomers of a molecule, or reactants, intermediates and products of a chemical reaction. If the valley is deep and with steep sides then the molecular structure is enough rigid and well defined.

On the other hand, if the valley is wide or shallow, the molecule is flexible and the concept of molecular structure is poorly defined. A reaction can be represented as a shift from the valley of the reactants to the valley of the products. Depending on the nature of the reactants and products, the reaction can be a simple conformational change, an isomerization, a unimolecular reaction or a bimolecular reaction.

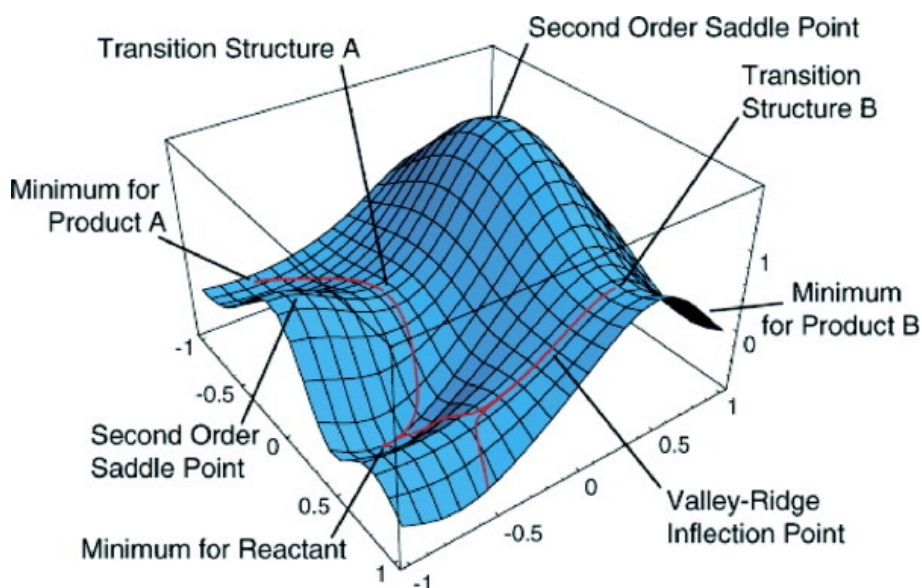


Figure 3.2. Surface model of potential energy with indicated minima, transition structures, second order saddle points and reaction paths [38].

A specific path through the potential energy surface describes the reaction mechanism. The transition state is the highest point on that particular reaction path that requires the least energy to go from the reactants to the products.

Its energy, structure and corresponding vibrational frequencies can be used to predict reaction rates through transition state theory. Both the minimum and transition structures can be identified through geometry optimization. Efficient methods are also available for following reaction paths once the structure of the transition state has been identified.

3.5 Geometrical optimization

Geometry optimization is the process of researching equilibrium geometries and transition states on the potential energy surface.

Since even for small molecules it is difficult to obtain functional forms that accurately describe the potential energy surfaces, most geometry optimization methods directly search for equilibrium and transition structures without building the entire potential energy surface.

Efficient methods of geometry optimization make use of the first derivatives

of the potential energy surfaces with respect to the geometric parameters. These derivatives can be obtained analytically, when it is possible to give them a closed mathematical form, or they can be calculated numerically. In some optimization algorithms, the second derivatives of the PES can also be used.

The first derivatives of the potential energy surface are also called gradients.

In classical mechanics, the first derivatives changed in sign correspond to the forces acting on the atoms in a molecule, as shown in the equation 3.18.

$$\frac{dVx}{dx} = -Fx \quad (3.18)$$

Hence, the points on the potential energy surface where the gradients, or forces, are zero are called stationary points. In the topological analysis of the potential energy surface, these points are indicated as critical points and their characterization is carried out through the calculation of the second derivatives.

The matrix of the second derivatives of the potential energy surface is called the Hessian matrix. In particular, the number of negative eigenvalues of the Hessian matrix at a critical point is known as the critical point index. A critical point with index 0 is a minimum, while a critical point with index 1 corresponds to a transition structure.

For a point on the energy surface, to be a minimum it must satisfy two conditions:

- The first derivatives, or equivalently the gradient or the forces, must be zero (that is, it must be a critical or stationary point). If the first derivatives are not zero there must be a neighboring point with lower energy;
- The matrix of the second derivatives or Hessian must be positive (i.e. with index 0). In other words, all the eigenvalues of the Hessian matrix must be positive.

It should be noted that all translations and rotations of the molecule and any redundancy in the internal coordinates must be removed before deriving the eigenvalues of the Hessian matrix. If one or more eigenvalues are negative, then the potential surface is a maximum along these directions and the point is not a minimum, but a saddle point. For a critical point to be a transition structure:

- The first derivatives must be zero and the energy must be a maximum along the reaction path that connects reactants and products;
- It must also be a minimum in all directions perpendicular to the reaction path.

Hence, a transition structure is a critical point with index 1, that is, one of the eigenvalues of the Hessian matrix must be negative and all the other eigenvalues must be positive. The eigenvector of the Hessian matrix corresponding to the negative eigenvalue represents a shift along the reaction path and is indicated as the transition vector.

A transition structure is also called a first-order saddle point. A saddle point of order n has n negative eigenvalues. This corresponds to a point which is a maximum in n directions and therefore does not represent a transition structure. In Figure 3.2, transition structures and saddle points of the second order (maxima) are shown.

3.5.1 Local minima: how to find them

Identifying a minimum equilibrium structure involves an optimization without constraints of the potential energy surface and, in this specific case, we can also speak of geometry minimization. The algorithms for minimizing nonlinear functions with many variables can be grouped into three broad categories, as reported in the table 3.1.

Categories	Examples
Methods that use only energy	Monovariate research, simplex method
Methods that use gradients	Conjugate gradients, quasi-Newton
Algorithms that require second derivatives	Newton or Newton-Raphson

Table 3.1. The algorithms for minimizing nonlinear functions with many variables can be grouped into this three broad categories.

The methods based on energy are those of more general applicability, but they are the slowest to converge. Methods using second derivatives converge very quickly, but analytical second derivatives are only available for a limited number of theoretical computational methods and are much more expensive than gradient computation. Gradient-based algorithms are the methods of choice for many levels of theory.

If analytical first derivatives are not available, it is usually more convenient to calculate them numerically rather than using energy-based optimization methods. Several algorithms have been developed for geometry optimization and the most used are the so-called quasi-Newton methods.

In Newton or quasi-Newton methods, the potential energy surface is approximated using a quadratic function 3.19 and 3.20:

$$E(x) = E_0 + g_0^t \Delta x + \frac{1}{2} x^t H \Delta x \quad (3.19)$$

$$g(x) = g_0 + H\Delta x \quad (3.20)$$

where

$$\Delta x = x_0 - x \quad (3.21)$$

is the shift vector, "g" is the gradient (first derivative), and "H" is the Hessian matrix (second derivative). In the minimum, the gradient is zero and the shift (step) towards the minimum can be obtained by solving a set of linear equations [3.22](#) and [3.23](#):

$$g(x) = g_0 + H\Delta x = 0 \quad (3.22)$$

$$\Delta x = -\frac{1}{H}g_0 \quad (3.23)$$

This is Newton's step and is the basis of many of the optimization methods that use the gradient. It has to be said that the efficiency of a quasi-Newton type method depends on six factors:

- The initial geometry;
- The coordinate system;
- The initial estimate (guess) for the Hessian matrix;
- Linear research;
- The method for updating the Hessian matrix;
- Control of stride length.

The initial geometry

Obviously, the closer the initial geometry is to the final optimized one, the fewer optimization steps will be needed. In structural calculations electronics with quantum methods, good initial geometries can be obtained from molecular graphics programs and molecular simulation programs, from molecular mechanics calculations or from calculations at a less accurate level of theory.

For molecules with more than a minimum, the initial structure should be close to that of the desired local minimum. Finding the global minimum is a much more difficult problem to deal with and is beyond the scope of these notes. Some references are given at the bottom.

The coordinate system

The coordinate system used during the optimization can have a very large effect on the speed of convergence of the geometry optimization. Cartesian coordinates are the simplest and provide an unambiguous representation for any structure. However, they are strongly coupled; for example, to change the length of a bond you need to change the x, y and z coordinates of two or more atoms.

An alternative is to use internal coordinates, such as bond lengths, bond angles, dihedral angles, etc. For acyclic molecules, it is easy to construct a non-redundant internal coordinate system, ie containing only $3N-6$ internal coordinates for the N atoms of the molecule. For a cyclic molecule, a coordinate system containing all bonds and angles would have more than the required $3N-6$ coordinates. For example, a six-link ring has 6 bonds, 6 bond angles, and 6 dihedral angles, for a total of 18 coordinates, while there are only 12 internal non-redundant degrees of freedom.

The initial estimate for the Hessian matrix

The initial estimate of the Hessian matrix will also influence the convergence rate. The closer the estimate is to the correct Hessian, the faster the convergence will be. Molecular Cartesian coordinates have strong anharmonic couplings between them and the Hessian therefore has many extra-diagonal elements. However, if a good Hessian estimate is available, the convergence speed of the optimization, even in Cartesian coordinates, can be quite satisfactory. In redundant internal coordinates, the coupling is smaller and the Hessian is almost diagonal.

For cyclic molecules, the non-redundant internal coordinates (e.g. coordinates that do not include ring-closing bonds) are also strongly coupled, but in the case of redundant internal coordinates the coupling is smaller and the Hessian may be or be almost diagonal. The initial empirical estimate of a diagonal Hessian matrix can be quite satisfactory in the case of redundant coordinates and can be easily transformed into other coordinate systems. In the case of *ab initio* quantum methods, the initial Hessian matrix can also be obtained from molecular mechanics or semiempirical calculations.

A very good initial estimate for high-level calculation methods is to use the Hessian matrix obtained either from a previous optimization or from a frequency calculation performed at a less accurate theory level. Some particularly difficult optimizations may require a very accurate initial Hessian matrix. In these cases, it can be obtained by calculating it numerically or analytically at the same level of calculation then used for optimization.

Linear research, the method for updating the Hessian matrix and the control of stride length

An accurate linear search may require additional calculations, but an approximate search can be performed without the need for further energy and gradient calculations. For example, you can make a best fit of the energy and direction of the gradient in the current point and in the previous one with a cubic or quadratic polynomial and then the minimum is searched using the polynomial thus obtained. The second step in quasi-Newton optimization is the updating of the Hessian matrix, from H^{old} to H^{new} . What we try to do, within the quadratic approximation expressed by equation 3.19, is to adapt the down gradient of the current point x_i and the down gradient of the previous point. This requirement leads to:

$$H^{new} \Delta x = \Delta g \quad (3.24)$$

There are numerous methods for updating the Hessian matrix from H^{old} to H^{new} . Some examples of these methods are: the Murtagh-Sargent, the symmetrical Powell, the Davidson-Fletcher-Powell (DFP) and the Broyden-Fletcher-Goldfrab-Shanno (BFGS). The latter is generally considered the best method in the case of geometry minimizations, and can be written as:

$$H^{new} = H^{old} + \frac{\Delta g \Delta g^t}{\Delta x^t \Delta g} - H^{old} \frac{\Delta x \Delta x^t H^{old}}{\Delta x^t H^{old} \Delta x} \quad (3.25)$$

This type of update is symmetrical and positive and minimizes the change norm of the Hessian matrix. Similar formulas are also available for updating the inverse Hessian matrix. Quasi-Newton geometry optimization methods, and related approaches, are suitable for finding minima of small to medium-sized molecules.

For difficult cases, the Hessian can be recalculated either after a few steps or at each step, rather than updating. The latter case is equivalent to the Newton or Newton-Raphson algorithm. Once the Hessian has been updated, a Newton step is performed on the model quadratic surface as given by equation 3.23. For this step to be carried out in the direction that descends towards the minimum, the Hessian must be positive, that is, all the eigenvalues must be positive. The positive character can be controlled and possibly forced, for example by diagonalizing the Hessian matrix and then changing the sign of the negative auto-values.

Some important considerations have to be taken into account. First of all, if the structure is far from the minimum (e.g. the gradients are still large) or if the potential energy surface is very flat (one or more small Hessian eigenvalues), then a simple Newton step can or be too long and bring the molecule to a region where the quadratic model is no longer valid. In these cases, it is advisable to take a shorter

step. For example, it is possible to limit the length of the step so as not to exceed a value τ considered reliable (trust radius). At the end of each optimization step there is a test to check the convergence. Checking the difference in energy between one step and the next is not very effective because the energy changes little near the minimum. The examination of the gradient (magnitude, RMS, and/or value of the maximum component) is a more reliable test for convergence. It can also control over the expected geometry change (displacements) may be necessary, since for fairly flat surfaces the displacements can still be large even if the gradient is already small.

3.5.2 The problem of the global minimum and characterization of the PES

When minimizing the geometry, given a starting structure, it is possible to locate only the closest minimum which is usually a local minimum. For a one-dimensional PES with two minima, as shown in Figure 3.3, we see that if we start from point A the gradient-based methods will take us to the closest minimum, a local minimum, while starting from the point indicated with B we will arrive at the minimum global (asterisk).

It is clear that for multi-dimensional cases like those typical of a relatively small molecule, the potential energy surface will be extremely complex and its exploration difficult. The localization of the different minima on the PES is also called conformational search.

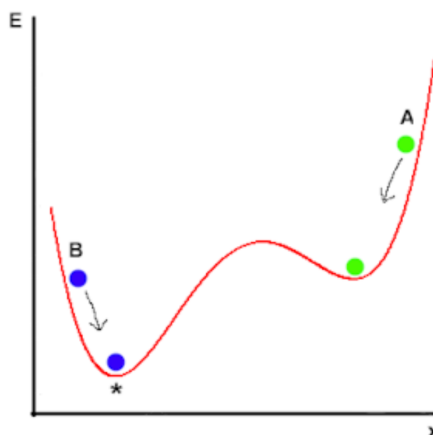


Figure 3.3. One-dimensional potential energy surface with two minima.

After the geometry optimization has reached convergence, it should be checked that the structure obtained corresponds to a true minimum. Since the optimizations tend to preserve the starting symmetry, because the gradients belong to the total-symmetric representation, it is not to be excluded that a neighboring structure with lower energy or with lower symmetry could exist. This can be checked by calculating the complete matrix of the second derivatives (the Hessian used for optimization is not sufficient as it normally does not contain any information relating to distortions with lower symmetry).

At this point, for the structure obtained to correspond to a minimum, all the eigenvalues must be positive. The characterization and classification of the stationary points of the PES therefore requires the exact calculation of the Hessian and its eigenvalues/eigenvectors. This is an expensive procedure, but within the quadratic (harmonic) approximation of the PES, i.e. a Taylor expansion truncated to the second order, the Hessian matrix corresponds to the matrix of harmonic force constants and beyond to mathematical information it also has an important chemical-physical significance.

At the stationary point, the diagonalization of the force constants matrix, weighted by the atomic masses, produces eigenvalues that are related to the harmonic vibrational frequencies and eigenvectors corresponding to the normal modes of vibration of the molecule. If all frequencies are real (positive eigenvalues) the structure is a minimum, if instead there is one and only one imaginary frequency (negative eigenvalue) the structure is a transition state.

In this case, the eigenvector represents the descending direction leading towards a minimum (products or reactants). The reaction path expressed in weighted coordinates for the masses is called the intrinsic reaction coordinate (IRC) and the path with the lowest energy is indicated as the minimum energy path (MEP).

3.5.3 Vibrational frequencies: how to calculate them

The vibrational frequencies of a molecule (N atoms) are calculated as follows:

- A geometry optimization is performed to search for a stationary point, possibly a minimum;
- Given the optimized structure, the second derivatives of energy are calculated with respect to the $3N$ Cartesian nuclear coordinates, with the origin in the center of mass;
- We construct the matrix of the weighted force constants for the atomic masses (mass-weighted force-constant matrix), W , whose elements are given by:

$$W_{ij} = \frac{1}{\sqrt{m_i m_j}} \frac{\delta^2 E}{\delta x_i \delta x_j} = \frac{1}{\sqrt{m_i m_j}} H_{ij} \quad (3.26)$$

Where i and j go from 1 to $3N$ and m is the mass of the atom with coordinates x and y .

- The eigenvalues and eigenvectors of the matrix \mathbf{W} are determined by solving the matrix equation:

$$\mathbf{W}\mathbf{L} = \mathbf{L}\mathbf{\Lambda} \quad (3.27)$$

Where \mathbf{L} is the eigenvector matrix and $\mathbf{\Lambda}$ is the eigenvalue vector λ_k . Therefore, the eigenvector λ_k corresponds to the eigenvalue L^k .

The whole procedure can also be seen as a transition from Cartesian coordinates to weighted coordinates for the masses, followed by a unitary transformation into a new coordinate system, represented by the normal modes of vibration, which make the \mathbf{W} matrix diagonal. It is important to note that the force constants matrix can be computed for any geometry but the transformation into normal coordinates is valid only in a stationary point, where the first derivatives vanish. Of the $3N$ eigenvalues, 6 are null and correspond to degrees of translational and rotational freedoms, the remaining $3N-6$ eigenvalues correspond to the vibrational degrees of freedom and are related to the vibrational frequencies by:

$$v_k = \frac{\lambda_k^{1/2}}{2\pi} \quad (3.28)$$

From the vibrational frequencies it is possible to derive, in the quantum case, the zero-point energy:

$$E_{ZPE} = \frac{1}{2} \sum_{k=1}^{3N-6} h\nu_k \quad (3.29)$$

It has to be said that the calculated values can also be very different from the experimental ones. In general, the effect of anharmonicity is more significant when light atoms such as hydrogen. In the specific case of water, the differences can reach almost 200cm^{-1} . The anharmonic effects can be estimated a posteriori with perturbative techniques.

3.6 ORCA

In this section will be given an insight on the tool ORCA, which has been useful in this work for the geometrical optimization.

ORCA is an ab initio quantum chemistry program package that contains modern electronic structure methods. The free version is available only for academic use at universities and the different geometries may be generated with Avogadro or other tools.

First of all, I will resume some hints made in the previous sections, in order to easily focus on the objective of this thesis.

3.6.1 Hartree-Fock method and basis set

In general, a molecule is a system composed by atoms. It has to be said that each atom is composed by:

- N_N Nuclei, composed by neutrons and protons;
- N_e Electrons.

Moreover, a molecule can be studied with Quantum Mechanics as a system of a set of N_N positive nuclei and a set of N_e electrons, respectively position $R_i = \{X_i, Y_i, Z_i\}$, charge Q_i e and position $r_i = \{x_i, y_i, z_i\}$, charge -e. The Quantum Mechanical Problem can be written as:

$$\hat{H}\Psi = E\Psi \quad (3.30)$$

Where:

- Ψ is the so-called molecular Wavefunction.

$$\Psi = \Psi\{R, r\} = \Psi\{X_1, Y_1, Z_1, \dots, X_{N_N}, Y_{N_N}, Z_{N_N}, x_1, y_1, z_1, \dots, x_{N_e}, y_{N_e}, z_{N_e}\} \quad (3.31)$$

$|\Psi\{R, r\}|^2$ is the probability of finding the molecule in a precise status where the nuclei and the electrons have coordinates R and r respectively.

- \hat{H} is the so-called molecular Hamiltonian.

$$\hat{H} = \hat{T}_N + \hat{T}_e + \hat{V}_{N_N} + \hat{V}_{N_e} + \hat{V}_{e_e} \quad (3.32)$$

Where $\hat{T}_N + \hat{T}_e$ is the kinetic contribution for nuclei and electrons, whereas $\hat{V}_{N_N} + \hat{V}_{N_e} + \hat{V}_{e_e}$ are the potential energies associated to nuclei-nuclei, nuclei-electrons and electrons-electrons interactions.

Proton mass is $1,67 \times 10^{-27}$ Kg, electron mass is $9,31 \times 10^{-31}$ Kg . The kinetic energy of nuclei is negligible and we can imagine the electrons moving in an average potential generated by nuclei. This translates in an equivalent QM problem related to the electron only:

$$[\hat{T}_e + \hat{V}_{N_e} + \hat{V}_{e_e}]\Psi_{el}(R, r) = E\Psi_{el}(R, r) \quad (3.33)$$

The nuclei are considered frozen, the electron wavefunction Ψ_{el} still depends on nuclear coordinates, but not on the nuclear velocities. $|\Psi_{el}(R, r)|^2$ probability of finding the electrons in a precise position r considering the nuclei in frozen coordinates R .

Furthermore, as announced before, the electrons feel the nuclei potential, in general, we can define the so-called Potential Energy Surface, which describes the energy of the molecule as a function of nuclei coordinates.

Then, each electron has lies in a molecular orbital. One idea is to write the electron wavefunction as a combination of molecular orbital wavefunction.

$$\Psi_{el} = \prod_i \Psi_i(x, y, z) = \Psi_1(x_1, y_1, z_1) \cdot \dots \cdot \Psi_{N_e}(x_{N_e}, y_{N_e}, z_{N_e}) \quad (3.34)$$

This is the most trivial way, but it does not consider anti-symmetry principle. A second possibility is the Slater-Determinant, that is for 2 electrons:

$$\Psi_{el} = \Psi_1(x_1, y_1, z_1) \cdot \Psi_2(x_1, y_1, z_1) - \Psi_2(x_2, y_2, z_2) \cdot \Psi_1(x_2, y_2, z_2) \quad (3.35)$$

In order to solve the QM problem, it is necessary to exploit two principles.

- The LCAO (Linear Combination of Atomic Orbitals)

$$\Psi_{MO}(x, y, z) = \sum_{i=1}^N c_i \Psi_{AO,i}(x, y, z) \quad (3.36)$$

- The variational principle

$$E = \frac{\int \Psi_{el} \widehat{H}_{el} \Psi_{el}^* dV}{\int \Psi_{el} \Psi_{el}^* dV} \quad (3.37)$$

Quantum Chemistry tools have to find the set of c_i minimizing the energy. This is the so-called Hartree Fock method.

$$\Psi_{MO}(x, y, z) = \sum_{i=1}^{N_e} c_i \Psi_{AO,i}(x - X_i, y - Y_i, z - Z_i) \quad (3.38)$$

The physical best motivated orbital is the so-called Slater-Type Orbital (STO), which is a solution of the Schroedinger equation. Even though they are computationally difficult to treat. For this reason, the atomic orbital of atom is generally expressed as a sum of gaussian functions:

$$\Psi_{AO,i}(x, y, z) = \sum_{j=1}^{N_e} k_j G_j(x, y, z) \quad (3.39)$$

Where G is a Gaussian Type Orbital (GTO). The idea is to fit the STO orbital with a set n of GTO orbitals.

STO-nG basis set, that is, n Gaussian functions fitting for the STO orbital: STO-3G, STO-4G, STO-5G, STO-nG. In figure 3.4 is given a practical example.

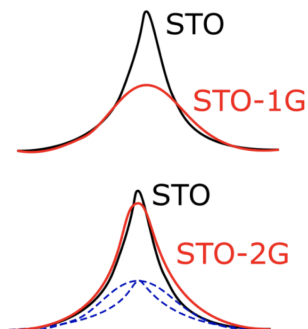


Figure 3.4. STO-nG basis set, that is, n Gaussian functions fitting for the STO orbital.

It is important to say that in some cases, also polarization functions can be used. Indeed, the electrons can move from their standard orbital as a response to polarization, for instance, in the Hydrogen atom, we can add a p orbital (generally not occupied) and mix it with an s orbital, thus allowing the electron to create a polarization. A second important set of functions is the set of diffuse functions, that are, GTOs with small exponent used to describe the regions far from nuclei.

It is important to notice that the most important orbitals playing a relevant role in the chemical reactions are the valence orbitals, therefore it makes no sense to express all the orbitals with the same number of GTOs. Here come the Split-valence Basis sets which are typically expressed with the notation

$$X - YZg \quad (3.40)$$

Where: X STOs are used for the core orbitals and the valence orbitals are represented with two atomic orbitals, one with Y GTOs, the second with Z GTOs.

3.6.2 Density Functional Theory (DFT)

As previously announced, the Hartree-Fock method consist in 5 main steps: position of the nuclei and elements, basis set, Hamiltonian operator, wavefunction and observable (Energy, Polarization, Electron Density,...). This is a very complex procedure.

An alternative approach to the Hartree-Fock method is the Density Functional Theory (DFT). The electron density is defined as:

$$\rho(r) = \int \dots \int |\psi(r_1, r_2, r_3, \dots, r_{N_e})|^2 dr_1 dr_2 \dots dr_{N_e} \quad (3.41)$$

The energy of the molecule can be written as a function of the electron density:

$$E = E[\rho(r)] \quad (3.42)$$

Mathematically, we have two contributions

$$E = E'[\rho] + \text{Functional} \quad (3.43)$$

Where $E'[\rho]$ is a closed-form equation describing the energy-density relation (for a set of N_e non-interacting electrons). N_e is a second term (functional, partially empirical) enabling taking into account the terms which are not (yet) included in the relationship.

3.7 The structure: choices

As said in the Theory Section 2.5.2, foreign atoms can be introduced into fullerene cages; these electric charge or magnetic centres can strengthen superconductivity [8]. In addition, cage size has also been shown to have a physical effect [8].

For example, C82 has a deformed cage with lower symmetry than C60, and X@C82 species (X = La, Gd, Tb, Dy, Ho, Er) have been studied as small and stable memory storage units. In particular, Ce@C82 has even demonstrated hysteresis in transport characteristics attributed to nanomechanical rearrangement [8].

Such efforts lead to interest in molecules with non-superimposable charge centres and structural centres, which may form stabilized electric dipoles in the molecule, exhibiting ferroelectric characteristics without long-range dipole ordering [8]. This would then realize the long-sought single-molecule electret (SME).

The purpose of this section is to summarize the logical steps that are suggested to discuss the structure, design and performances of a Gd@C82 SME. In this optics, it is a brief introduction to set the very practical part of the work, in order to easily move then in the simulations part (section 4).

3.7.1 The cage

As previously stated, writing in Nature Nanotechnology, Zhang et al. report an endohedral metallofullerene (Gd@C82) single-molecule electret device, demonstrating its non-volatile memory capabilities [4].

SME behaviours can be observed in a molecule containing an internal cavity, in which a trapped ion shuttles between two or more energetically stable sites. The direction of the electric polarization switches with the ion position [4].

At a temperature range where the thermal energy is adequately lower than the energy barrier between the stable ion sites, suppression of ionic inter-site movement occurs, thereby resulting in semi-permanent molecular polarization. However, applying an electric field to the SME within this temperature range can alter individual ion site energy, thus inducing inter-site ion transfer with polarization reversal [4].

Consequently, SMEs exhibit ferroelectric characteristics (for example, polarization hysteresis and spontaneous polarization), without long-range dipole ordering. In addition, Zhang et al. reveal the SME nature of the Gd@C82 molecule by indicating the existence of two Gd stable sites inside C82 through theoretical calculations and observing the dielectric relaxation process between them [4]. Finally, the authors fabricate a single-molecule transistor comprising a Gd@C82 molecule in the nanogap between a pair of Au electrodes. They create the nanogap through a feedback-controlled electromigration-break-junction method [4].

It has to be said that Zhang et al. attribute the SME behaviour to the manipulation of Gd sites within the C82 cage.

An interesting observation is that the behaviour of single-electron transport in Gd@C82 varies depending on the location of the Gd ion because the two stable Gd@C82 sites are non-equivalent [4].

This asymmetry is central to the employment of Gd@C82 molecules as memory elements. In particular, information can be stored as the Gd ion position is adjusted by the gate voltage, while the known position of the Gd ion, obtained from I_{DS} measurements, can be read as stored information. This two-state behaviour is highly reproducible and stable for over a month [4].

The switching between the two non-equivalent molecular polarization states can modify the physical properties and electronic states of the molecule; thus, this mechanism will be useful for the development of new types of single-molecule memory devices that combine external light and magnetic fields [4].

Additionally, because an asymmetric energy structure is easier to design with SMEs than SMMs, SMEs possess an intrinsic advantage as memory elements. Although the commercialization of single-molecule devices presents various limitations, such as chip-scale integration, the work of Zhang et al. provides an important demonstration for future non-volatile memories based on electrets [4].

Coming back to the present work, for all these reasons, I have decided to employ

the C82 cage, but the wanted behaviour could be expected also with other cages that provide an asymmetry on the structure, since information can be stored as the encapsulated ion position is adjusted by the gate voltage and the known position of the Gd ion can be read as stored information.

ATK tool provides different possible cages of C82, in figure 3.5 are shown four possible configurations and in figure 3.6 the one that I have chosen (the most similar to the one used in the papers found in literature). It has to be said that they all satisfy the isolated pentagon rule (IPR).

The isolated pentagon rule (IPR) is a general rule for determining the stability of all-carbon fullerene cages composed of hexagons and pentagons. Fullerenes that violate this rule have been deemed too reactive to be synthesized [35].

The stabilization of non-IPR endohedral fullerenes depends on charge transfer from the encapsulated metal clusters (endoclusters) to fullerene cages, the electronic properties of empty all-carbon cages, the matching size and geometries of fullerene and endocluster, as well as the strong coordination of the metal ions to fused pentagons [35].

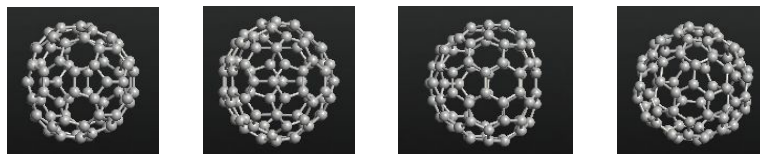


Figure 3.5. Some of the C82 fullerene provided by ATK tool, from left: named No.2 (82 atoms, symmetry group C_s), named No.4 (82 atoms, symmetry group C_s), named No.7 (82 atoms, symmetry group C_{3v}) and named No.8 (82 atoms, symmetry group C_{3v}).

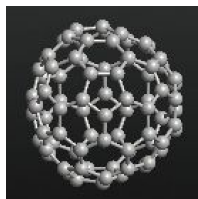


Figure 3.6. The C82 cage chosen. In the tool it is named No.5 (82 atoms, symmetry group C_2).

3.7.2 The encapsulated atom

Secondly, the molecule that should be encapsulated in the cage should be selected. In the recent years, different species encapsulated in C82 cage have been studied as small and stable memory storage units, the most famous ones are Lanthanum (La), Gadolinium (Gd), Terbium (Tb), Dysprosium (Dy), Holmium (Ho) and Erbium (Er). I have decided to use the Gadolinium since it is one of the most discussed in literature. Hereafter I will give some general information on it.

Gadolinium

Gadolinium is a soft, shiny, ductile, silvery metal belonging to the lanthanide group of the periodic chart. The metal does not tarnish in dry air but an oxide film forms in moist air. Gadolinium reacts slowly with water and dissolves in acids. It becomes superconductive below 1083 K. It is strongly magnetic at room temperature [36].

Moreover, it has a lot of uses, in fact it has found some use in control rods for nuclear reactors and nuclear power plants; it is used to make garnets for microwave applications and its compounds are used for making phosphorous for colour TV tubes. Metallic gadolinium is rarely used as the metal itself, but its alloys are used to make magnets and electronic components such as recording heads for video recorders. It is also used for manufacturing compact disks and computer memory [36].

Gadolinium is one of the more abundant rare-earth elements. It is never found as free element in nature, but it is contained in many rare minerals. The main mining areas are Cina, USA, Brazil, Sri Lanka, India and Australia with reserves expected to exceed one million tonnes. World production of pure gadolinium is about 400 tonnes per year [36].

Encapsulation: where?

After the choice of the encapsulated specie, it is important to understand where to place the Gadolinium inside the C82 cage. The authors of [4], as explained in section 2.5.1, found two configurations significantly more stable than the others, so I have decided to replicate both of them taking into account the information given in the additional paper of their research. In particular, as you can easily see in figure 3.7, I have selected the two faces referring to the subfigures I and IV of image 2.9 of the paper, and then I have placed the Gd atom inside the cage referring to the distances given by the table 2.1. In particular for the configuration I, the Gd atom is placed at a distance of 2.45 Å from the selected face and for the IV configuration the Gd atom is placed at a distance of 2.34 Å from the respective selected face of the cage. The two configurations correspond to the one of the paper found in

literature, it has to be said that the coordinate system provided from atk has the z direction corresponding to the x of the one of the paper (and viceversa).

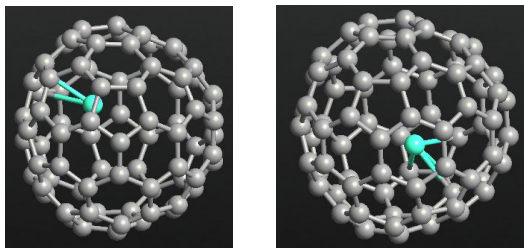


Figure 3.7. On the left it is shown the configuration I, on the right configuration IV. The C82 cage is represented in grey, the Gd atom is light blue. The figure on the left follows the coordinate system reported in fig. 3.8, the other on the right has been rotated a bit in order to better see the position of the Gd atom.

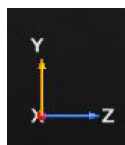


Figure 3.8. This is the coordinate system used with the atk tool. It is remarkable that the z of atk corresponds to the x in the images of the paper.

3.7.3 Electrodes and the final structure

Once the cage and the encapsulated atom are chosen, it should be chosen the device structure. In other words, two architectures are possible: a molecular wire, so a two-terminal device, or a molecular transistor, with one or more gates. Since the fabrication process is more complex and thus expensive for molecular transistors than for the wires, I have chosen to start with studying and testing a molecular wire. After that, when the wire is defined, it can be also added a gate. In this way it is possible to confirm an eventual improvement on the behaviour.

After that, the contact material and eventually the presence of anchoring groups should be selected. The anchoring groups by definition are functional groups aimed in anchoring the molecule to the contacts.

This point is very important since the contact-molecule interface strongly determines the quality and the regime of transport. As suggested in literature, I have chosen to employ no anchoring group and metal electrodes of gold (Au - with

orientation (111)). It has to be said that gold contact technology is already widely used and known for molecular junctions and it is demonstrated in literature that carbon is capable of forming strong covalent bonds with gold, consequently making an anchoring group superfluous.

Furthermore, the main parameter to be fixed in a molecular wire is the gap distance between the two electrodes and so the length between the contacts and the C82 molecule. In order to do that, it is useful to choose a distance that optimizes the sensitivity to the target. It has to be said that in the articles found in literature describing this experiment, there is no mention on the parameter they have fixed.

As it will be explained, I have started with a certain distance, but then I had to change in order to reach the wanted results (see later). In fact, the last chosen distance was the one corresponding to the covalent gold-carbon bond length. This corresponds to the equilibrium distance in case of chemisorption. It is important to note that the gold electrode has greater dimensions in relation to C82 cage, thus leading effectively to chemisorption.

By definition, chemisorption is a chemical adsorption process, caused by a reaction on an exposed surface, which creates an electronic bond between the surface and the adsorbate. During the chemical reaction, a distinct chemical species is created on the adsorbent surface, which causes the bond to be created [46]. This concept will be well explained in section 4.6.1.

In figure 3.9, you can see the three final structures, the one with the empty C82 cage and the others corresponding to the configuration I and IV. The device with the empty cage has been generated to study the differences of behaviour between the cage alone and with the presence of the Gd atom.

In addition to the geometrical choices, it is useful to verify if the molecular channel is sensitive to the target. This can be performed at equilibrium by confirming a change in the DOS or in the transmission spectrum. This will be treated in sections 4.5.1 and 4.5.2. It is remarkable that this analysis can be performed on the isolated C82 cage (or Gd@C82-I or IV) and so without the contacts, but it has to be said that the disadvantage of doing so, especially in single molecules channels, is that the influence of contacts on the final DOS can be significant and can modify a lot the wanted results.

For this reason I have chosen to perform a preliminary study on the equilibrium DOS and transmission spectrum of the entire device, considering so also the contacts.

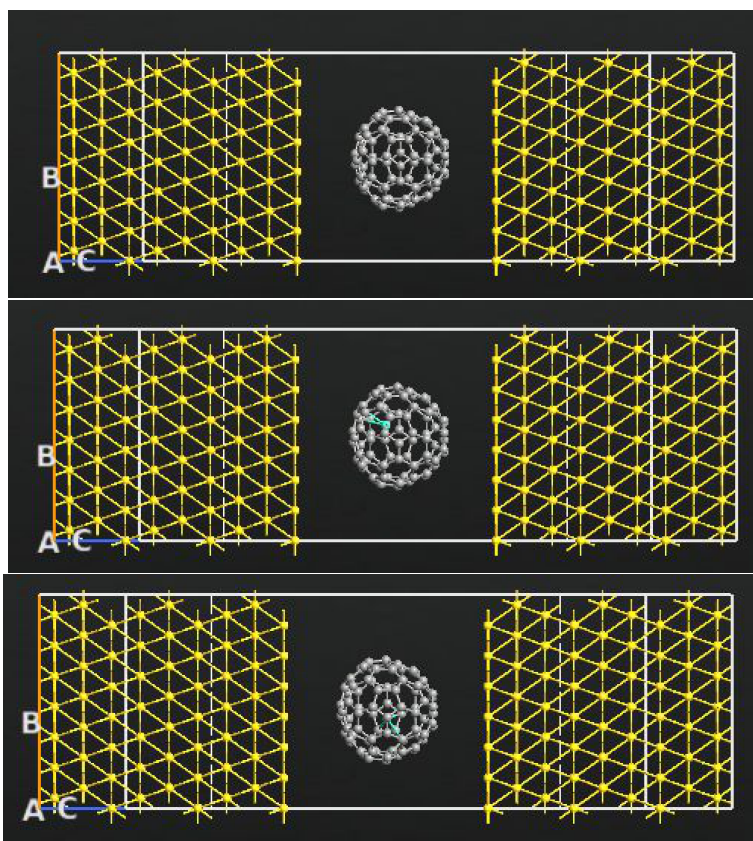


Figure 3.9. The final devices. In the first on the top you can see the one with the empty C82 cage, the second one exploits the I configuration and the third one the IV. In yellow are represented the gold electrodes.

3.8 Optimization results

After having realized the structure, I have proceeded by doing a geometrical optimization.

So after having extracted the file .xyz of the structures I have made on the ATK tool (Gd@C82-I and Gd@C82-IV), I have created the file to run on Orca (.inp).

In figure 3.10, you can see the choices made. As shown, I have given the following commands:

- *B97* Functional;
- *D3*: Grimme-D3 Corrections;

- Use *def2-TZVPP* Basis Set (Valence triple-zeta with two sets of polarization functions);
- *opt*: Optimize Geometry;
- *ChelPG*: Charge calculation
- *%output* section: Plot molecular orbitals and basis sets;
- *GdC82.xyz* is the file extracted from the geometry made in *atk*.

After some weeks and different tries, the simulation did not convert. For this reason I have decided to do some modifications, as you can see in figure 3.11.

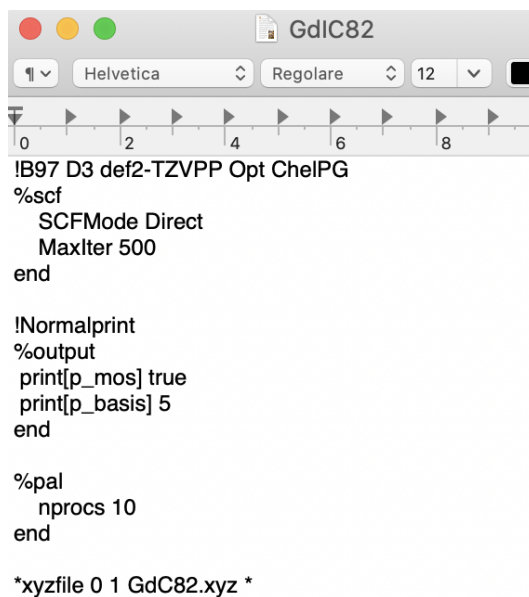
- *B97* Functional;
- *D3*: Grimme-D3 Corrections;
- Use *def2-SVP* Basis Set (Valence triple-zeta with two sets of polarization functions);
- *SlowConv*: Convergence facilitator;
- *ChelPG*: Charge calculation;

I have taken the simulation monitored very often. It has to be said that it has always given a good prospective of convergence since the energy change was very very small.

However, at the end of almost 36 days and 500 cycles, unfortunately, it could not reach any convergence. In figure 3.12 you can see the timing reported at the end of the output file, while in 3.14 it is possible to observe the values reached at the 499th iteration: the energy change was very small (about -0.00000088613).

It is interesting to know that at the end of the output file (.out), it was presented a warning (reported in figure 3.13), that states that the wavefunction did not converged yet, although there were given signs of convergence. It is a good point (and a good hint to insist with this method), however for time constraints I have decided to proceed with the geometries that I have made.

It has to be said that in the following chapter, the utilized structures are the one that I have made without any optimization, but I have tried to make them as reasonable as possible.



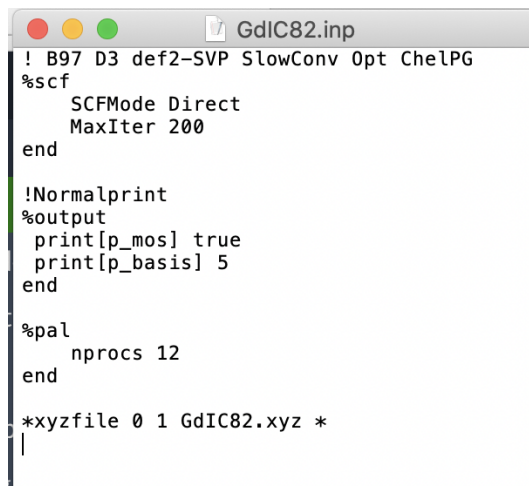
```
IB97 D3 def2-TZVPP Opt ChelPG
%scf
  SCFMode Direct
  MaxIter 500
end

!Normalprint
%output
print[p_mos] true
print[p_basis] 5
end

%pal
  nprocs 10
end

*xyzfile 0 1 GdC82.xyz *
```

Figure 3.10. Geometrical optimization, input file, structure Gd@C82-I: first try.



```
! B97 D3 def2-SVP SlowConv Opt ChelPG
%scf
  SCFMode Direct
  MaxIter 200
end

!Normalprint
%output
print[p_mos] true
print[p_basis] 5
end

%pal
  nprocs 12
end

*xyzfile 0 1 GdIC82.xyz *
```

Figure 3.11. Geometrical optimization, input file, structure Gd@C82-I: second try.

```

-----
TIMINGS
-----
Total SCF time: 35 days 12 hours 17 min 14 sec

Total time      .... 3068234.460 sec
Sum of individual times  .... 3067835.479 sec (100.0%)

Fock matrix formation  .... 3044929.731 sec ( 99.2%)
XC integration         .... 4962.582 sec (  0.2% of F)
Basis function eval.  .... 357.411 sec (  7.2% of XC)
Density eval.         .... 1488.167 sec ( 28.4% of XC)
XC-Functional eval.   .... 23.857 sec (  0.5% of XC)
XC-Potential eval.    .... 777.308 sec ( 15.7% of XC)
Diagonalization       .... 19482.739 sec (  0.6%)
Density matrix formation  .... 319.477 sec (  0.0%)
Population analysis    .... 0.000 sec (  0.0%)
Initial guess         .... 42.897 sec (  0.0%)
Orbital Transformation  .... 0.000 sec (  0.0%)
Orbital Orthonormalization  .... 0.000 sec (  0.0%)
DIIS solution         .... 3043.055 sec (  0.1%)
Grid generation       .... 17.579 sec (  0.0%)
Warning: (DFTVMD): Non-parameterized functional used for dispersion correction !
Warning: (D3BJ): Non-parameterized functional used for dispersion correction !

Please define all necessary parameters (s6, s8, a1, and a2) in the %method block!
[file orca_tools/Tool-Misc/qcdfvtdw.cpp, line 36139]: ERROR in DFT dispersion correction!

```

Figure 3.12. Screenshot of the timing at the end of the second try of geometrical optimization: it did not convert after 35 days and 500 cycles.

```

-----
WARNING
The wavefunction IS NOT YET CONVERGED! It shows however signs of
convergence. Therefore the wavefunction will be stored and can be
used as input for another calculation.
DO NOT USE THIS WAVEFUNCTION FOR ANYTHING ELSE. It is NOT RELIABLE
-----

```

Figure 3.13. A warning presented at the end of the output file: they wavefunction did not convert, but there are signs of convergence.

```

-----
!          ITERATION 499          !
-----
Total Energy      : -3890.102419799146 Eh
Energy Change     : -0.000000888613 Eh
MAX-DP           : 0.001237956643
RMS-DP           : 0.000010804779
Actual Damping    : 0.0000
Actual Level Shift : 0.0000 Eh
Int. Num. El.     : 527.99536245 (UP= 263.99768122 DN= 263.99768122)
Exch.+Correl.(+NL) : -399.85314162
DIIS-Error        : 0.000363570159
DIIS coefficients:
  0.07897  0.03886  0.01545  0.30034  0.57438

*****
*                      ERROR                      *
*          SCF NOT CONVERGED AFTER 500 CYCLES          *
*****

```

Figure 3.14. It has not been reached any convergence after 500 cycles. In the picture are shown the values of the 499th iteration.

Chapter 4

Results

4.1 Cage C82 and the two stable configurations

As anticipated in chapter 3, this master thesis work will focus on the analysis of three devices: the one that involves the empty C82 cage and the two different configurations previously called I and IV (please see section 3.7) that include the encapsulation of the Gd cluster inside the C82 cage in two different stable sites.

Hereafter I will expose the analysis computed on these structures and the results obtained, providing comments and also some hints of useful theory.

In the first part (4.2) I will consider the C82 molecule alone and with the encapsulated atom, without the electrodes. After that, I will study the entire structure with the electrodes (4.4).

4.2 Mulliken population

In order to understand this property, it is necessary to analyze a bit of theory. This theoretical part will be very useful also to understand the obtained results.

4.2.1 What is electronegativity

By definition, electronegativity is a measure of the tendency of an atom to attract a bonding pair of electrons [40].

The Pauling scale is the most commonly used. Fluorine (the most electronegative element) is assigned a value of 4.0, and values range down to caesium and francium which are the least electronegative at 0.7 [40].

It is interesting to know that if we consider a bond between two atoms, A and B with equal electronegativity, each atom may be forming other bonds [40]. In addition, if the atoms are equally electronegative, both have the same tendency to attract the bonding pair of electrons, and so it will be found on average half way between the two atoms [40]. To get a bond like this, A and B would usually have to be the same atom. It is possible to find this sort of bond in, for example, H_2 or Cl_2 molecules [40].

This type of bond could be thought of as being a *pure* covalent bond, where the electrons are shared evenly between the two atoms [40].

On the other hand, if B is slightly more electronegative than A, it will attract the electron pair rather more than A does. That means that the B end of the bond has more than its fair share of electron density and so becomes slightly negative [40]. At the same time, the A end (rather short of electrons) becomes slightly positive.

Moreover, if B is a lot more electronegative than A, the electron pair is dragged right over to B's end of the bond. To all intents and purposes, A has lost control of its electron, and B has complete control over both electrons. Indeed Ions have been formed [40].

4.2.2 Mulliken Electronegativity

A method for estimating electronegativity was developed by Robert Mulliken (1896-1986; Nobel Prize in Chemistry 1966) who noticed that elements with large first ionization energies tend to have very negative electron affinities and gain electrons in chemical reactions [41].

It has to be said that the energy needed to remove one or more electrons from a neutral atom to form a positively charged ion is a physical property that influences the chemical behavior of the atom [42]. By definition, the first ionization energy of an element is the energy needed to remove the outermost, or highest energy, electron from a neutral atom in the gas phase [42].

Furthermore, the electron affinity is defined as the change in energy (in kJ/mole) of a neutral atom (in the gaseous phase) when an electron is added to the atom to form a negative ion. In other words, the neutral atom's likelihood of gaining an electron [43]. Conversely, elements with small first ionization energies tend to have slightly negative (or even positive) electron affinities and lose electrons in chemical reactions [41].

Mulliken recognized that an atom's tendency to gain or lose electrons could

therefore be described quantitatively by the average of the values of its first ionization energy and the absolute value of its electron affinity [41].

Robert S. Mulliken proposed that the arithmetic mean of the first ionization energy (E_{I1}) and the electron affinity (E_{ea}) should be a measure of the tendency of an atom to attract electrons [41]. It can be said that this definition is not dependent on an arbitrary relative scale, it has also been called *absolute electronegativity*. Using the definition of electron affinity, it is possible to write Mulliken’s original expression for electronegativity as in equation 4.1 [41]. As known from Maths, the magnitude of a quantity is a positive number. But it has to be said that this definition of electron affinity, for most elements, produces negative values for the electron affinity. This is why vertical lines indicating absolute value are needed in Equation 4.1 to make sure that we are adding two positive numbers in the numerator [41].

$$\chi = \frac{|E_{I1} - E_{ea}|}{2} \quad (4.1)$$

In a more practical way:

- Elements with a large first ionization energy and a very negative electron affinity have a large positive value in the numerator of Equation 4.1, so their electronegativity is high [41];
- Elements with a small first ionization energy and a small electron affinity have a small positive value for the numerator in Equation 4.1, so they have a low electronegativity [41].

Finally it is remarkable that the Mulliken electronegativity can only be calculated for an element for which the electron affinity is known. The Mulliken electronegativity of an atom is sometimes said to be the negative of the chemical potential [41]. To be more precise, from [41] it is observed that by inserting the energetic definitions of the ionization potential and electron affinity into the Mulliken electronegativity, it is possible to show that the Mulliken chemical potential is a finite difference approximation of the electronic energy with respect to the number of electrons [41]:

$$\mu_{Mulliken} = -\chi_{Mulliken} = -\frac{|E_{I1} - E_{ea}|}{2} \quad (4.2)$$

4.2.3 Mulliken Populations analysis

Mulliken population analysis is historically the most important method for calculating atomic charges [44]. The Mulliken populations method allows to evaluate the partial atomic charges from calculations made through computational methods

[44]. The concept of atomic charge is used by chemists to explain the chemical behavior of a species. It considers a fictitious charge that is attributed to each atom present in a molecule considering the bonding electrons delocalized in the vicinity of the more electronegative atoms that make up the molecule itself [44].

It has to be declared that in reality, the atomic charge is not a measurable physical quantity. This is due to the fact that the electrons have a diffuse charge distribution that can be arbitrarily assigned to one of the atomic centers. Therefore, different methods have been developed to calculate the atomic charge starting from wave functions, including that of the Mulliken populations [44].

With this method it is possible to characterize the electric charge distribution in a molecule and the nature of the bonding, antibonding and non-bonding molecular orbitals [44].

In order to be more correct, it has to be said that molecular orbital theory is involved with the combination of atomic orbitals to form new molecular orbitals. These new orbitals happen from the linear combination of atomic orbitals to form bonding and antibonding orbitals [45]. The bonding orbitals are at a lower energy than the antibonding orbitals, so they are the first to bridge. By computing the molecular orbitals, it is easy to calculate the order of the bond [45].

It is remarkable that electrons that spend most of their time between the nuclei of two atoms are placed into the bonding orbitals. Therefore, electrons that spend most of their time outside the nuclei of two atoms are placed into antibonding orbitals [45]. This is because there is an increasing in electron density between the nuclei in bonding orbitals, and a decreasing in electron density in antibonding orbitals. In addition, placing an electron in the bonding orbital stabilizes the molecule because it is in between the two nuclei [45].

Instead, placing electrons into the antibonding orbitals will decrease the stability of the molecule. Electrons will fill according to the energy levels of the orbitals. In other words, they will first fill the lower energy orbitals, and then they will fill the higher energy orbitals [45]. If a bond order of zero is obtained, that means that the molecule is too unstable and so it will not exist [45].

If we consider a normalized molecular orbital consisting of two atomic orbitals which are also normalized we have [44]:

$$\Psi_i = c_{ij}\varphi_j + c_{ik}\varphi_k \quad (4.3)$$

Afterwards, the charge distribution is described as density probability from the square of the wave function [44]:

$$\Psi_i^2 = c_{ij}^2\varphi_j^2 + c_{ik}^2\varphi_k^2 + 2c_{ij}\varphi_j c_{ik}\varphi_k \quad (4.4)$$

Proceeding with mathematical tricks and so integrating on all the electronic coordinates, taking into account that both the molecular orbitals and the atomic orbitals are normalized, we have [44]:

$$1 = c_{ij}^2 + c_{ik}^2 + 2c_{ij}c_{ik}S_{jk} \quad (4.5)$$

where S_{jk} is the superposition integral of the two atomic orbitals [44].

Finally, Mulliken's interpretation of this result is that an electron present in a molecular orbital φ_t provides [44]:

- c_{ij}^2 to the electronic charge in the atomic orbital φ_j [44];
- c_{ik}^2 to the electron charge in the atomic orbital φ_k [44];
- $2c_{ij}c_{ik}S_{jk}$ to the electron charge in the superposition region of the two atomic orbitals [44].

Therefore, the terms c_{ij}^2 and c_{ik}^2 represent the population of the atomic orbitals and $2c_{ij}c_{ik}S_{jk}$ the population of the superposition orbital [44]. Moreover, the population of the overlap orbital is greater than zero for a bonding molecular orbital, less than zero for an antibonding molecular orbital and equal to zero for a non-bonding orbital [44].

These populations can be listed in a matrix form for each molecular orbital [44]. It has to be considered that if there are two electrons in a molecular orbital then the populations must be doubled. Each column and each row of the matrix correspond to an atomic orbital and the elements of the diagonal provide the populations of the atomic orbital [44]. The elements not belonging to the diagonal provide the overlapping populations. The population matrix P_i is the following:

$$\begin{array}{cc} c_{ij}^2 & 2c_{ij}c_{ik}S_{jk} \\ 2c_{ij}c_{ik}S_{jk} & 2c_{ik}^2 \end{array}$$

Table 4.1. The population matrix.

Therefore, to be more precise, since there is a population matrix for each molecular orbital it is better to use a matrix that takes into account the net population so that there are a lower number of data. This matrix is given by the sum of all the population metrics for the occupied orbitals [44]:

$$NP = \sum_{i=occupied} P_i \quad (4.6)$$

By definition, the net population matrix gives the populations of the atomic orbitals and the populations of the overlapping orbitals resulting from all electrons

in all molecular orbitals [44]. Moreover, the elements of the diagonal provide the total charge in each atomic orbital and the elements outside the diagonal provide the total population of overlap that characterizes the total contribution of the two atomic orbitals to the bond present between the two atoms [44].

4.2.4 Settings

In order to study this property, I have considered separately the three main cases: C82 cage alone and the two stable cases of Gd@C82 (I and IV) mentioned in the previous chapters.

With the purpose to proceed in a meaningful way, I have used these setting that I will expose below, please refer to figs. 4.1, 4.2, 4.3, 4.4 and 4.5. Hereafter I will mention the case of the empty cage, but the same settings have been used also in the other two cases.

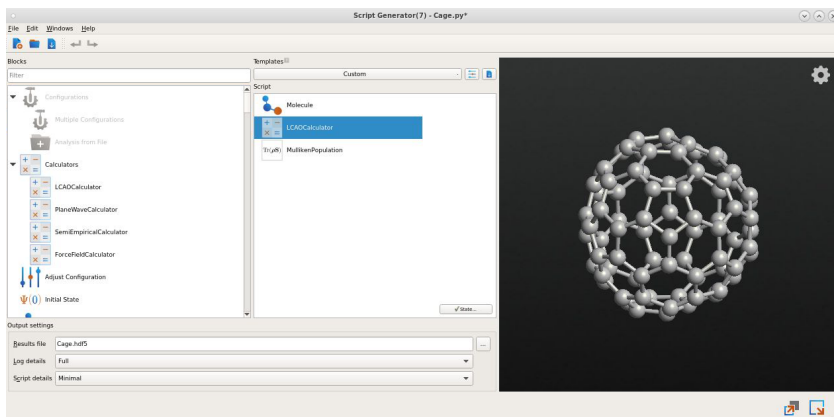


Figure 4.1. Script generator: molecule on the right and the selected simulations.

After having selected the wanted analysis as shown in fig. 4.1, I have proceeded with the related settings. As you can see from figure 4.2, the first thing to decide is the exchange correlation functional, in other words how accurate to represent the electron-electron interaction.

There are different classes of functionals and it has to be said that the most important aspect is understand their dissimilar level of approximation. In this way it is possible to choose the most suitable for the wanted application, and decide if it is necessary to use a more precise one depending on the structure to simulate. The possible choices are [47]:

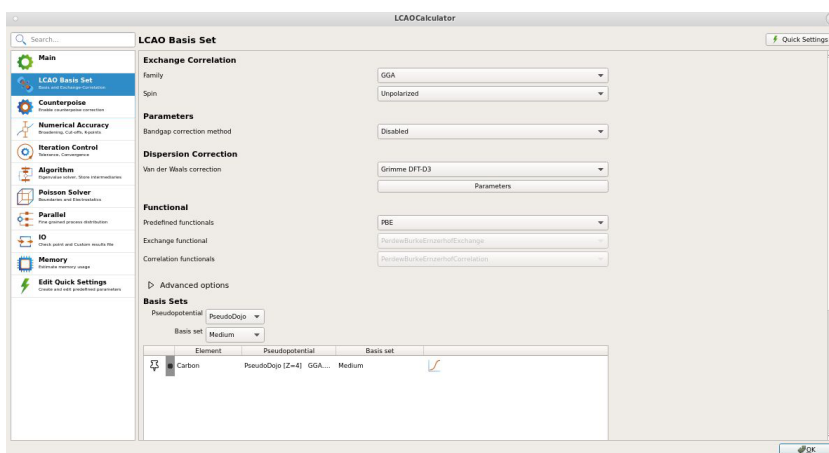


Figure 4.2. LCAO calculator: basis sets.

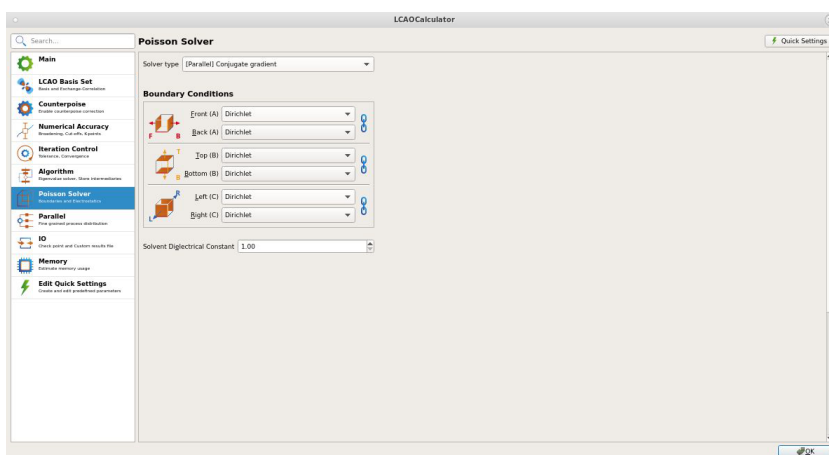


Figure 4.3. LCAO calculator: Poisson solver.

- LDA (Local Density Approximation): the electron density is assumed to be gradually varying, so the exchange-correlation energy can be obtained using formulae derived for an equal electron density. Its direct improvement is given by LSDA (Local Spin Density Approximation).
- GGA (Generalized Gradient Approximation): the exchange-correlation functional dependent not only on the electron density but also on its derivatives.

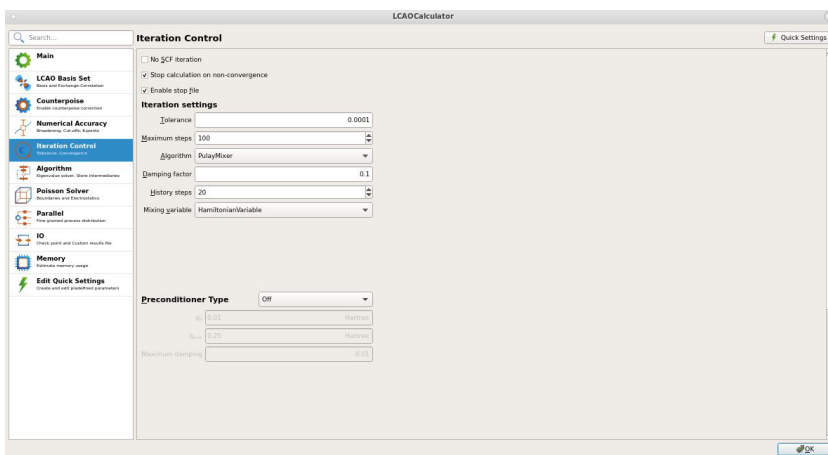


Figure 4.4. LCAO calculator: iterations.

- Meta-GGA: extension of GGA so that the exchange and correlation functionals depend on higher order derivatives of the electron density.
- Generalized RPA (Generalized Random Phase methods): consider also virtual molecular orbitals.

I have used the GGA one, selecting the corrections class Grimme-D3, which with Grimme-D2 is noted to be a practical tool to describe weak intermolecular interactions [48]. In addition, it is known to include also empirical methods to account for dispersive interactions in practical calculations within the DFT framework [48]. Moreover, the functional used is PBE and it is remarkable that functionals like it are derived entirely from theory (can be considered *ab initio*).

In ATK there are different methods for the solution of the Poisson's equation. As you can see from figure 4.3, I chose the *Conjugate Gradient*, which is a method for solving linear systems and solves the Poisson's equation in real space. Furthermore, it is very efficient for parallel computations.

Finally, it is known that Poisson's equation is a second-order differential equation. For this reason, in order to reach the solution it is necessary to set the boundary conditions. So, I have selected the Dirichlet boundary conditions which, by definition, force the solution to attain certain a priori prescribed values for a subset of the degrees of freedom in the model [49]. In more practical words, Dirichlet boundary conditions are used because they enable the potential to fluctuate and finally reach convergence.

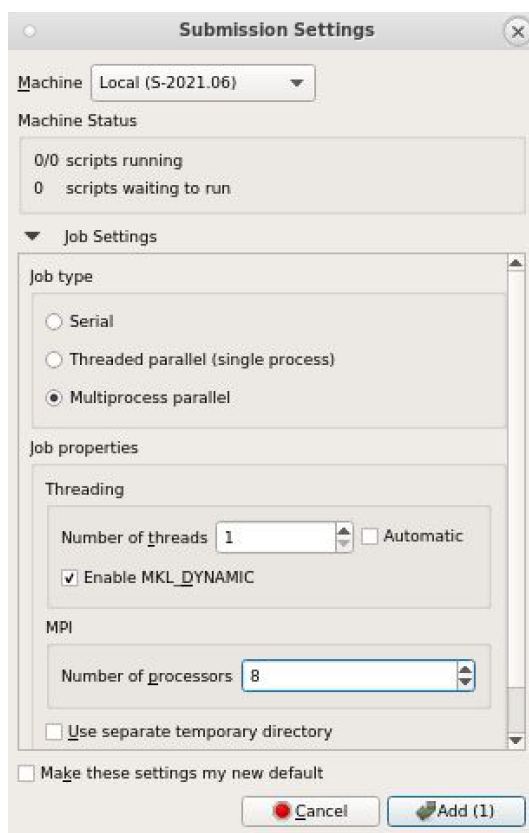


Figure 4.5. Final settings before running.

4.2.5 Results

From the obtained output files, it can be easily seen how the presence of the Gd atom perturb the C82 cage.

As previously announced, Mulliken understood that the propensity of an atom of gain/lose electrons can be described quantitatively by the average of the values of its first ionization energy and the absolute value of its electron affinity.

If we take a step back, it is known from literature that the introduction of metal atoms into the Fullerene cages cause an increase of the electron affinity with respect to the correspondent empty cages (as anticipated in section 2.3).

In fact, after having analyzed the results obtained by the converged Mulliken population analysis, it can be immediately noted that there is a remarkable difference in the outputs obtained with configuration I and IV respect to the configuration with the empty C82 cage.

As you can find the Appendix section, these output *Mulliken Population Reports* show the number that represents the Mulliken Population of each orbital, for each spin (for each shell, the spin-up populations are listed on the first line, spin-down on the second one) [39].

If for example, for simplicity, we consider the first Carbon atom (called θ) of each configuration, we find for the empty cage a value of 2.801, for the Gd@C82-I case 4.011 and for Gd@C82-IV case 4.008. With the encapsulation of the Gd atom we reach a value greater of the 43.2 %.

4.3 Molecular Energy Spectrum

Theoretical remarks

It is known that a quantum-mechanical system or an atom confined spatially (i.e. bounded) can carry on specified discrete values of energy. These values are defined as energy levels and usually refer to the energy levels of the electrons in the analyzed atoms. It has to be said that this does not happen in a general classical particle where instead can be reached any amount of energy.

To be more precise, in chemistry, a principal energy level (or electron shell) could be considered as the orbit of one (or more) electron around the nucleus of the atom. The closest one respect to the nucleus is called *First shell* and then there is the second one called again *Second shell* and so on. It is remarkable that all the shells coincide with the respective quantum numbers (i.e. $n=1, 2, 3, \dots$).

Every shell can hold a well defined amount of electrons. This number is given by a formula that says that the n^{th} shell can carry up to $2(n^2)$ electrons. For example, the *First shell* can contain 2 electrons, the *Second shell* can contain 8 electrons (i.e. $2+6=8$), the *Third shell* can contain 18 electrons (i.e. $2+6+10=18$) and so forth. It is important to know that the electrons are attracted to the nucleus and so the electrons of the atom will stay in outer shells just if the inner one is completed.

An interesting fact is that if an atom is at the lowest reachable energy level, it is defined as *at ground state*. On the other hand, if an atom is at the highest reachable energy level, it is defined as *excited*.

But what about molecules? It is known that, in a molecule, chemical bonds between atoms are built for stability objectives. In other words, the sum of the energy levels of the bounded atoms is lower than the one that could be reached without that bonding. To be more precise, the orbitals of separated atoms influence the energy levels of the other to give birth to *bonding* and *antibonding* molecular orbitals. In fact, if we consider bonding orbitals, their energy level is lower respect to the antibonding ones. Then, in order to let the molecule be stable, the electrons of the covalent bonding have to stay in the lower energy orbital.

To conclude, it is significant to recognize that, in an approximate but more practical point of view, the molecular energy state (which can be also named as the eigenstate of the molecular Hamiltonian) can be defined as the sum of different energies: electronic, nuclear, vibrational and rotational.

4.3.1 Molecular energy spectrum of the three cases

Coming back to the present work, it is necessary to say that there are many types of graphs that represent the energy levels.

In this thesis, it will be presented the one obtained from the simulation with the ATK tool. All the data have been then reworked and showed then in chapters 4.5.2, 4.7.2 and 4.9.2 (respectively for the first, second and third case; i.e. empty C82 cage, Gd@C82 - I and - IV) where they have been studied according to the Device Density of State of each structure (subsections 4.5.3, 4.7.3, 4.9.3, 4.6.5, 4.8.4 and 4.10.4).

4.4 The device

In the following section, I will consider the entire structure, which is composed by the C82 molecule and the Au electrodes. Also in this section I will study the three cases: the one with the empty C82 cage and the two different configurations I and IV.

4.4.1 A general overview

I have started considering the usage of LCAO with GGA family of exchange correlation and Grimme DFT-D3 for the dispersion correction, but it took very long. For example, for a Transmission Spectrum, it took more two months.

For this reason (time constraints) I could not proceed in this way and the possibilities where actually two: proceed with another method (less accurate, but faster) or change cage and molecule (considering a smaller cage, for example C28, the computational time would reduce a lot).

Since I was very curious to see what kind of results I would have obtained leaving the famous C82 cage, I have proceeded just changing method.

Moreover, in the first section, I will expose the settings used for the simulation, considering the same structure (the one with the empty C82 cage) but different computational methods. Then I have considered the results obtained by the EHT method, as regards the DFT ones I could not reach the results in these months. After that, I have continued the analysis of the structures (the other two configurations with the encapsulation of the Gd atom) using the less accurate method. In each Section (referring to the three different structures), I start exposing the results obtained with the first configuration and a certain "big" distance between the electrodes and the molecule (about 6.5 Å). After having analyzed the results, I have decided to move to a different configuration and so limitate that distance to a smaller one (see later).

Before going through the following section, it is important to underline that it is not always possible to use the wanted method or the one that is known to be the most accurate to represent the studied physics. In particular in these treated topics, the time constraints play a very important role since the simulation can last months. All the students generally start the work with some expectations and a very well defined program (in terms of time above all), but during the different steps they should be prepared to change method (maybe moving to one less accurate) or even change physics or chemistry. Anyway, if one must change the method using one not much accurate, it has to be recognized that the results could be reasonable but they not always represent the reality.

4.5 The empty C82 cage

In this section I will refer to the device reported in 4.6: empty cage C82 with the electrodes. The analysis will start with the Transmission Spectrum at equilibrium and the Device Density of state and then the IV characteristic. As previously announced, I have started my work considering a more accurate and precise method (LCAO calculator set with GGA family of exchange correlation and Grimme DFT-D3 for the dispersion correction), but due to time constraints I had to change moving to a less careful one (Semi-empirical calculator with the use of the extended Huckel parametrization).

Hereafter I will expose the setting used and the obtained results, also comparing the two methods.

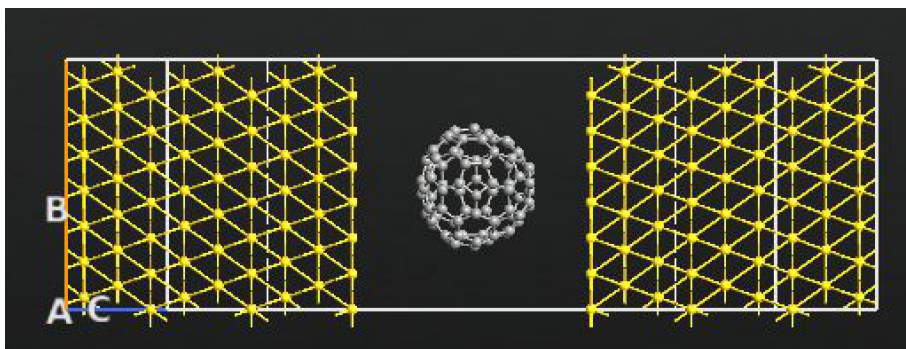


Figure 4.6. The first studied device: empty C82 cage and the electrodes.

4.5.1 Transmission spectrum at the equilibrium

As previously announced, the final Density of States and transmission spectrum can be influenced by the presence of the electrodes. Furthermore, considering the entire structure (also with the electrodes) the transmission spectrum can be obtained in a acceptable manner. Infact, without electrodes, it would not have sense talking about transmission.

Settings

DFT The choices made to set the LCAO calculator are the same used in section 4.2.4, so please refer to figs. 4.2, 4.3, 4.4 and 4.5.

Semi-empirical For the second used method, I have used the semi-empirical calculator, with the selection of the extended Huckel parametrization. The transmission spectrum analysis has been performed with the settings reported in tab. 4.2.

Range of energy	$E_0 = -13\text{eV}$, $E_1 = 13\text{eV}$, Points = 101
Sampling (k-points)	Sampling: $n_a = 3$, $n_b = 3$
Parameter of the zero Energy	Average Fermi level
Infinitesimal	1e-06 eV
Calculator of self-energy	Recursion

Table 4.2. Equilibrium transmission spectrum analysis settings.

Results and considerations

In figure 4.7 it is shown the obtained transmission spectrum of the first device in exam (i.e. C82 cage without the encapsulation of the Gd atom), obtained with the settings reported in 4.5.1.

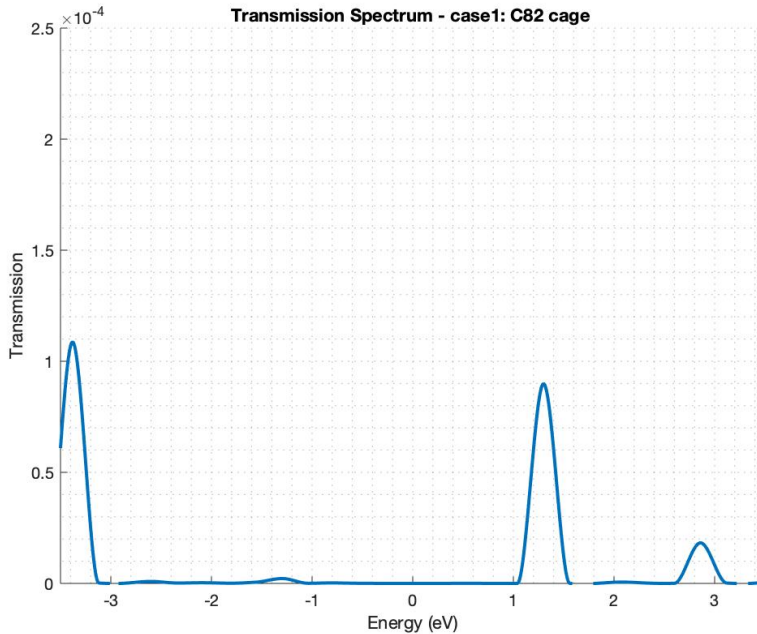


Figure 4.7. Transmission spectrum of the first device: empty C82 cage.

It can be easily seen that the transmission peaks are tight and imply a very low amount in terms of transmittivity. This is right since the coupling factor between the electrodes and the C82 molecule is small (we are in the case of weak coupling). It has to be said that this leads to the fact that the electrodes inject in the channel not a lot of charge and so "low conduction". In other words, if we integrate the transmittivity in the bias window range we obtain low current. This can then be observed in the section 4.5.4, where you can find the obtained values of the current.

4.5.2 Density of state

After that, I have proceeded with the Device Density of States, which is very important in terms of transport. In fact, by definition, it figures out the number

of electron states that take part to conduction.

Settings

Semi-empirical For this analysis, I have used the semi-empirical calculator, with the selection of the extended Huckel parametrization. As regards the settings of the Device Density of States analysis, I have chosen, in both cases (as you can see in tab. 4.3), an energy range from -13 to 13 eV (with 101 points). I have decided to take inspiration from the paper found in literature, but then I have immediately moved to a smaller range from -5 to 5 eV in order to reduce the amount of time needed for the computational part. The graphs are then reported in an even smaller range since I have aligned them to the one obtained from the new improved structures (see later).

Range of energy	$E_0 = -13\text{eV}$, $E_1 = 13\text{eV}$, Points = 101
Sampling (k-points)	Sampling: $n_a = 3$, $n_b = 3$
Parameter of the zero Energy	Average Fermi level
Infinitesimal	1e-06 eV
Calculator of self-energy	Recursion

Table 4.3. Device DOS analysis settings.

Results and considerations

In the image 4.8 you can see the DOS of the single C82 molecule. This can be done selecting, in the DOS analyzer, the wanted atoms (in this case the C82 molecule) as you can see in fig. 4.9.

I have decided to analyze the different contributions of the orbitals (s, p, d, f separately) in order to understand which is the dominant one. In Fig. 4.9 (in the right top of the screenshot) you can also see that it is possible to select the wanted orbitals and to extract the corresponding data. After having exported the different information, I have reworked them with Matlab obtaining the graphs that will be shown in the following chapters. Moreover, in fig. 4.8, it can be easily seen that the greater contribution is given by the p orbital (given in yellow), while no contribution is given by the d and f ones. If you observe carefully the totality of the DOS behaviour is quite well described by the single contribution of the p-type state.

After having obtained the results considering the C82 molecule alone, I have considered the electrodes separately left and right. The obtained results are shown in fig. 4.10, where it is possible to notice that the major contribution is given by the d orbital in both cases. The two graphs are similar but not the same, in fact the

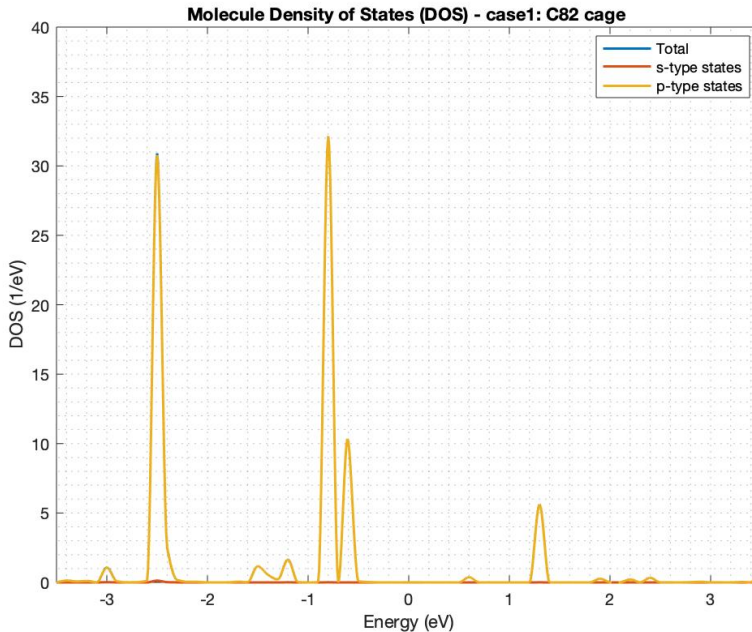


Figure 4.8. Device Density of States of the single C82 molecule (part of the first device).

contribution of the electrode on the right seems stronger than the other (DOS is doubled). Finally, in fig. 4.11, you can see the DOS graph of the entire device with the empty cage. It is possible to notice that the peaks of transmission correspond to the DOS ones.

4.5.3 Molecular energy spectrum vs DDOS

Taking into account the basic theoretical concepts analyzed the subsection 4.3, it is possible to summarize that when a molecule is bounded to two metallic electrodes, an exchange of charge occurs between the molecule and two electrodes. This causes for sure a shift of the molecular energy states and also broadening of the energy level. In fact we pass from discrete energy levels to broadened peaks.

Moreover, considering the molecule, the levels of the energy at equilibrium associate the "Fermi" level. In addition, all the levels that exceed the latter are named Lowest Unoccupied Molecular Orbitals and the others underneath are termed Highest Occupied Molecular Orbitals (respectively LUMOs and HOMOs). In fig. 4.12

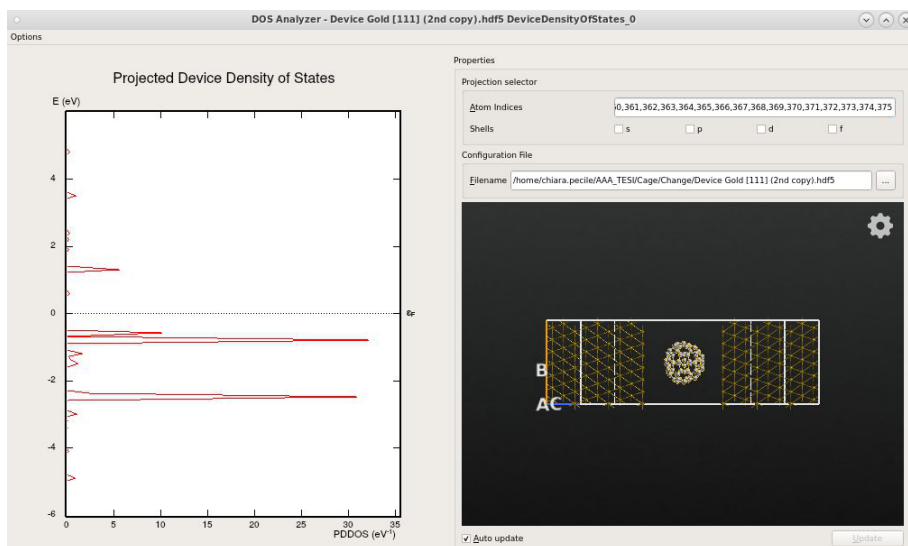


Figure 4.9. Picture of the DOS analyzer, on the right it is possible to see the selection of the C82 molecule done in order to realize the graph 4.8, on the top you can see the possible selection of the s, p, d and f orbitals.

you can see the graph of DOS of the molecule of the case in exam (e.g. considering the influence of the electrodes) with the energy states of the molecule considered without the influence of the electrodes. It can be observed that, with the non negligible influence of the electrodes, the HOMOs and LUMOs are a bit shifted and broadened.

4.5.4 IV characteristic

At this point, I have moved to the IV characteristic, which is one of the most important graphs for this study. First of all, in more theoretical words, we can say that it has been computed the integral of the bias window at the different bias voltages. In table 4.4 are reported the data obtained from the simulation. It can be easily noted that the obtained current with this configuration is very small. This could be expected from the analysis of the previous graphs, however it does not respect the wanted prospect. In fact in the paper found in literature, the current was measured in nA.

In figure 4.13 you can find the plot of obtained results.

This result suggested to do more and proceed with some changes in order to reach some improvements. Since the current was too low, I have decided to shorten

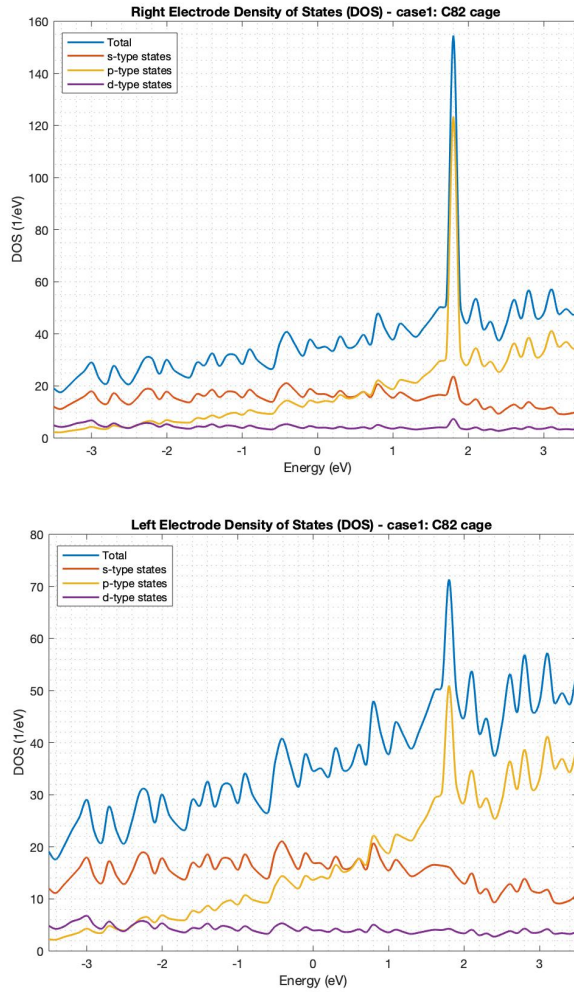


Figure 4.10. Device Density of States of the single electrodes, respectively right and left, reading from the top side (part of the first device in exam).

the distance between the electrodes and the molecule C82. In the section below you can find all the followed procedure.

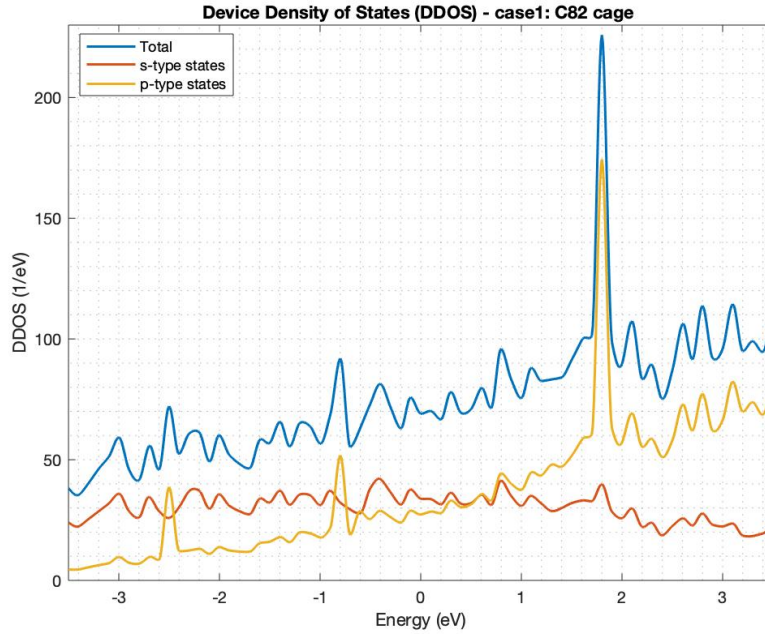


Figure 4.11. Device Density of States of the first device in exam.

Bias (V)	Current (A)
0.000000	0.000000e+00
-0.100000	-2.244320e-12
-0.200000	-6.153054e-13
-0.300000	-4.651179e-13
-0.400000	-7.760044e-13
-0.500000	-4.026153e-12
0.100000	3.101876e-13
0.200000	2.275729e-13
0.300000	3.552274e-13
0.400000	2.693904e-12
0.500000	7.060794e-11

Table 4.4. IV curve report - case1: empty C82 cage.

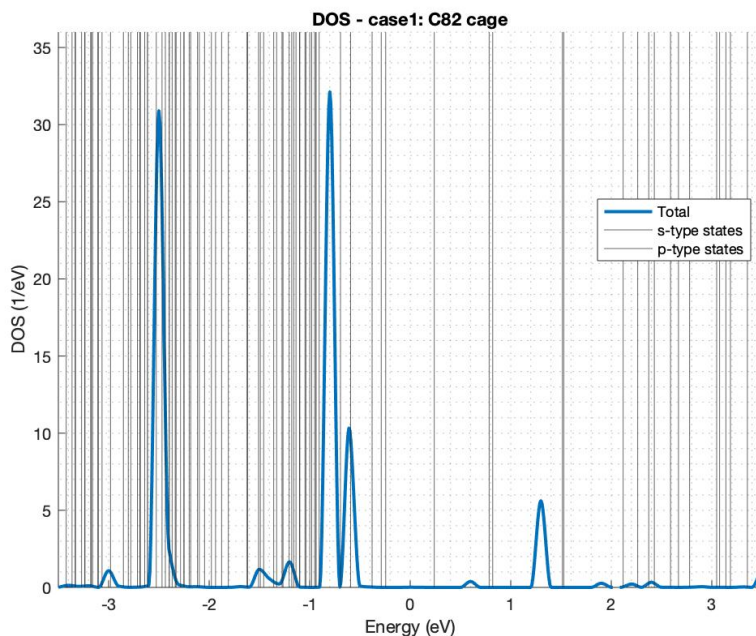


Figure 4.12. Device density of States vs Molecular energy spectrum - case 1: empty C82 cage.

4.6 Improvements

As explained before, I have started this work producing a device setting its features on my own. Certainly I have tried to follow the information provided by the papers found in literature and use this hints in a reasonable way. However, studying the obtained results, it can be easily seen that something can be for sure improved. At this point, especially observing the current obtained, I have decided to change the distance between the electrodes and the molecule. Observing some recent works, I discovered that a possible solution is set the distance at 2.4 \AA , which is known to be the shorter distance that leads to a stable configuration. This measure is the shorter distance that can lead to an equilibrium in terms of Chemisorption. This concept will be explained in the section 4.6.1. It must be said that this value is given from a very similar case, but not the one considering this type of molecule (C82).

At this point it is important to describe and analyze an important aspect: the Chemical Adsorption.

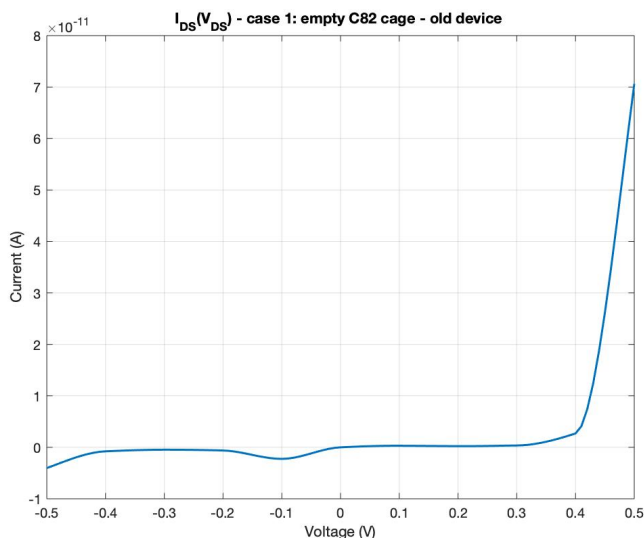


Figure 4.13. Plot of the IV curve - case 1: empty C82 cage, old device (higher distance between molecule and electrodes).

4.6.1 Chemical Adsorption

In general, the Chemical Adsorption is the process that manages the bonding of a molecule to (in general) a surface [50]. If we consider an even more generic case, when we refer to this process, we call "adsorbate" the chemical specie that we are considering and "adsorbent" the surface where the "adsorbate" is adsorbed. This process can happen in two modes: Chemisorption and Physisorption.

Chemisorption and Physisorption

By definition, Chemisorption is a bonding activity based on a chemical process [50] that implies the creation of connections (i.e. bonds) between the adsorbate and the adsorbent. This suggests that there is a considerable interaction between the orbitals of these two protagonists and so high energies involved for the bonding (that can be ionic or covalent). Moreover, we can say that in order to break the created bond and liberate the adsorbate, it is needed a great amount of energy.

On the other hand, Physisorption is the activity that involves the attraction of a the adsorbate to the adsorbent. By definition it is caused by the force that occur between the two protagonists. It is also known as "van der Waals adsorption"

since it is mainly due to van der Waals attraction [51]. Contrarily to the previous process, the interaction between adsorbent and adsorbate is weak and no alteration happens at the original chemical structure. In general, there is no creation of chemical bonds between the two characters.

If we move to a more specific case, so the one considered in this work, from theory it is known that, in systems that involve molecular wires (i.e. with metal electrodes), one of the most important factors that manages the transport in the system is the type of interface. Depending on the different cases, the molecule can be "chemisorbed" or "physisorbed" toward the contact [51]. The nature and severity of the process performed can be considerably changed depending on the chemical species involved. Moreover, depending on the strength of the interaction between the adsorbate and the adsorbent it is possible to determine different cases: weak or strong chemisorption and weak or strong physisorption.

If we consider weak Chemisorption we could have a small charge transfer between the molecule and the contact (to reach equilibrium). Then in the case of strong Chemisorption we are in presence of strong covalent bonds and a charge transfer occurs in order to reach the equilibrium. It has to be said that this usually happens with the exploitation of a specific anchoring group to create the wanted bonds (not our case). On the other hand, for the case of weak Physisorption there is no transfer of charges between the molecule and the contact. Then, in the case of strong Physisorption we could have a transfer of charge even if the molecule is not strongly coupled with the contact surface.

To summarize, Chemisorption happens if a covalent bond is constructed between the contact and the molecule. A covalent bond is strong and this also allows a small transfer of charge. Besides, this process leads to a substantial interaction and also to a "high level of orbital delocalization" [51]. Furthermore, Physisorption happens if there is a weak coupling between the molecule and the contact. This leads to a very small broadening and normally there is no transfer of charges. In addition to this, it has to be said that when we have to realize a structure, we have to take into account that there are two important measures of distance between the molecule and the electrodes that lead to an optimal geometry and equilibrium in terms of chemisorption and physisorption specifically. For this purpose, during my work I had to change this distance (reduce it) in order to reach improvements on transmittivity. You can see the obtained results in the subsection 4.6.3.

Hereafter you can find the new device referring to the configuration with the empty C82 cage and all the analysis performed on it.

4.6.2 The new device: empty C82 cage

In order to realize the new device with shorter distances of the molecule respect to the electrode, I started from the structure I had and passed to the bulk configuration.

Here, after some trials, I could reach the wanted distance moving firstly the left electrode and then the right one. Since the structure of the C82 molecule is not symmetrical, it was no possible to set a specific distance from the nearest "point" of the electrode and all the atoms of the C82 molecule involved in the region that faces the latter. So I tried to set a distance a bit less than 2.4 \AA (2.3208 \AA) for the nearest atom and a bit more for all the other atoms next to the electrode. After that I have fitted again the cell and realized the device from bulk.

In Fig. 4.14, it is shown an example of distance between the molecule and an electrode of the previous device. On the other hand, in Fig. 4.15 there are shown the distances that characterize the new device.

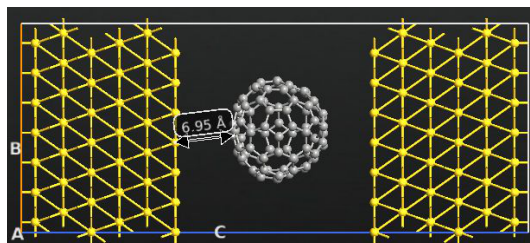


Figure 4.14. Example of the distances of the previous configuration, between the left electrode and the C82 molecule.

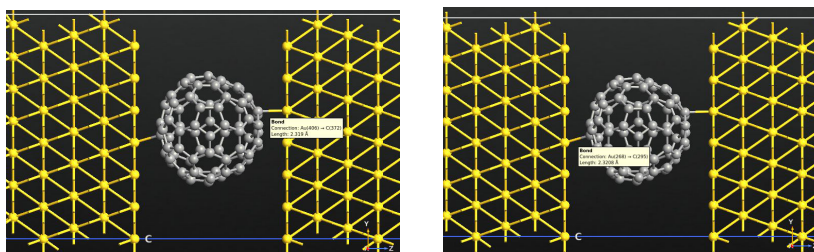


Figure 4.15. Final distances set in the new device. In these pictures you can see the lower ones; In particular you can also see the references of the atoms considered to calculate the distance (in the small white note).

In fig. 4.16 you can see the final new structure. It is important to know that the lines that connect the molecule to the electrodes have no specific meaning (they

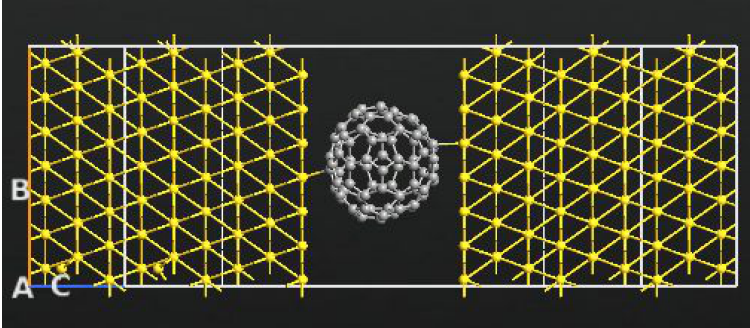


Figure 4.16. The new device - case 1: empty C82 cage.

do not represent a covalent bond), they are just a way how ATK tool represents small distances. The following subsections expose the different analysis that have been performed on this device.

4.6.3 Transmission spectrum at the equilibrium

Settings

All the analysis has been performed in the same way as the previous case (see 4.5.1), a part of the range of energies used. I have decided to reduce it in order to reduce the computational time. In the image 4.17 you can see the window of the settings used in this case.

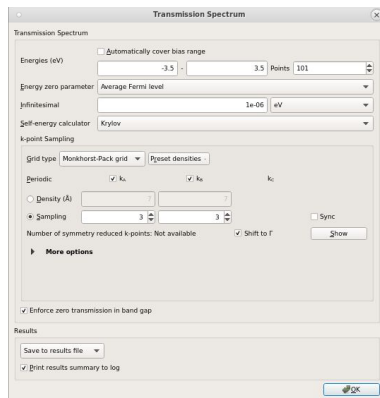


Figure 4.17. Settings: Transmission Analyzer of the new device - case 1: empty C82 cage.

Results and comments

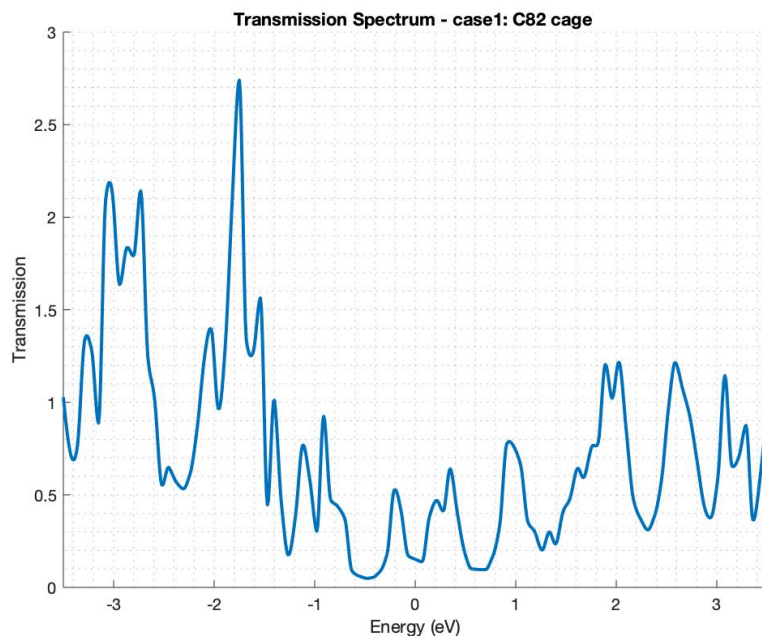


Figure 4.18. Transmission spectrum of the new device - case 1: empty C82 cage.

Observing the graph 4.18, you can easily see that the transmittivity is increased a lot. This was for sure the wanted and expected result. The peaks are more broadened and we can also say that now we have moved from weak coupling to strong coupling, where we can appreciate the creation of covalent bonds. Referring to the theory exposed in section 4.6.1, we are in the Chemisorption case, so we are in presence of a greater interaction between the molecule and the electrodes. This is a very good point since we can now appreciate easily the behaviour of the device and finally reveal if it behaves as SME.

As anticipated above, it is important to take into account that in this case the electrodes play a non-negligible role in the Transmission spectrum of the system (also in the DOS of the system). This because their distance from the molecule is short and so there is a sort of superimposition of the states of the molecule and the ones of the electrodes. This important influence would not happen if there was a greater distance between the electrodes.

Finally, observing this graph it is important to do a special remark. Considering the tool ATK, the given $T(E)$ is not the actual total transmission coefficient. In order to reach the definite transmission probability, it can be performed a more specific procedure studying the transmission eigenstates and eigenvalues. The latter are named transmission eigenvalues that represent the transmission quantum mechanical operator, then the others can be estimated by their projection in the surfaces of the real space. It has to be said that these surfaces are named transmission eigenchannels and, in a more practical overview, they represent the "place" where transmission happens. It is known from theory that the eigenvalues related to transmission are the definite transmission coefficients. Moreover, they are always normalized to 1.

Instead, coming back to the graph exposed in this subsection, the obtained value is greater than 1. However, this is right since there is the possibility that different transmission eigenvalues can sum at a fixed energy. Since they are normalized to 1, their sum can reach obviously a value greater than 1. In more practical words, this means that more transmission channels are available (more than 1). So, electrons can be transferred from Source to Drain through different paths, which means dissimilar channels and so eigenstates.

4.6.4 Density of state

The analysis of the DOS has been computed in the same way as reported in section 4.5.2. Below you can find the results obtained from the new device.

Results and comments

In the image 4.19 you can observe the DOS of the single C82 molecule. Comparing it with the previous case, it is possible to note that we have a lot of peaks more and also a greater amount in terms of DOS ($1/eV$). Then, as in the previous case, I have analyzed the different contributions of the orbitals. After having exported the different information, I have reworked them with Matlab. You can easily notice that the greatest contribution is given again by the p orbitals (yellow). The final DOS of the molecule is mainly the same of the p-type states.

Then in fig. 4.20 it is possible to observe the final graph of the DOS of the entire device. It can be observed the presence of only 3 peaks. Two of them are very small, one is of the order of 10^8 $1/eV$. Here the greatest contribution is given by the p-type states. This behaviour is very different from the one obtained with the older device. In fact in the previous case, the peak was a lot smaller. Then in fig. 4.21 it is possible to observe the behaviour of the two different electrodes. Again you can see a big difference respect to the previous case, in fact the peaks now are described by a greater amount in terms of $1/eV$. Their behaviour, we

can say, is symmetrical and the major contribution to their final graph is given by p-type states in both cases.

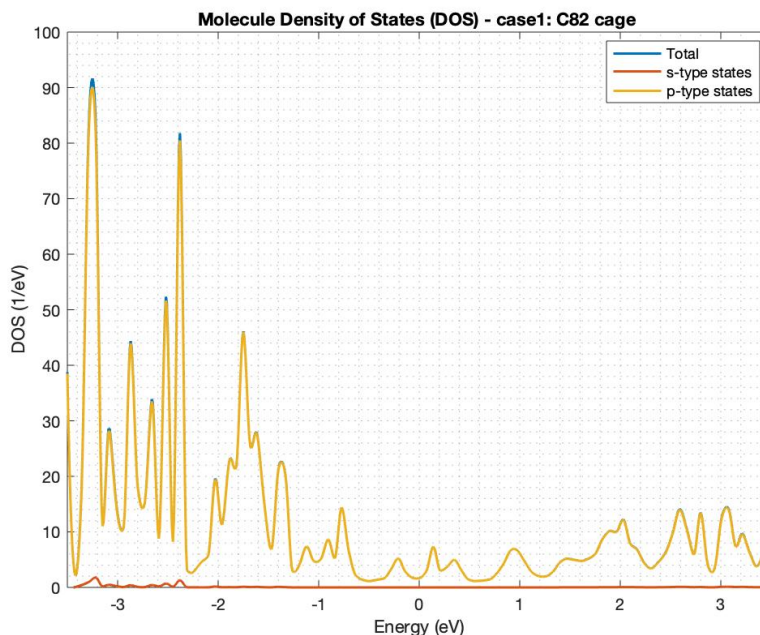


Figure 4.19. Device density of States of the molecule of the new device - case 1: empty C82 cage.

4.6.5 Molecular energy spectrum vs DDOS

Taking into account the basic theoretical concepts analyzed the subsection 4.3, we can finally add that when a molecule is bounded to two metallic electrodes, an exchange of charge occurs between the molecule and two electrodes. This causes for sure a shift of the molecular energy states.

Moreover, considering the molecule, the levels of the energy at equilibrium associate the "Fermi" level. In fig. 4.22 you can see the graph of DOS of the molecule of the case in exam (e.g. considering the influence of the electrodes) with the energy states of the molecule considered without the influence of the electrodes. It can be observed that, with the non negligible influence of the electrodes, the HOMOs and LUMOs are a bit shifted and broadened.

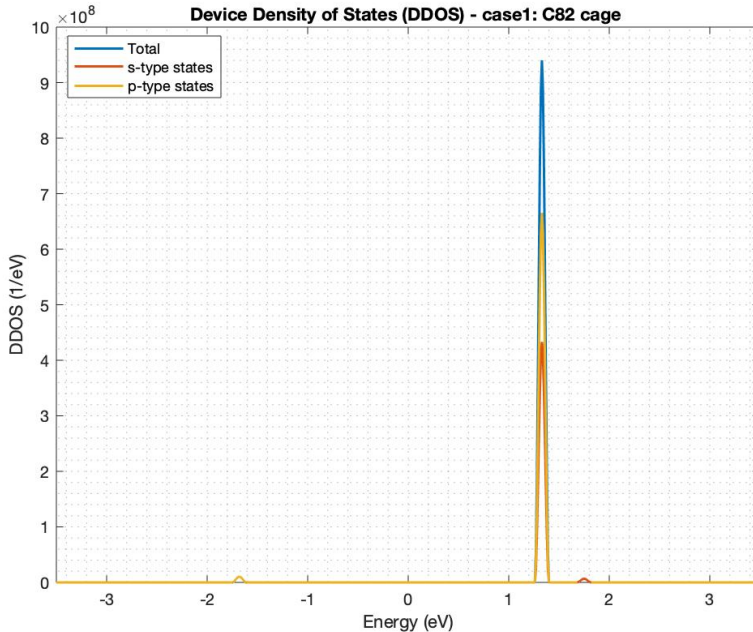


Figure 4.20. Device density of States of the entire new device - case 1: empty C82 cage.

4.6.6 IV characteristic

At this point, I have moved to the IV characteristic. As announced in the subsection 4.5.4, it is one of the most important analysis for this study. In table 4.5 are reported the data obtained from the simulation. It can be easily seen that the obtained current in this case has increased a lot. This was for sure expected and gives us the possibility to better appreciate the behaviour..

In figure 4.23 you can find the plot of obtained results. In the subsection 4.6.7 you can see the graph that analyzes the differences between the old and the new device of this first case.

Moreover, this result is the real consequence of the improvements made on the structure. In the 5 section you can find different observations related on these aspects. After this configuration, with the empty cage, let's move to configuration Gd@C82-I.

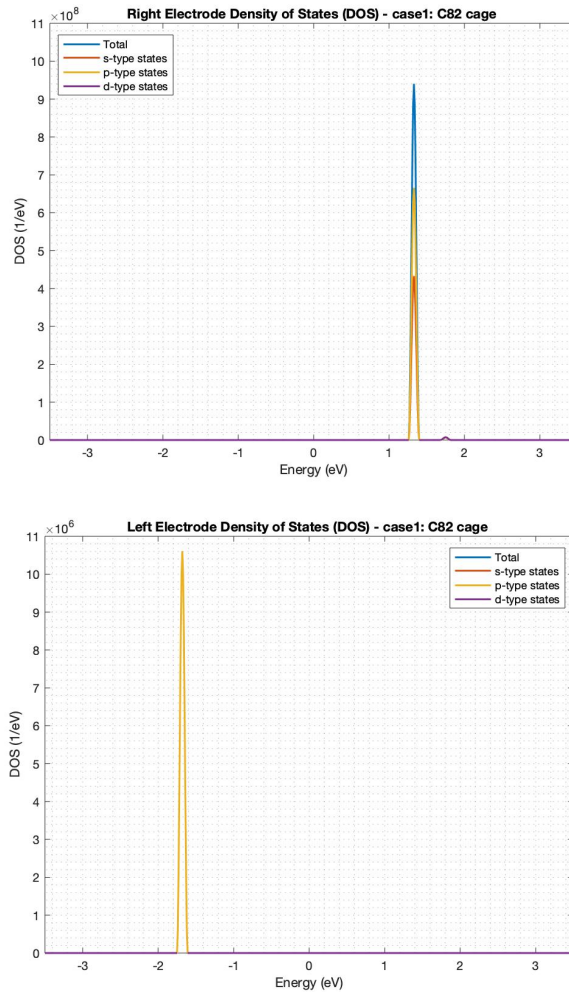


Figure 4.21. Device Density of States of the single electrodes, respectively right and left, reading from the top side - case 1: empty C82 cage..

4.6.7 IV curve: old vs new device

As previously announced, I have created a graph to compare the two curves related to the case 1 device. So in fig. 4.24 you can see the obtained graph, in linear scale. As expected, the current of the old device is very small compared to the new one. In fact, with this scale it is not possible to appreciate the differences between the

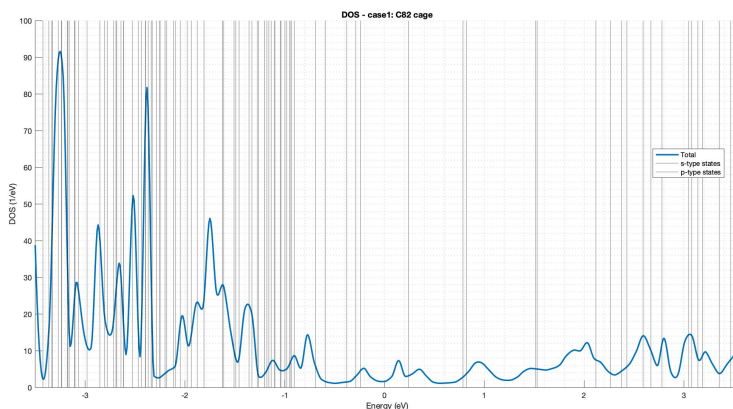


Figure 4.22. Device density of States vs Molecular energy spectrum - case 1: empty C82 cage.

Bias (V)	Current (A)
0.000000	0.000000e+00
-0.100000	-1.444865e-06
-0.200000	-2.755594e-06
-0.300000	-4.248485e-06
-0.400000	-5.904285e-06
-0.500000	-7.637758e-06
0.100000	1.617926e-06
0.200000	3.904488e-06
0.300000	7.172438e-06
0.400000	1.015110e-05
0.500000	1.340551e-05

Table 4.5. IV curve report - case1, new device: empty C82 cage.

two behaviours. Therefore, I decided to use the semilogarithmic scale (y axis). You can find this graph in fig. 4.25. In this case we can easily see that the behaviour is practically the same, except from the values of current.

4.7 Gd@C82 - I

In this section I will refer to the device reported in 4.26: cage C82 with the encapsulated Gd atom and the electrodes. The configuration has been called Gd@C82-I

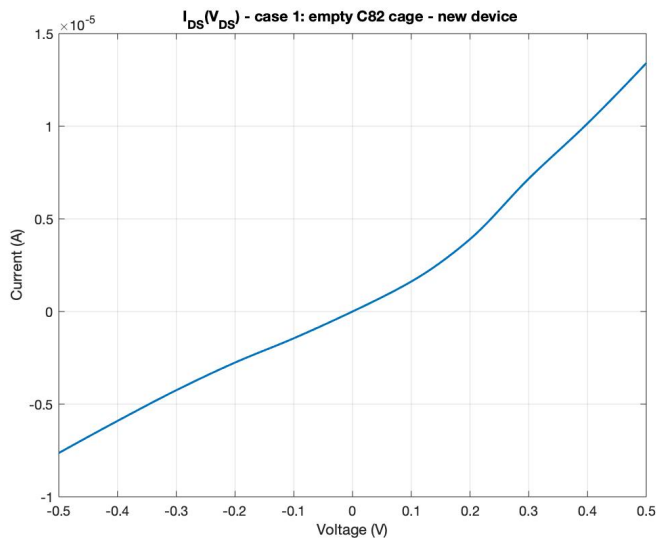


Figure 4.23. Plot of the IV curve - case 1: empty C82 cage, new device.

referring on what announced in the chapter 2.5.2 (the research reported in [4]).

4.7.1 Transmission spectrum at the equilibrium

Settings

I have used the semi-empirical calculator, with the selection of the extended Huckel parametrization. The transmission spectrum analysis has been performed with the settings reported in tab. 4.6.

Range of energy	$E_0 = -13\text{eV}$, $E_1 = 13\text{eV}$, Points = 101
Sampling (k-points)	Sampling: $n_a = 3$, $n_b = 3$
Parameter of the zero Energy	Average Fermi level
Infinitesimal	1e-06 eV
Calculator of self-energy	Recursion

Table 4.6. Transmission spectrum analysis settings - Gd@C82-I.

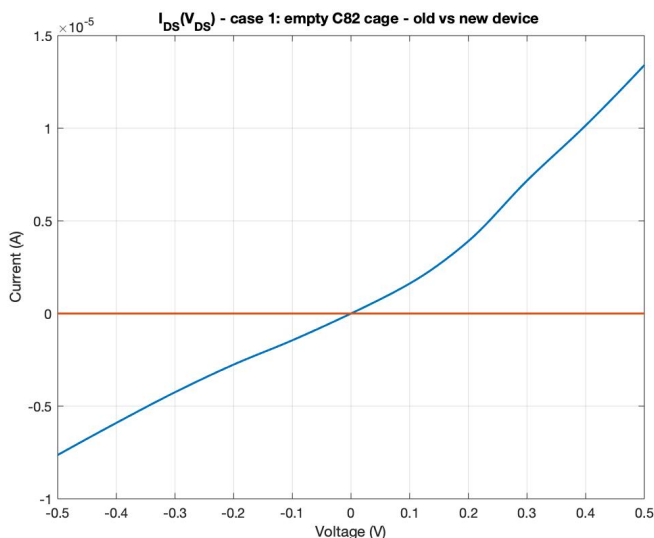


Figure 4.24. Plot of the IV curve - case 1: empty C82 cage, old vs new device. Linear scale.

Results and considerations

In figure 4.27 it is shown the obtained transmission spectrum of the second device in exam: Gd@C82 - I. It can be easily seen that there is a lot of difference respect to the case with the empty C82 cage. In fact we have less peaks and this means less current (see subsection 4.7.4).

This result is very different to the one presented in literature. This could be explained by the fact that I have used a less accurate method respect to the one used in the paper. Moreover, another possible contribution is given by a too high distance between the molecule and the electrodes. However, it can also be said that if we refer to the figures reported in chapter 2.5.1, it is very difficult to deeply study them since their are a bit confusing from a very practical point of view. In the final chapter you can find then some useful observations also on this aspect.

This result (together with the other) suggested to do some improvements on the structure, as explained in section 4.6. Also for this structure I have made some changes that will be exposed in section 4.8.

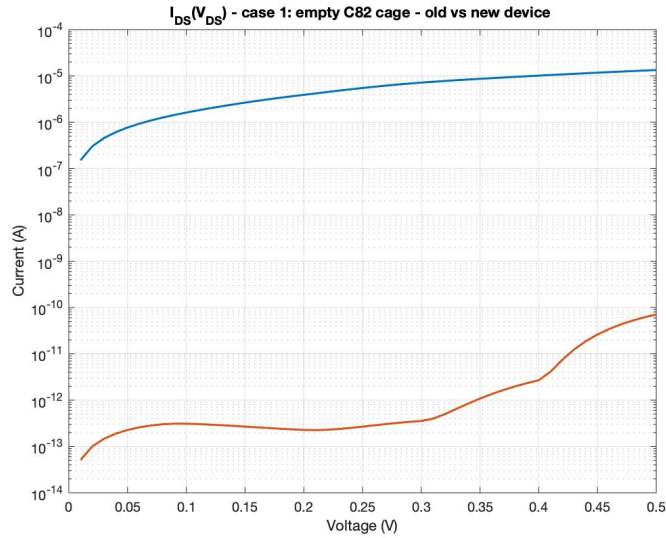


Figure 4.25. Plot of the IV curve - case 1: empty C82 cage, old vs new device. Semilogarithmic scale (y).

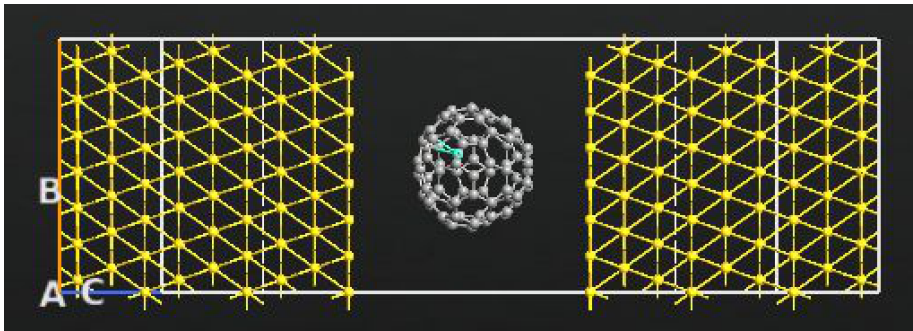


Figure 4.26. The second studied device: C82 cage with the encapsulated Gd atom and the electrodes.

4.7.2 Density of state

Settings

For the Device Density of States analysis, I have chosen, as you can see in tab. 4.7, an energy range from -13 to 13 eV (with 101 points). As announced in the previous section, I have decided to take inspiration from the paper found in literature, but

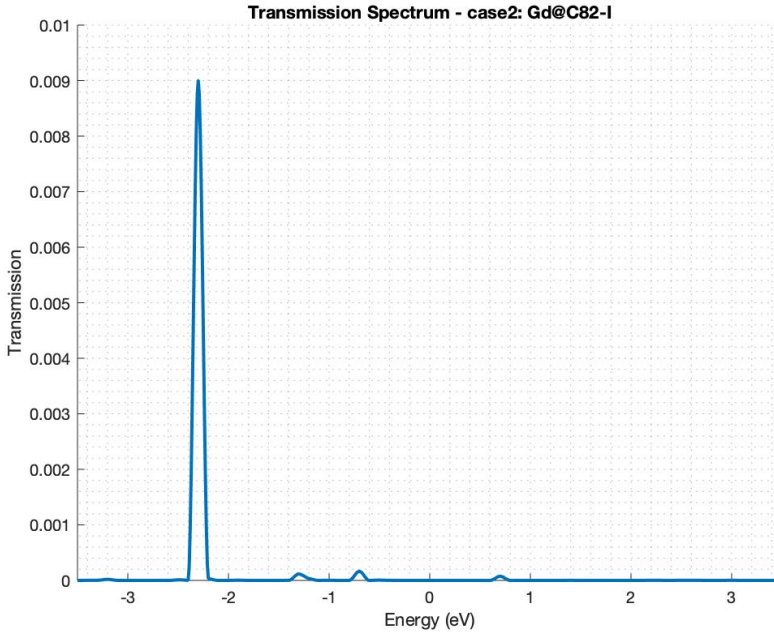


Figure 4.27. Transmission spectrum of the second device: Gd@C82 - I.

then I have moved to a lower range (as you can see from the reported graphs).

Range of energy	$E_0 = -13\text{eV}$, $E_1 = 13\text{eV}$, Points = 101
Sampling (k-points)	Sampling: $n_a = 3$, $n_b = 3$
Parameter of the zero Energy	Average Fermi level
Infinitesimal	$1\text{e-}06$ eV
Calculator of self-energy	Recursion

Table 4.7. Device DOS analysis settings - Gd@C82-I.

Results and considerations

In the figure 4.28 you can see the DOS of the single Gd@C82 molecule, of the device take in exam in this chapter. This can be done selecting, in the DOS analyzer, the wanted atoms, as explained before. In figure 4.29 you can see the DOS Analyzer where I have extracted the data: on the left the graph provided by atk with both

contributions of spin, on the right the configuration in exam (where is possible to select the atoms to analyze) and on the right top the possibility to select the different orbitals to perform a deeper analysis of the case.

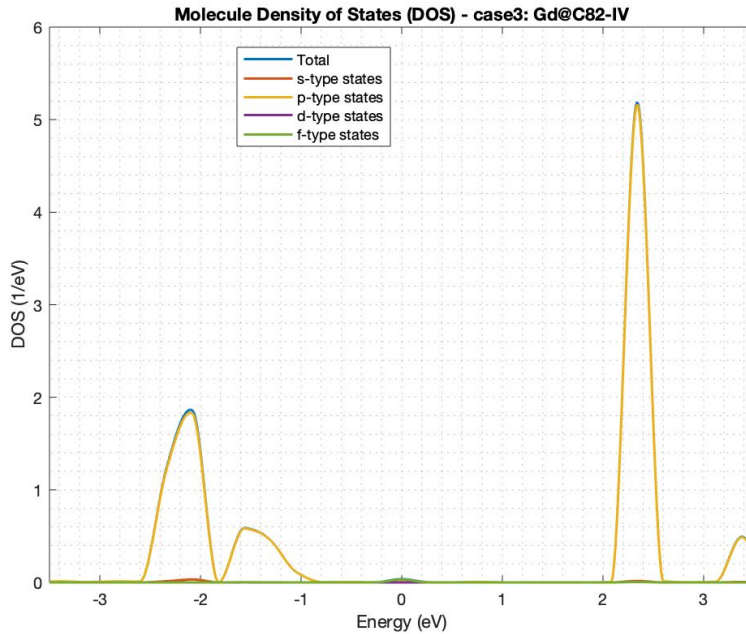


Figure 4.28. Device Density of States of the single Gd@C82 molecule - configuration I (part of the second device).

As for the previous device, I have decided to analyze the different contributions of the orbitals in order to discover which is the dominant one. After having exported the data, I have reworked them with Matlab. Furthermore, in figure 4.28, you can see that the greater contribution is given by the p orbital (in yellow), while the other orbitals' contribution can be seen in the other different colours.

Subsequently, I have considered the electrodes separately left and right. The obtained results are shown in fig. 4.30, where is possible to notice that the major contribution is given by the p orbital in both cases.

In the end, in the image 4.31, you can see the DOS of the entire device with the encapsulation of the Gd atom in the position I.

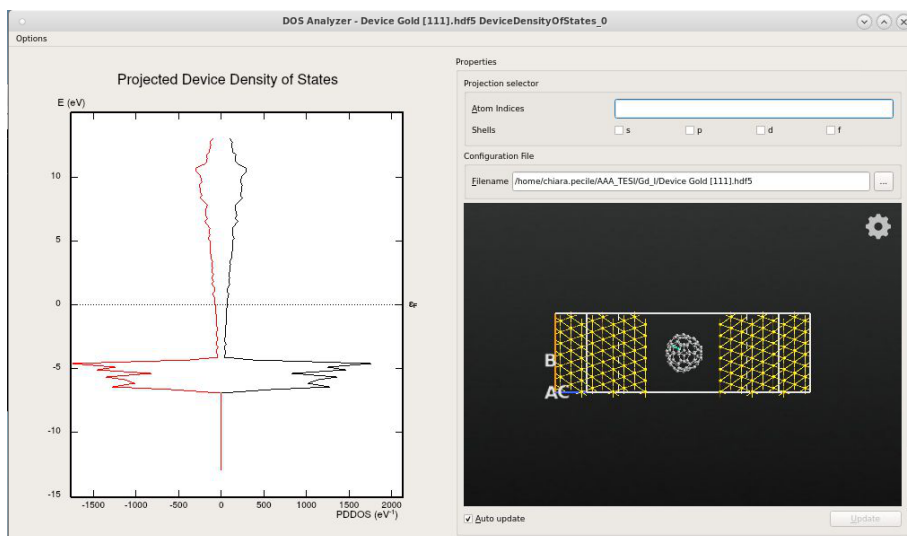


Figure 4.29. Picture of the DOS analyzer, on the top you can see the possible selection of the s, p, d and f orbitals and on the left the representation given by the ATK tool of the DDOS of this system (both contributions of spin).

4.7.3 Molecular energy spectrum vs DDOS

Again, considering the basic theoretical concepts analyzed the subsection 4.3, it is possible to summarize that when a molecule is bounded to two metallic electrodes, an exchange of charge occurs between the molecule and two electrodes. This causes for sure a shift of the molecular energy states. In fig. 4.32 you can see the graph of DOS of the molecule of the case in exam (e.g. considering the influence of the electrodes) with the energy states of the molecule considered without the influence of the electrodes. It can be observed that, with the non negligible influence of the electrodes, the HOMOs and LUMOs are a bit shifted and broadened.

4.7.4 IV characteristic

In table 4.8 are reported the data obtained from the IV curve report. It can be easily noted that the obtained current, also with this configuration, is very small. This was expected even more respect to the previous case, in fact referring to the transmission spectrum we had very few and poor peaks. However, as anticipated, this does not respect the expectations I had. In fact in the paper found in literature, the current was greater.

This is one of the reasons that suggested to perform some changes in the realized

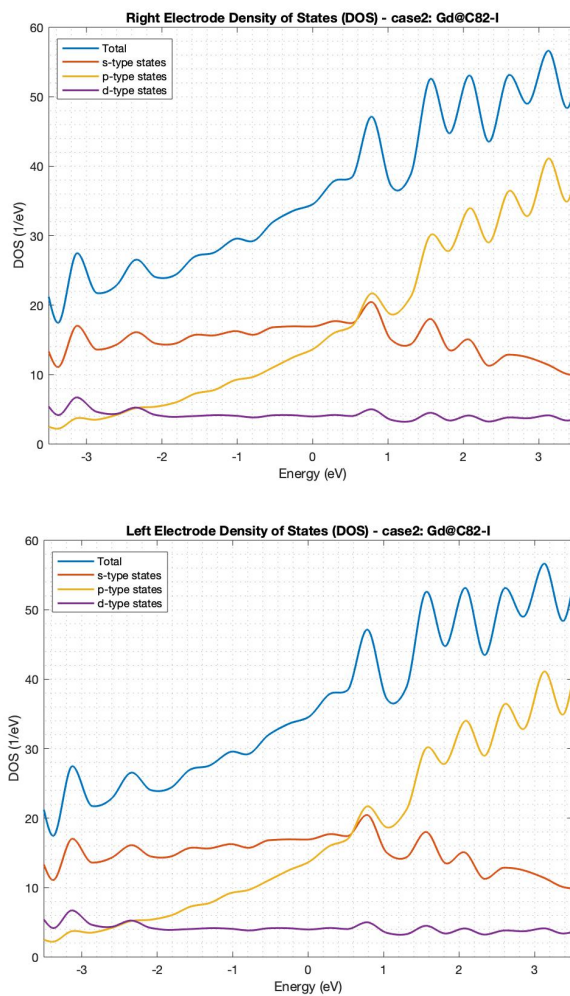


Figure 4.30. Device Density of States of the single electrodes, respectively left and right, reading from the top side (part of the second device in exam).

structure. Again, I have reduced the distance between the electrodes and the Gd@C82 molecule. Here after you can find the new structure and all the analysis performed on it.

In figure 4.33 you can find the plot of obtained results.

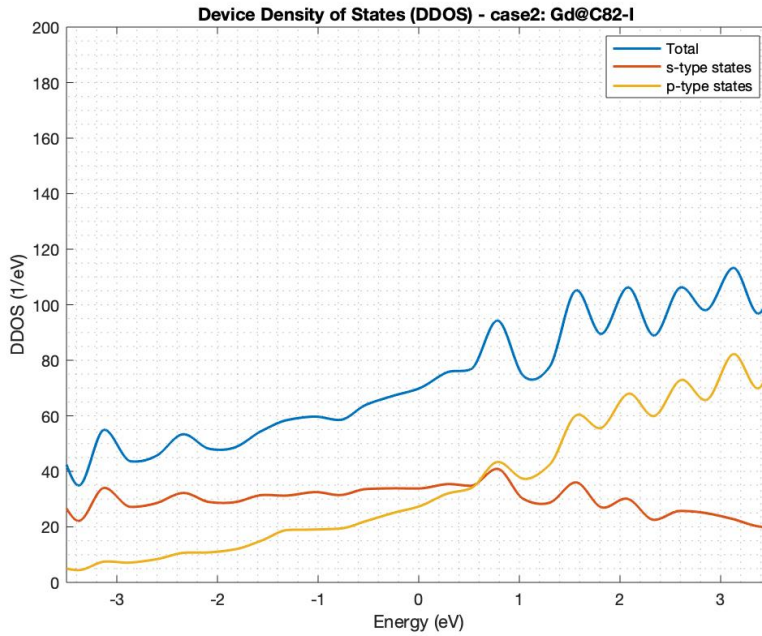


Figure 4.31. Device Density of States of the second device in exam.

Bias (V)	Current (A)
0.00000	0.000000e+00
-0.10000	-5.692985e-13
-0.20000	-3.803744e-13
-0.30000	-3.095533e-12
-0.40000	-1.896156e-12
-0.50000	-2.176001e-09
0.10000	8.321331e-13
0.20000	7.056005e-13
0.30000	8.154646e-09
0.40000	2.360706e-11
0.50000	3.012767e-11

Table 4.8. IV curve report - case2: Gd@C82 - I.

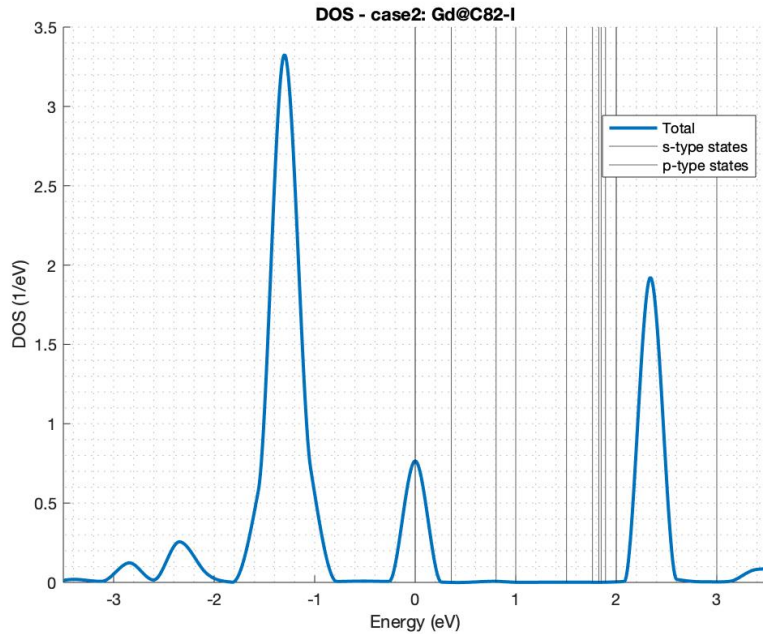


Figure 4.32. Device density of States vs Molecular energy spectrum - case 2: Gd@C82-I.

4.8 Improvements

Since the obtained result do not satisfy the expectations I had at the beginning, in order to reveal the SME behaviour, as I had already explained in section 4.6, I made some changes in the distance between the electrodes and the Gd@C82 molecule.

4.8.1 The new device: Gd@C82 - I

As in the case previous case, I have shorten the distance to a value of 2.4 Angstrom. Please refer to section 4.6 for deeper details.

In the picture 4.34 you can see the new device of the configuration Gd@C82-I. Then, from the analysis point of view, I have proceeded as done before.

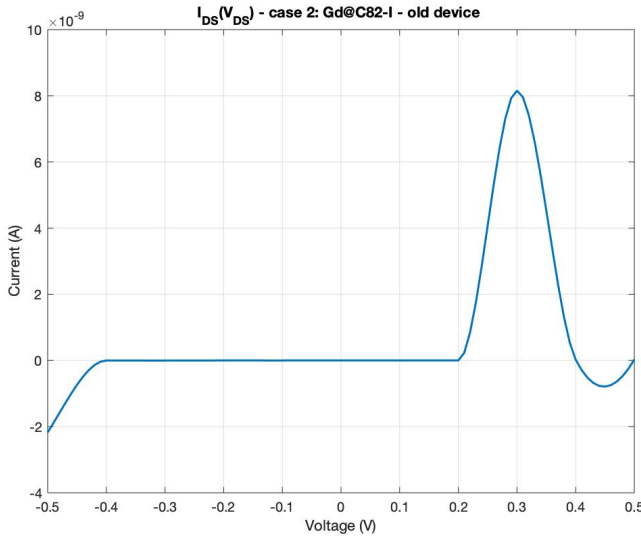


Figure 4.33. Plot of the IV curve - case 2: Gd@C82-I, old device.

Figure 4.34. The new device - case 2: Gd@C82 - I.

4.8.2 Transmission spectrum at the equilibrium

Settings

All the analysis has been performed in the same way as the previous cases (see [4.5.1](#)), a part of the range of energies used. I have decided to reduce it in order to reduce the computational time. In the image [4.17](#) you can see the window of the settings used in this case.

Results and comments

Observing the graph [4.35](#), you can easily see that the transmittivity is increased a lot, respect to the previous old case. As in the case of the empty C82 cage, this was the expected result: the peaks are more broadened and we have passed from weak coupling to strong coupling. This is a very good point since we can now appreciate easily the behaviour of the device (see section [4.10.2](#) to see the differences between the graphs and the conclusive chapter [5](#) to appreciate the behaviour obtained).

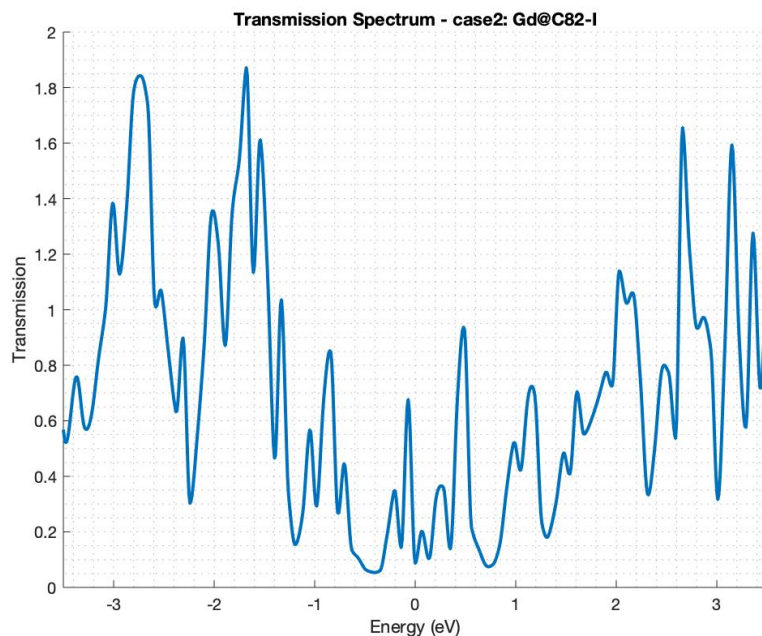


Figure 4.35. Transmission spectrum of the new device - case 2: Gd@C82-I.

4.8.3 Density of state

The analysis of the DOS has been computed in the same way as reported in section 4.5.2. Below you can find the results obtained from the analysis of the new device.

Results and comments

In the image 4.36 it is shown the DOS of the single Gd@C82 molecule. As in the previous case, it has been analyzed separately the different contributions of the orbitals. After having reworked he obtained data, I have reported them in some graphs with Matlab. It is note very easy to notice that the greatest contribution is given again by the p orbitals. Its contribution is described by the yellow line and the blue line (that can be seen just in the extremely top of the peaks) describes the totality of the DOS of the molecule.

Then in fig. 4.37 it is possible to observe the final graph of the DOS of the entire device. It can be observed that are present just two peaks. Here the greatest contribution is given by the p-type states. It has to be said that this behaviour

is very different from the one obtained with the older device. In fact in this case the peaks are much greater. Then in fig. 4.38 it is possible to observe the behaviour of the two different electrodes. Again you can see a big difference respect to the previous case, in fact the peaks now are described by a even greater amount but also they are very different between them. The major contribution to their final graph is given by p-type states in both cases.

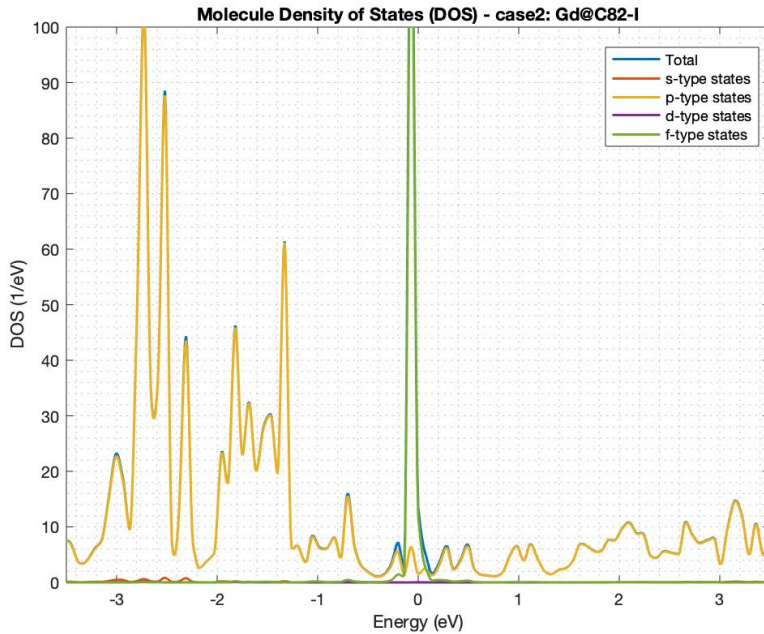


Figure 4.36. Device density of States of the Gd@C82 molecule of the new device - case 2: Gd@C82-I.

4.8.4 Molecular energy spectrum vs DDOS

Taking into account the basic theoretical concepts analyzed in subsection 4.3, we can finally add that when a molecule is bounded to two metallic electrodes, an exchange of charge occurs between the molecule and two electrodes. This causes for sure a shift of the molecular energy states. This can be seen for sure in fig. 4.39 where it is shown the graph of DOS of the Gd@C82 molecule of the case in exam (e.g. considering the influence of the electrodes) with the energy states of the molecule considered without the influence of the electrodes.

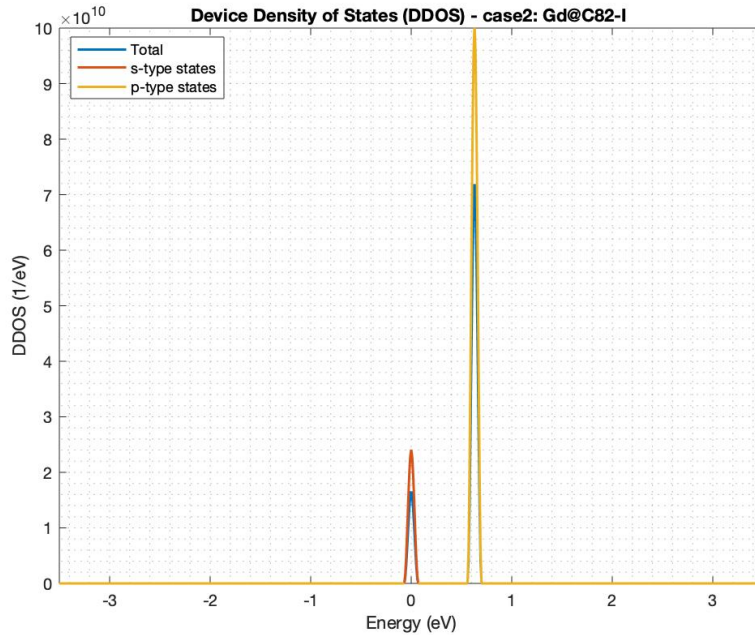


Figure 4.37. Device density of States of the entire new device - case 2: Gd@C82-I.

4.8.5 IV characteristic

At this point, I have considered the IV curve study. In table 4.9 are reported the data obtained from the simulation. It can be easily seen that the obtained current, also in this case, is extremely increased. This was for sure expected and gives us the possibility to better appreciate the behaviour.

In figure 4.40 you can find the plot of obtained results. In the subsection 4.8.6 you can see the graph that analyzes the differences between the old and the new device of this first case.

Besides, it has to be said that also in this case, the result is the real consequence of the improvements made on the structure. In the 5 section you can find different observations related on these aspects. After this configuration, let's now move to configuration Gd@C82-IV.

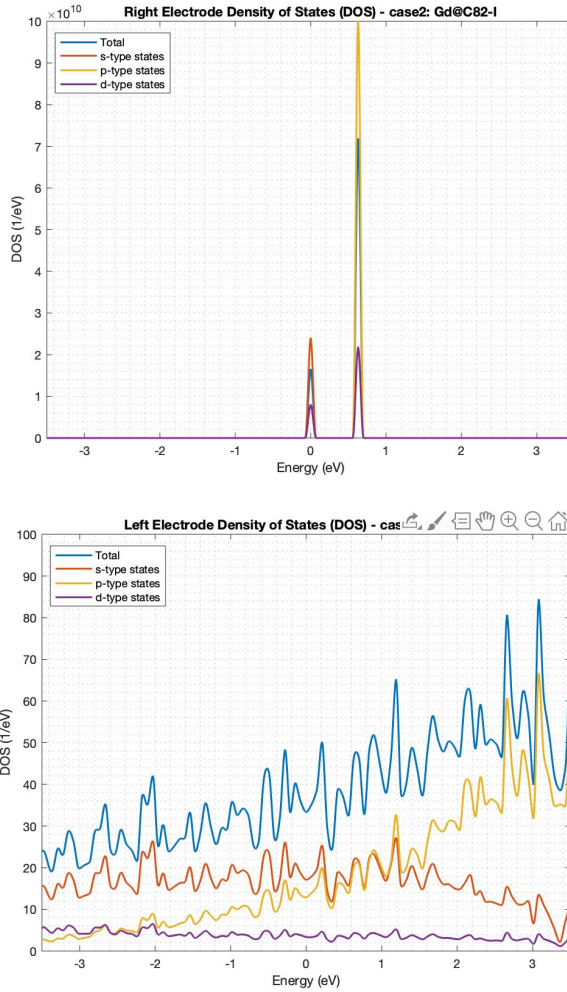


Figure 4.38. Device Density of States of the single electrodes, respectively right and left, reading from the top side - case 2: Gd@C82-I.

4.8.6 IV curve: old vs new device

Also in this case, I have created a graph to compare the two curves related to the case 2 device. So in fig. 4.41 you can see the obtained graph, in linear scale. As expected, the current of the old device is very small compared to the new one. In fact, with this scale it is not possible to appreciate the differences between the two

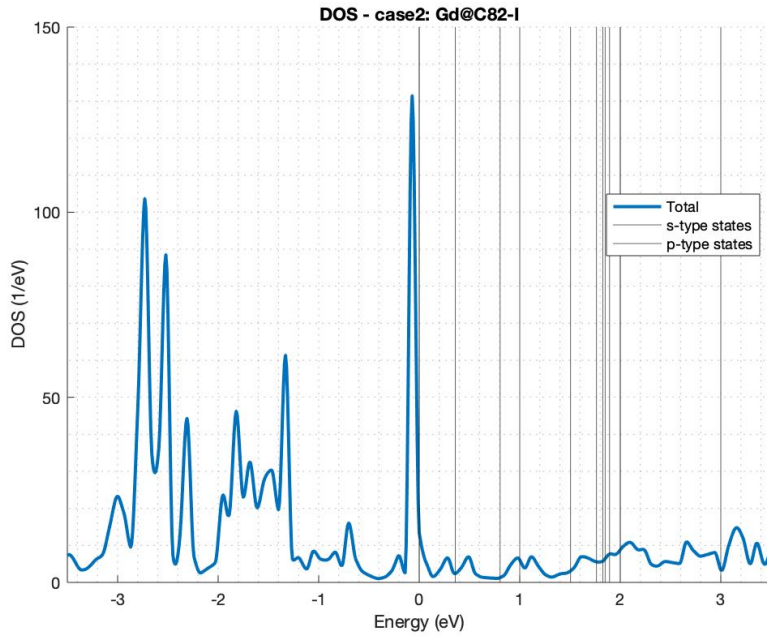


Figure 4.39. Device density of States vs Molecular energy spectrum - case 2: Gd@C82-I.

Bias (V)	Current (A)
0.000000	0.000000e+00
-0.100000	-2.269805e-06
-0.200000	-3.817398e-06
-0.300000	-6.224794e-06
-0.400000	-7.532781e-06
-0.500000	-9.564935e-06
0.100000	2.889196e-06
0.200000	5.488512e-06
0.300000	8.158617e-06
0.400000	1.088267e-05
0.500000	1.367802e-05

Table 4.9. IV curve report - case2, new device: Gd@C82-I.

behaviours. The same as I have done for the previous case (case 1 - empty C82

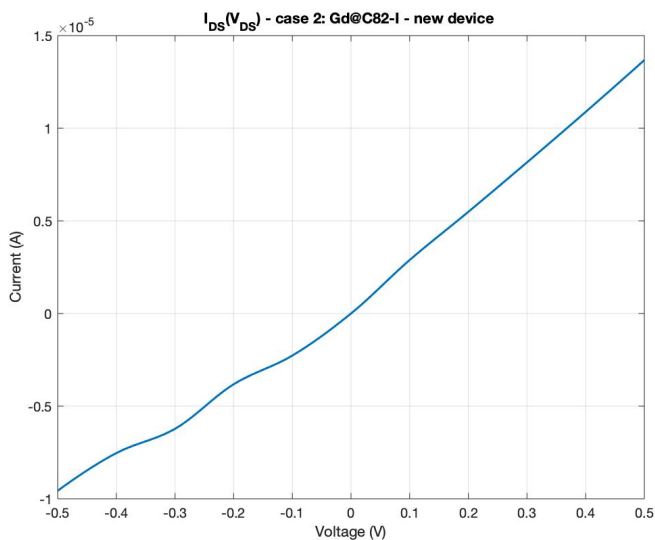


Figure 4.40. Plot of the IV curve - case 2: Gd@C82-I, new device.

cage in subsection 4.6.7), I decided to use the semilogarithmic scale (y axis). You can find this graph in fig. 4.42. In this case we can easily see that the behaviour of the new device is very strange and different respect to the one obtained with the older one.

4.9 Gd@C82 - IV

In this section I will refer to the device reported in 4.43: cage C82 with the encapsulated Gd atom and the electrodes. The configuration has been called Gd@C82-IV referring on what announced in the chapter 2.5.2 (the research reported in [4]).

4.9.1 Transmission spectrum at the equilibrium

Settings

I have used the semi-empirical calculator, with the selection of the extended Huckel parametrization. The transmission spectrum analysis has been performed with the settings reported in tab. 4.10.

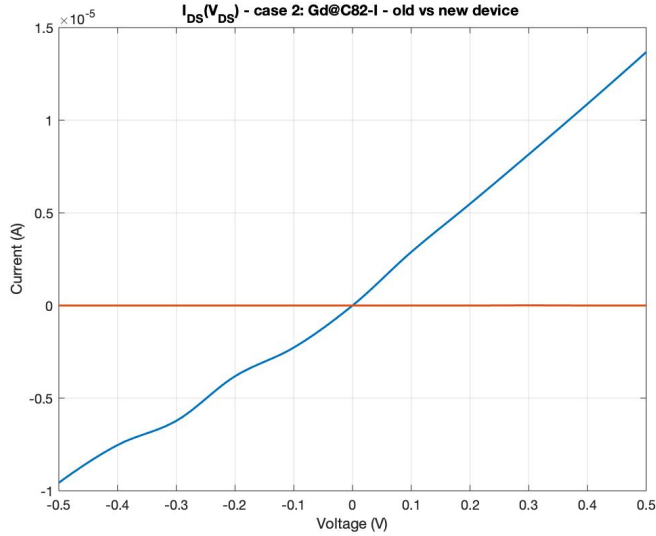


Figure 4.41. Plot of the IV curve - case 2: Gd@C82-I, old vs new device. Linear scale.

Energy range	$E_0 = -13\text{eV}$, $E_1 = 13\text{eV}$, Points = 101
k-point sampling	Sampling: $n_a = 3$, $n_b = 3$
Contributions	All
Energy zero parameter	Average Fermi level
Infinitesimal	1e-06 eV
Self-energy calculator	Recursion

Table 4.10. Transmission spectrum analysis settings - Gd@C82-IV.

Results and considerations

In figure 4.44 it is shown the obtained transmission spectrum of the third and last device in exam: Gd@C82 - IV. There can be easily noticed some differences from the first case with the empty cage.

First of all more peaks and so more current. Then also the HOMO - LUMO gap has reduced and this means better transmission.

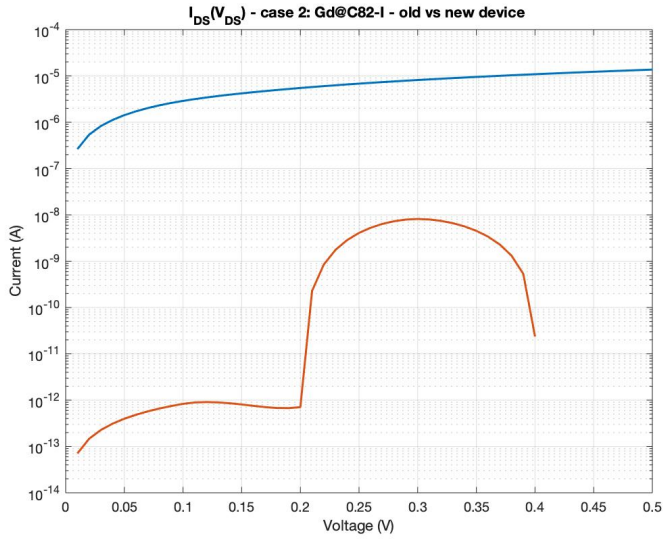


Figure 4.42. Plot of the IV curve - case 2: Gd@C82-I, old vs new device. Semilogarithmic scale (y).

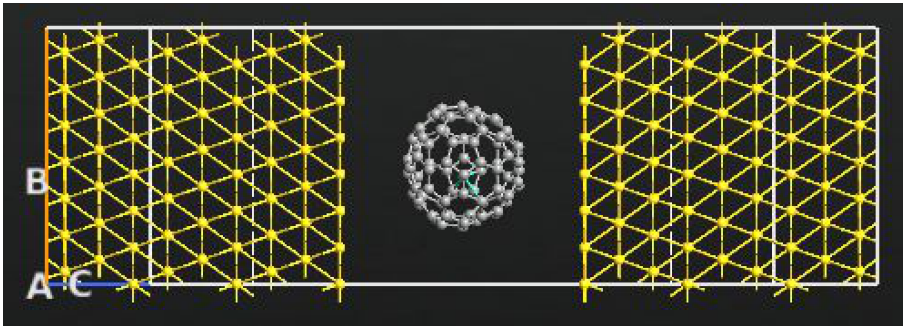


Figure 4.43. The third studied device: C82 cage with the encapsulated Gd atom and the electrodes.

4.9.2 Density of state

Settings

For the Device Density of States analysis, I have chosen, as you can see in tab. 4.11, an energy range from -13 to 13 eV (with 101 points).

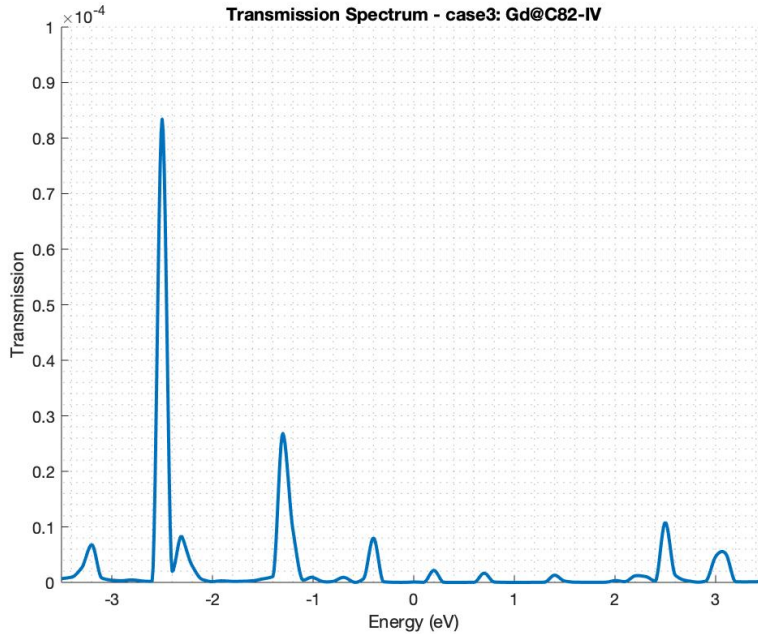


Figure 4.44. Transmission spectrum of the third device: Gd@C82 - IV.

Energy range	$E_0 = -13\text{eV}$, $E_1 = 13\text{eV}$, Points = 101
k-point sampling	Sampling: $n_a = 3$, $n_b = 3$
Contributions	All
Energy zero parameter	Average Fermi level
Infinitesimal	1e-06 eV
Self-energy calculator	Recursion

Table 4.11. Device DOS analysis settings - Gd@C82-IV.

Results and considerations

In the image 4.46 you can see the DOS of the single Gd@C82 molecule, configuration IV which is part of the third and last device. This can be done as explained before.

As for the previous devices, I have decided to consider the different contributions of the orbitals in order to realize which is the dominant one. After having exported the data, I have reworked them with Matlab. Furthermore, in figure 4.46,

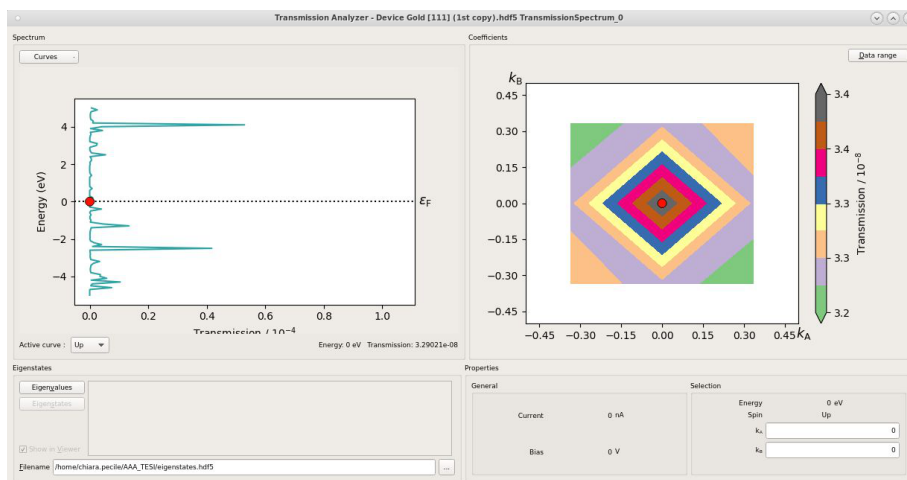


Figure 4.45. Transmission Analyzer in ATK: example for the third device Gd@C82 - IV.

you can see that the greater contribution is given by the d orbital.

After this step, I have studied the electrodes. As done before I have considered them in a separate way: respectively left and right. The obtained results are shown in the image 4.47, where is possible to notice that the major contribution is given by the p orbital in both cases.

In the end, in the image 4.48, you can see the DOS of the entire device (i.e. Gd@C82 - IV).

4.9.3 Molecular energy spectrum vs DDOS

Again, considering the basic theoretical concepts analyzed the subsection 4.3, it is possible to summarize that when a molecule is bounded to two metallic electrodes, an exchange of charge occurs between the molecule and two electrodes. This causes for sure a shift of the molecular energy states. In fig. 4.49 you can see the graph of DOS of the molecule of the case in exam (e.g. considering the influence of the electrodes) with the energy states of the molecule considered without the influence of the electrodes. It can be observed that, with the non negligible influence of the electrodes, the HOMOs and LUMOs are a bit shifted and broadened.

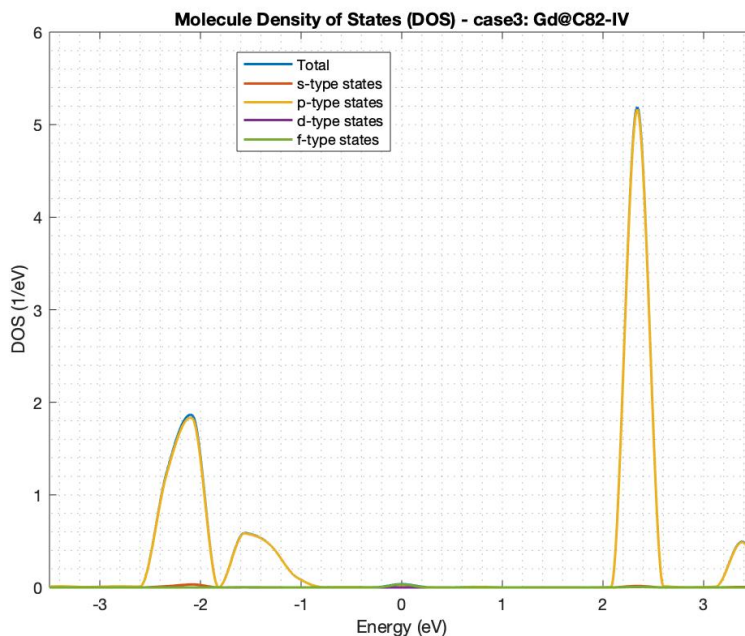


Figure 4.46. Device Density of States of the single Gd@C82 molecule - configuration IV (part of the third device).

4.10 Improvements

As done for the other two cases, I have proceeded doing some changes on the previous structure. I have shortened the distance between the electrodes and the molecule. Below you can see the new device realized for the third configuration Gd@C82-IV.

4.10.1 The new device: Gd@C82 - IV

The procedure followed is the same as in the previous cases. The distance between the molecule and the Au contacts has been shortened to reach the measure 2.4 Angstrom. Please refer to section 4.6 for more details.

In fig. 4.50 you can see the new device related to the third configuration: Gd@C82-IV. For the analysis I have proceeded as done before.

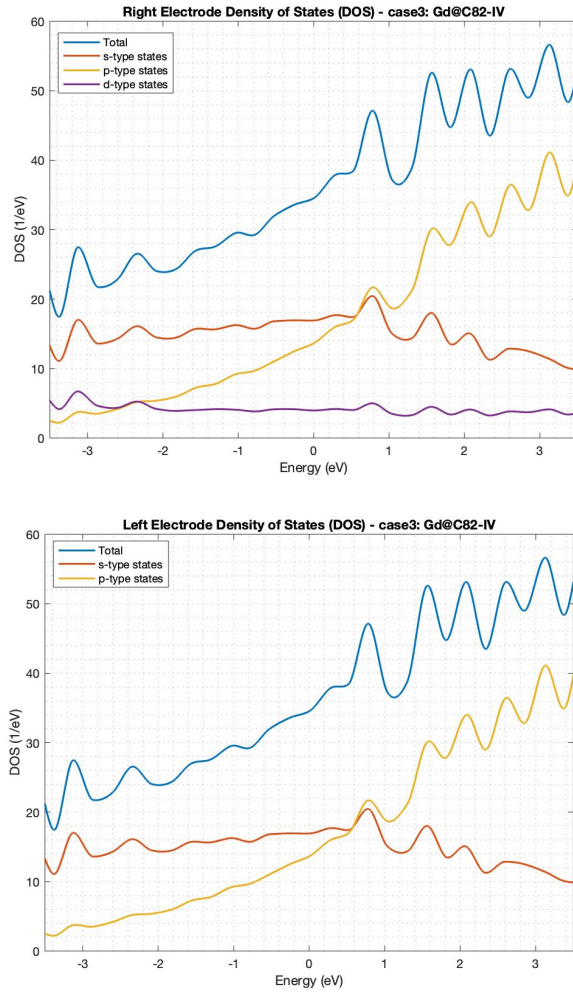


Figure 4.47. Device Density of States of the single electrodes, respectively left and right, reading from the top side (part of the third device in exam).

4.10.2 Transmission spectrum at the equilibrium

All the analysis has been performed in the same way as the previous cases (see 4.5.1), a part of the range of energies used. I have decided to reduce it in order to reduce the computational time. In the image 4.17 you can see the window of the settings used in this case.

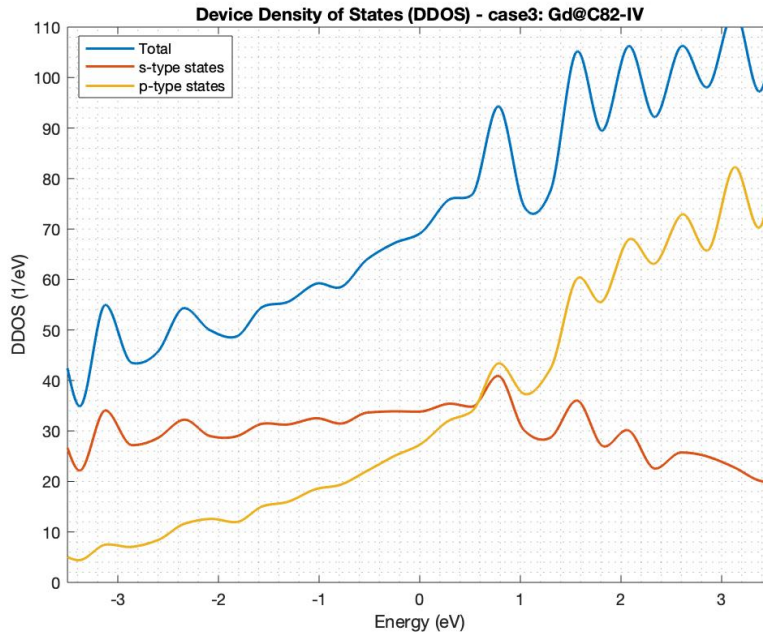


Figure 4.48. Device Density of States of the second device in exam.

Results and comments

Observing the graph 4.51, you can easily see that the transmittivity is increased a lot. As anticipated before, this was the expected result: the peaks are more broadened and we have passed from weak coupling to strong coupling. This is a very good point since we can now appreciate easily the behaviour of the device. In the conclusive chapter 5 you can then find the description of the behaviour obtained.

4.10.3 Density of state

The analysis of the DOS has been computed in the same way as reported in section 4.5.2. Below the results obtained are reported.

Results and comments

In the image 4.52 it is shown the DOS of the single Gd@C82 molecule. As in the previous case, it has been analyzed separately the different contributions of the

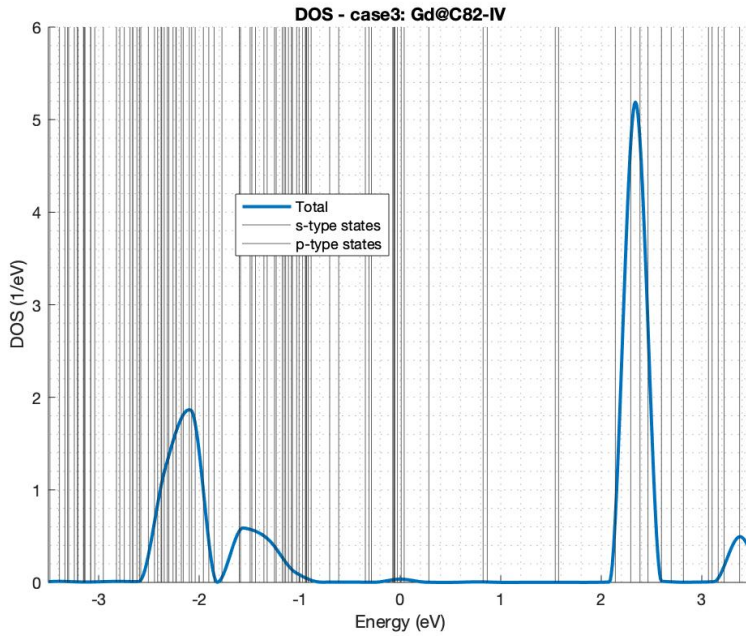


Figure 4.49. Device density of States vs Molecular energy spectrum - case 3: Gd@C82-IV.

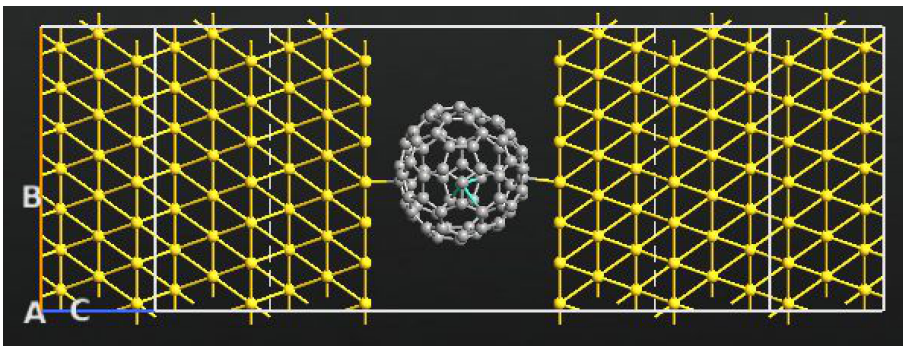


Figure 4.50. The new device - case 3: Gd@C82 - IV.

orbitals. It can be noted that the greatest contribution is given again by the p orbitals, but also by the f-type ones. The contribution of the p-type is described

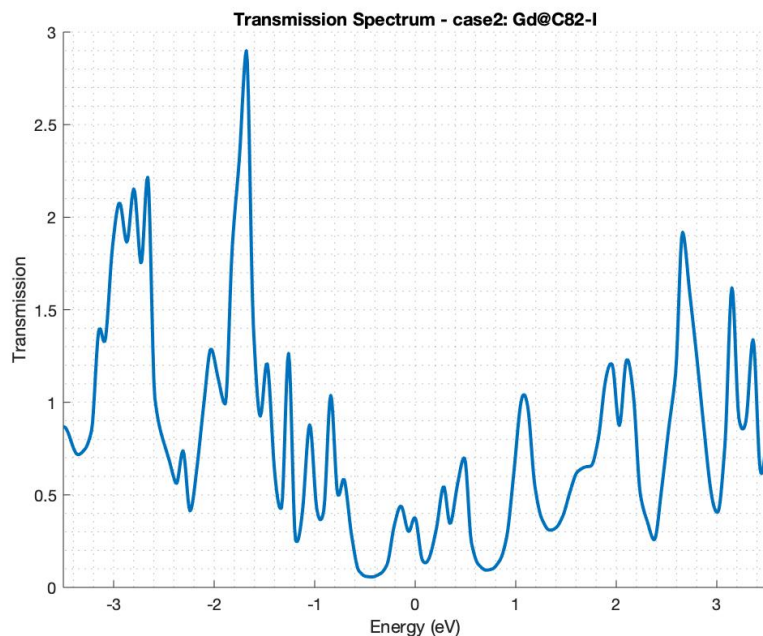


Figure 4.51. Transmission spectrum of the new device - case 3: Gd@C82-IV.

by the yellow line, the one of the f-type with green line and the blue line (that can be seen just in the extremely top of the peaks) describes the totality of the DOS of the molecule.

Then in fig. 4.53 it is possible to observe the final graph of the DOS of the entire device. It can be observed that are present just of one peak. Here the greatest contribution is given by the p-type states. It has to be said that this behaviour is dissimilar from the one obtained with the older device. In fact in this case the peak is much greater. Then in fig. 4.54 it is possible to observe the behaviour of the two different electrodes. Again you can see a big difference respect to the previous case, in fact the peaks now are described by a even greater amount but also they are very different between them. As in the previous case (e.g. Gd@G82-I new device), the major contribution to their final graph is given by p-type states in both cases.

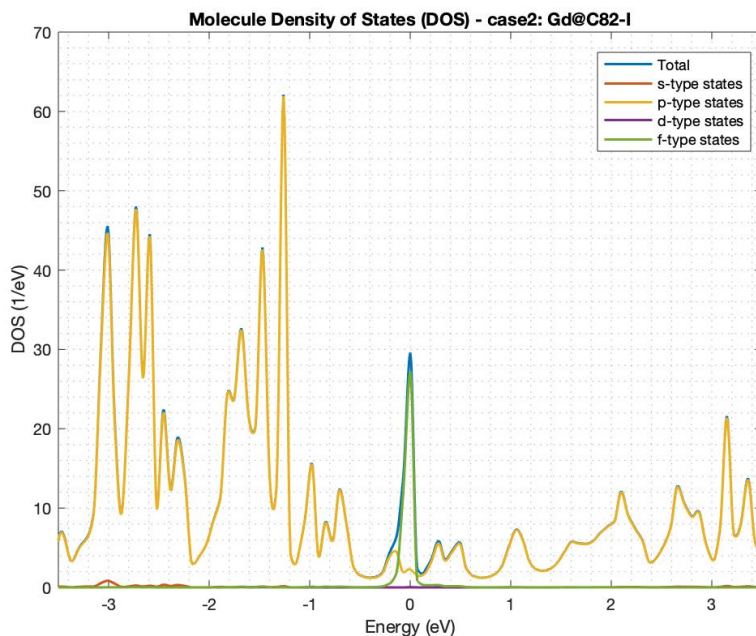


Figure 4.52. Device density of States of the Gd@C82 molecule of the new device - case 2: Gd@C82-I.

4.10.4 Molecular energy spectrum vs DDOS

Taking into account the basic theoretical concepts analyzed in subsection 4.3, we can summarize saying that when a molecule is bounded to two metallic electrodes, an exchange of charge occurs between the molecule and two electrodes. This leads to a shift of the molecular energy states. In fig. 4.55 you can again see this behaviour. In fact, in the graph it is reported the DOS of the Gd@C82 molecule of the case in exam (e.g. considering the influence of the electrodes) with the blue line and the energy states of the molecule considered without the influence of the electrodes (black lines).

4.10.5 IV characteristic

At this point, I have considered the IV curve study. In table 4.12 are reported the data obtained from the simulation.

In figure 4.56 you can find the plot of obtained results. Then, in the 5 section

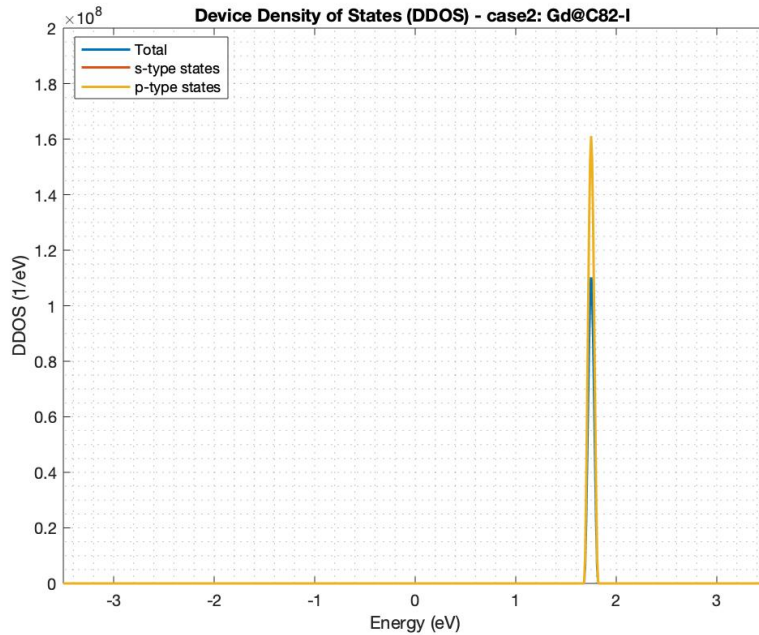


Figure 4.53. Device density of States of the entire new device - case 2: Gd@C82-I.

Bias (V)	Current (A)
0.000000	0.000000e+00
-0.100000	-2.361808e-06
-0.200000	-3.166265e-06
-0.300000	-4.075369e-06
-0.400000	-4.376760e-06
-0.500000	-6.836099e-06
0.100000	1.547168e-06
0.200000	4.513231e-06
0.300000	5.279078e-06
0.400000	7.928024e-06
0.500000	8.119042e-06

Table 4.12. IV curve report - case3, new device: Gd@C82-IV.

you can find different observations related to the differences between configuration I and IV.

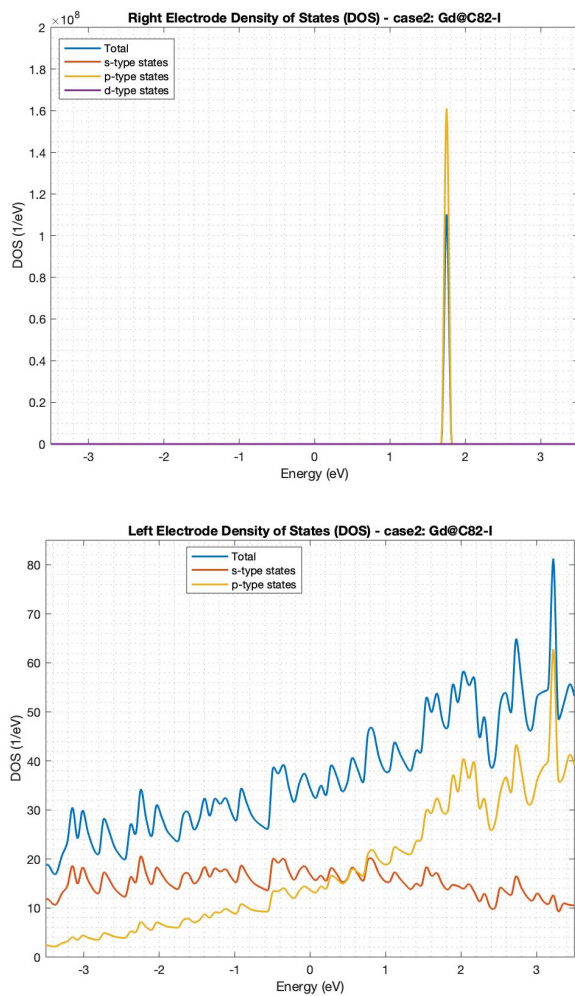


Figure 4.54. Device Density of States of the single electrodes, respectively right and left, reading from the top side - case 2: Gd@C82-I.

4.11 Nudged Elastic Band (NEB)

One of the main benefits provided by QuantumATK tool related to the study of electronic properties is the prediction on the reaction mechanisms using the Nudged Elastic Band (NEB) method [39].

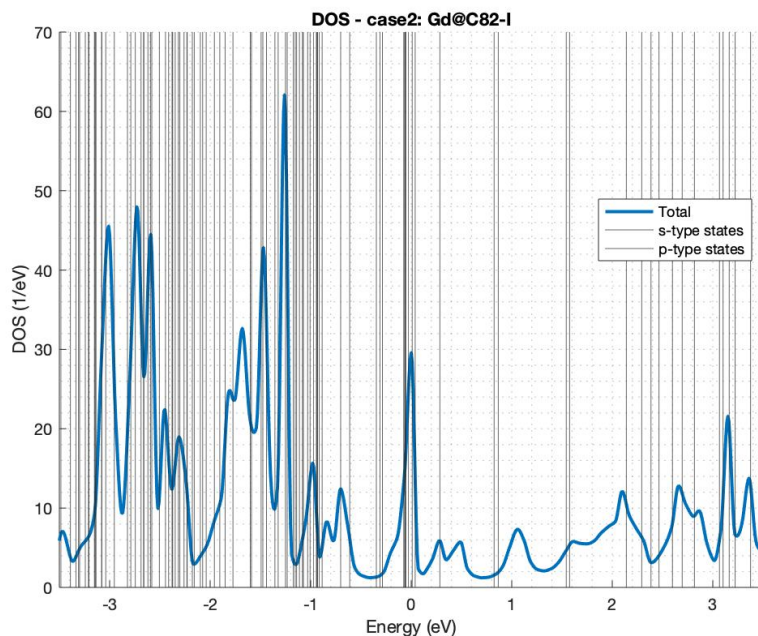


Figure 4.55. Device density of States vs Molecular energy spectrum - case 3: Gd@C82-IV.

This technique is used in order to uncover saddle points and minimum energy paths between the reactants and the products. It works by enhancing a few transitional images along the reaction path [52]. In individual image, the lowest energy achievable is found and the procedure evolves by maintaining equal spacing to adjacent images. In practical words, this "optimization" is forced by adding spring forces along the band between the images [52].

It has to be said that this can be certainly done with and without an electric field. Moreover it is performed considering also the analysis of transition states, reaction pathways and reaction barriers [39].

4.11.1 NEB tools in ATK and a bit of useful theory

The ATK program provides a NEB tool which allows to:

- Set up the wanted path;
- Edit the obtained images both individually or collectively;

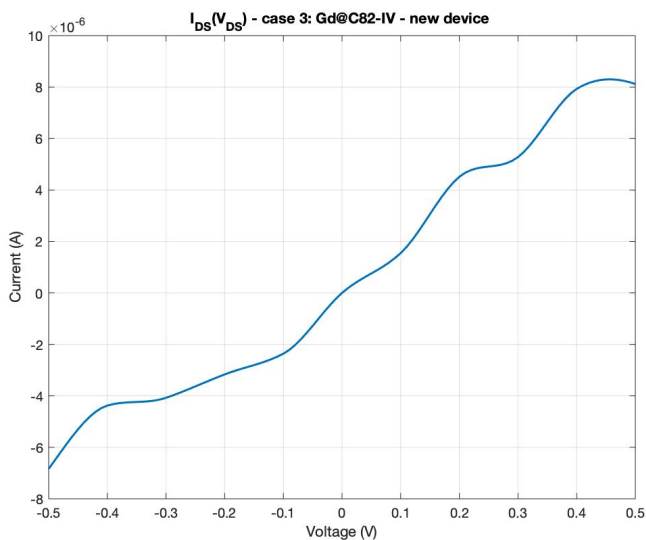


Figure 4.56. Plot of the IV curve - case 3: Gd@C82-IV, new device.

- Perform a preliminary optimized NEB path with the use of Image Dependent Pair Potentials (IDPP);
- Select the wanted algorithm for the interpolation (see later).

A deeper look

As you can also see later in the practical section 4.11.2, in order to perform the NEB calculation, the initial and final configurations have to be selected. At the beginning of a NEB computation, these geometries have to be optimized. This is done because it is important to minimize their energy (you can find more info in the section 3.5). Subsequently, it is done an approximation of the reaction path. Practically, a set of images is produced by means of an interpolation method that involves the initial and the final molecules, in this case [53]. It is possible to set the instructions to obtain also an intermediate. This can lead to a simplification of the process since the interpolation is done between the preliminary and intermediate state, and then between the intermediate and closing ones [53]. At the end, it is performed a concurrent optimization of all the images and so it is found the final reaction path. It must be said that in this process the images are not self-determining from each other, in fact every imaged depends on the neighboring one. For this reason, all the forces parallel to the reaction path obtained at each step

are deleted. So, a further "spring force" is added in order to maintain the middle images among their own neighbors. This allows to have a perfect distribution of the images (and so the different states) along the reaction path. To conclude, it must be precised that that NEB method is a computationally expensive method. In fact, it involves thousands of energy evaluations [53].

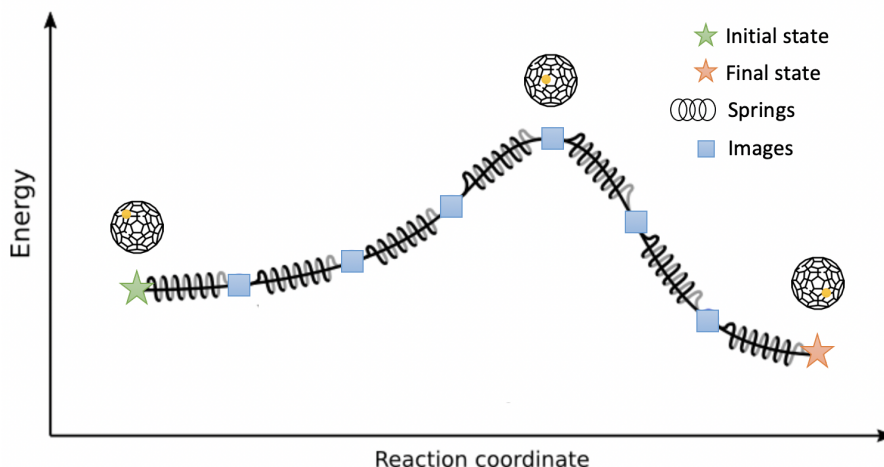


Figure 4.57. A practical example of the reaction path computed with NEB.

In figure 4.57 it is shown the NEB process. Starting from the initial system, in the path followed to reach the final structure, you can see the intermediate steps and so the related images. Between all the images you can see the added "spring forces" as explained before. The simulation at the end provides a scheme where it is possible to analyze the variation of the energy in correspondence of the variation of the configuration of the molecule in exam. In fact, on the y axis it is placed the energy (eV) and on the x axis the coordinates related to the reaction process.

4.11.2 NEB performed on the created structures

After having performed the simulations on the different created devices, I came back to the single molecules configurations: Gd@C82-I and Gd@C82-IV. The purpose of this section is to obtain the amount of energy needed to change configuration and so, in practical words, to move from figuration I to IV and viceversa.

The different steps are inspired by the tutorial provided by ATK manual (for more see [54]) and some further studies and tries done by myself.

First of all, in the *Builder* page of ATK I have selected the NEB window and set the two different configurations: the initial and the final one. I have firstly analyzed the case of the movement from I to IV. In the image 4.58 you can easily see the settings needed to create the NEB simulation process: the selection of the initial and final states, the selection of the method used for the interpolation and the maximum distance between the images. I have left the latter as default. As regards the interpolation algorithm, the ATK tools give us access to 3 different possibilities: LI - Linear Interpolation, HLC - Halgren Lipscomb and IDDP - Image Dependent Pair Potential [39]. I chose to select the linear one. After that, it is possible to proceed with the settings.

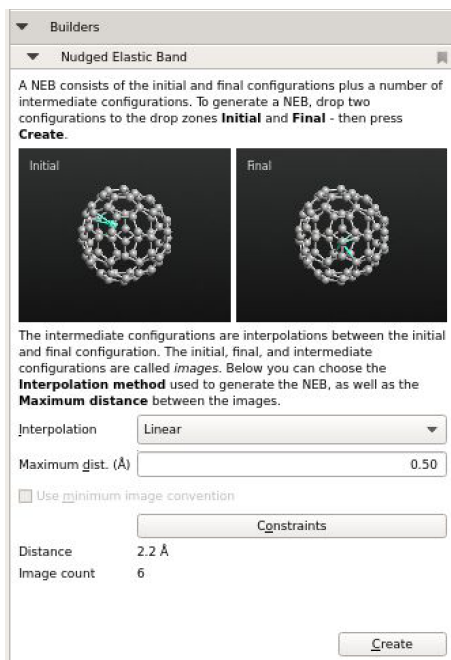


Figure 4.58. Creation of the NEB analysis. Since the NEB consist of the initial and final configurations, the tool requires them. In this case you can see the initial state Gd@C82-I and the final one Gd@C82-IV. The selected interpolation method is the linear one.

Later, after the creation of the NEB process, ATK provides a first sequence of states as you can observe in the image 4.59. Proceeding with the *Script Generator*, I have selected the *ForceFieldCalculator* (as suggested in the tutorial) and the *OptimizedGeometry* tool. This can be easily seen in fig. 4.60.

As regards the geometrical optimization, the NEB path is optimized using a limited-memory BFGS (l-BFGS) method. With this technique gives the optimized configuration as a combination of all NEB images. You can observe the other settings in fig. 4.62.

For the *ForceFieldCalculator*, the situation is more complex. In fact, with the ATK tool it is possible to select a huge amount of different analysis. Each of these analysis studies the relation between the different types of molecules. At this point, I have tried to select a setting that included both Gd and C. However this was not possible since the Default choices did not consider the Gd atom with C in general. So what I have decided to do is to select the Tersoff Single Type potential in the *Potential Editor* of the *ForceFieldCalculator* window and edit it in order to include the Gd specie. Tersoff Single Type potential is used to act between particles analyzing their interactions. In the screenshot 4.62 you can observe what I have done (I have left the values on the right by default).

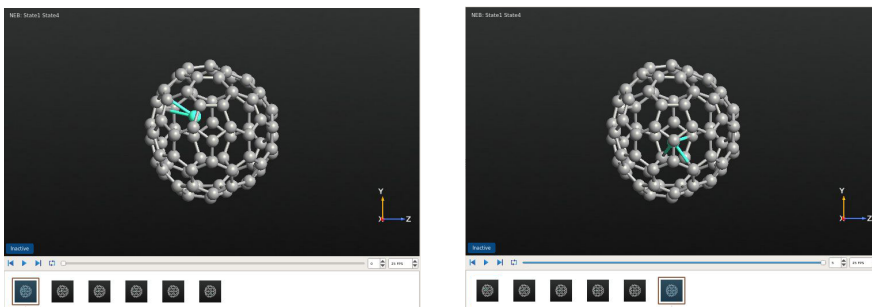


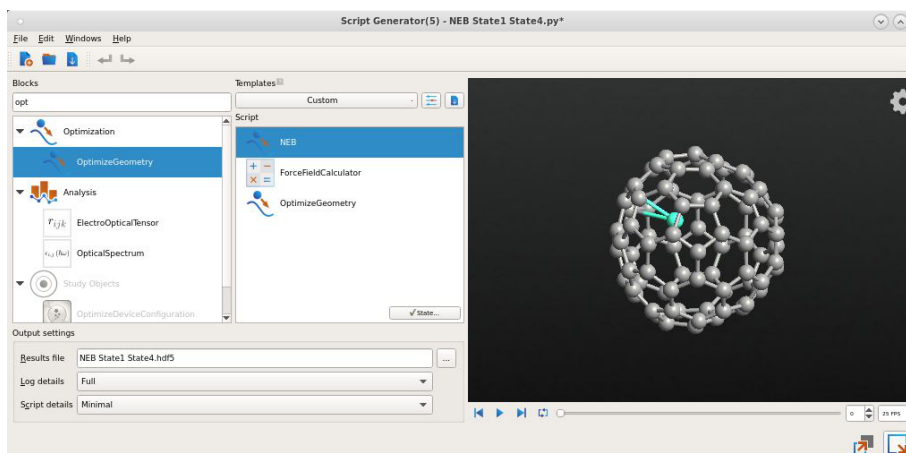
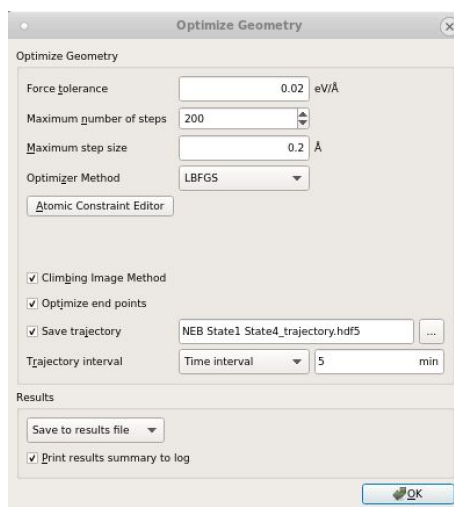
Figure 4.59. First sequence of states given by ATK, after the creation for the NEB analysis. In the first image Gd@C82-I, in the second one Gd@C82-IV. Below are shown the additional images.

4.11.3 Results and observations

In the case presented in the paper [4], the electrochemical potential that was necessary to pass from configuration I to IV is about +70 meV. On the other hand, in order to move from IV to I, it is necessary to employ an electrochemical potential of -87 meV. In fig. 4.63 you can see a practical scheme in order to appreciate this concept.

Considering the present case and so the structures analyzed in this work, the electrochemical potential needed to move from one configuration to the other is about 4 eV. In fig. 4.64 you can observe the graph that summarize the event.

This results have been obtained with ATK. Firstly, I have studied the movement

Figure 4.60. *Script Generator* of the NEB simulation.Figure 4.61. *Optimize Geometry* window of the NEB simulation.

from configuration I to IV. In the figures 4.65, 4.66 and 4.67 you can see the *NEB analyzer window* of the *movie tool*. In this window you can appreciate, on the left side, the Energy (eV) in function of the coordinated related to the reaction (Angstrom). On the right it is possible to see a video of the transition from one state to the other. Correspondingly to the movement of the right image, a grey

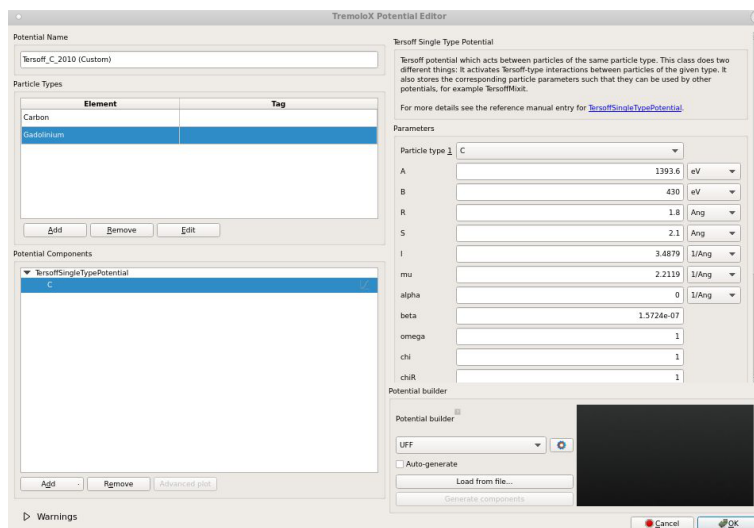


Figure 4.62. *Potential Editor* window of the NEB simulation (Forced Field calculator).

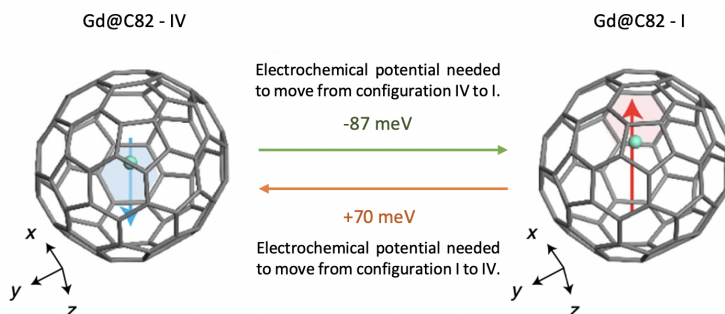


Figure 4.63. Needed energy to move from configuration I to IV (and viceversa) according to the analysis of the paper [4].

bar moves on the graph on the left in order to define the energy needed in that precise position.

In the image 4.65 you can see the initial state Gd@C82-I with an energy employed equal to 0 eV. Since for the reader it is not possible to observe the transition with the video given by ATK, in the following image 4.66 I have reported a "middle" position. I have chosen it randomly, but it is interesting to see the transition of the energy (grey vertical barrier on the graph).

Finally in fig. 4.67, it is possible to see the final state reached (Gd@C82-IV),

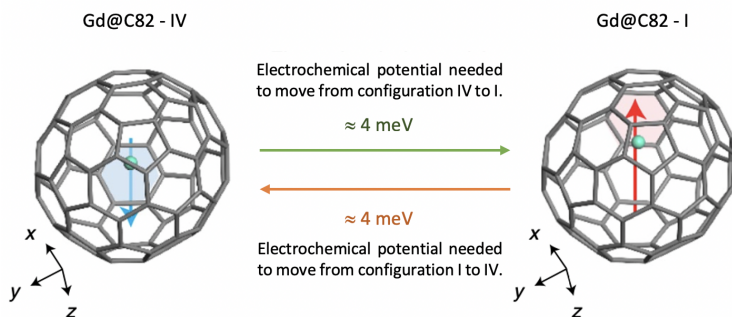


Figure 4.64. Needed energy to move from configuration I to IV (and viceversa) according to the analysis on the structures created in this work.

again the energy in that moment is 0 eV.

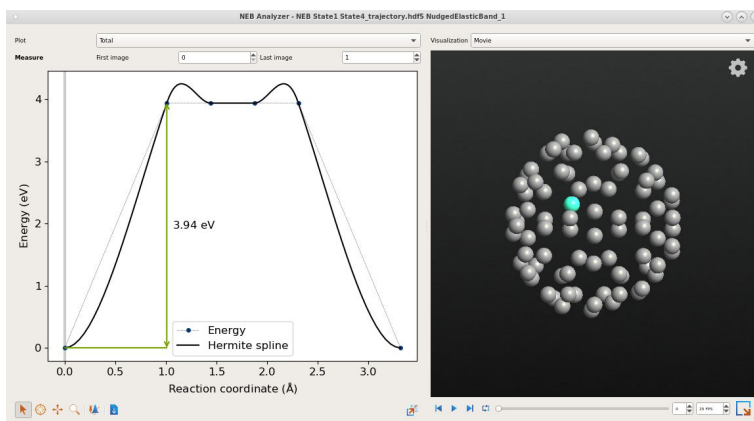


Figure 4.65. Needed energy to move from configuration I to IV, according to the analysis on the structures created in this work. In this picture, the Gd atom is in the starting position (Gd@C82-I).

The same has been done for the other case: moving from IV to I. As before I have reported here the initial and final state, but also a middle one chosen randomly (refer to figs. 4.68, 4.69 and 4.70).

With a first sight, the graphs seem the same in the two cases. In fact the energy needed is roughly 4 eV in both cases (3.93597 eV). There are two peaks present in correspondence of a translation of 1.2 Angstrom and 2.3 Angstrom. In the first

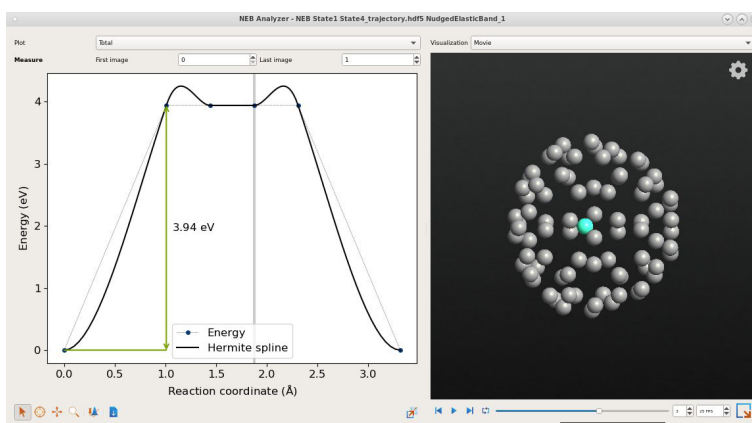


Figure 4.66. Needed energy to move from configuration I to IV, according to the analysis on the structures created in this work. In this picture, the Gd atom is in a "middle" position respect to the initial and final ones.

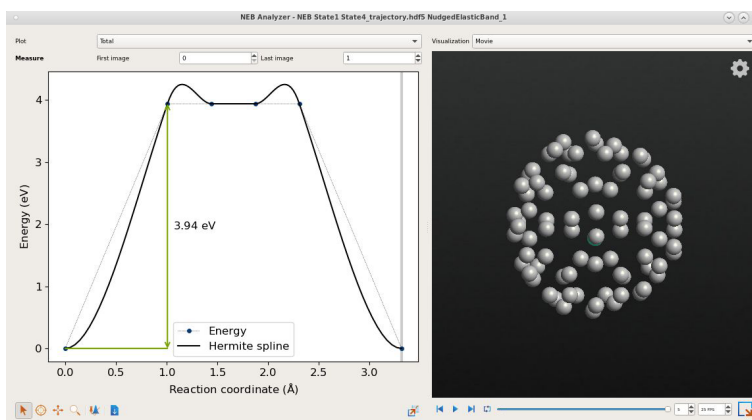


Figure 4.67. Needed energy to move from configuration I to IV, according to the analysis on the structures created in this work. In this picture, the Gd atom is in the final position (Gd@C82-IV).

analysis, so the one that considers the movement from configuration I to IV, the peaks reached a value of 4.19825 eV. On the other hand, the second analysis showed peaks of 4.23002 eV. So it is possible to see a small difference between the two cases. It can be said that for the first transition it is needed a bit lower amount of energy.

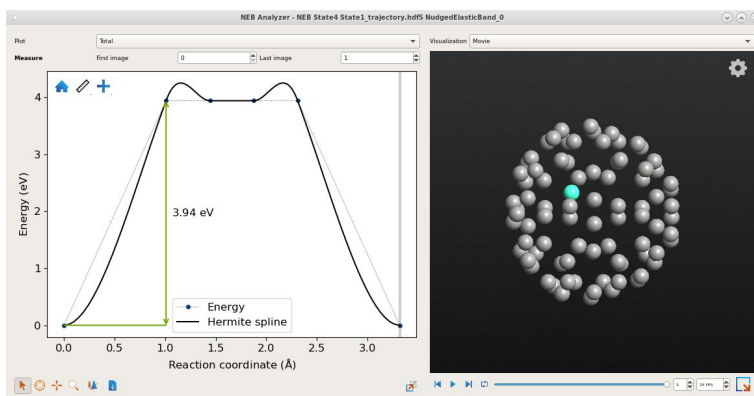


Figure 4.68. Needed energy to move from configuration IV to I, according to the analysis on the structures created in this work. In this picture, the Gd atom is in the starting position (Gd@C82-IV).

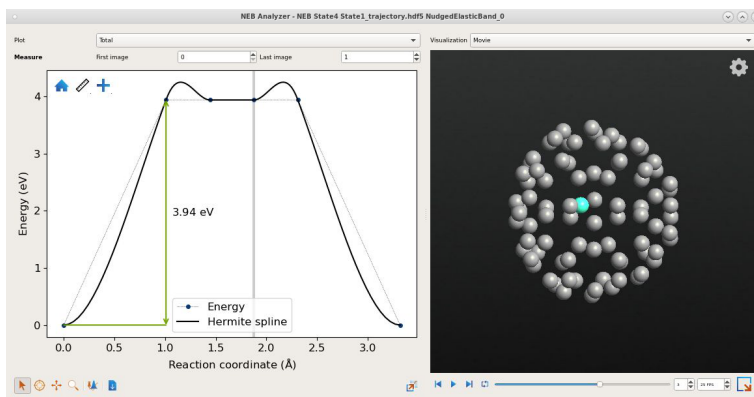


Figure 4.69. Needed energy to move from configuration IV to I, according to the analysis on the structures created in this work. In this picture, the Gd atom is in a "middle" position respect to the initial and final ones.

To conclude, it is important to observe that these results differ a lot respect to the ones presented in the paper [4]. This could be obviously expected since the structure is not the same. We can summarize the differences in different steps:

- Different C82 cage utilized. This for sure changes a lot the results since an alteration on the structure of the cage changes in turn the possible positions that can be used for the Gd atom inside it. The presence of dissimilar possible configurations gives rise to important changes in the result according to the

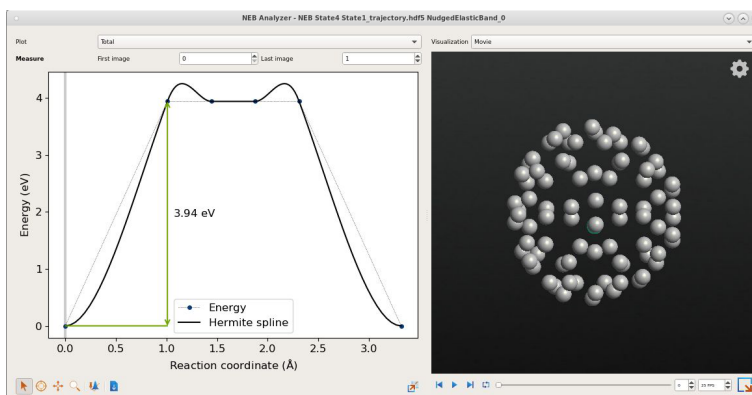


Figure 4.70. Needed energy to move from configuration IV to I, according to the analysis on the structures created in this work. In this picture, the Gd atom is in the final position (Gd@C82-I).

choices. The cage I have used in this work is similar but not the same respect to the one presented in the paper;

- Not exact position of the Gd atom, referring to the stable sites presented in literature. The procedure has been followed in a reasonable way, however possible issues can occur with a small error given by the distances of the Gd atom respect to the selected face of the cage.
- The usage of another tool and different settings: as explained before, for example, in fig. 4.62 I have reported the *Potential Editor* of the Forced Field Calculator which presents the settings I have made by myself. With a change on these settings it could be reached an important chance on the results.
- At the end it has also to be mentioned the tool that is utilized during the work.

Nevertheless, these consideration do not change the fact that in this work, all the procedures and the methods have been chosen in a reasoned way. So, it has to be said in the end, that the results obtained, even if they are very different respect to the ones obtained from the researchers, are logical and plausible.

Chapter 5

Conclusions

At the end of this work there are different details to be discussed. The first aspect to be mentioned is that the molecular scope is multidisciplinary. This means that it involves different fields of studying, above all Physics, Chemistry, Maths and Engineering. This factor plays a vital role in the effort that has to be computed by the researcher that wants to face this subject area. In fact, if we consider the present work, it has been very challenging for me, as Electronic Engineer, to "engineer" the device starting from a totally physical and chemical point of view. So it has to be said that the most complex and delicate steps in this field are the one involved to link all the different disciplines to fill the gap that strictly separates them. Indeed, in order to deal with the Single-Molecule Electret, especially at the beginning, I had to focus my studies on very theoretical aspects that I had not the pleasure to deepen during my Master courses. This includes not only Physical theory, but also a lot of Chemistry, which was the most tricky part for me.

The second one is for sure the fact that the information available on this topic, so on the Single-Molecule Electret, are very few and sometimes the material was not enough to perfectly act on the discovery of this so specific field. In section [5.2](#) you can find more considerations on this important aspect including the third aspect to be treated: the possible existence of other types of SMEs. This point is very interesting and for this reason I have dedicated an additional section to give some hints for future works ([5.2](#)).

Considering the obtained results on the new devices, the first think to note is the difference among the currents. In fact with the configuration IV, we have a lower current respect to the configuration I. This testifies a difference between the two different configurations. This results remark that the two position of the Gd atom lead to two different situations. But, at the end, if these currents are so

different and so maybe represent logic states 0 and 1, a memory cell based on this device could work? To know the answer you should go to section 5.1.

5.1 Comments and final application

Considering the obtained results, it is possible to see that there is a difference between the two different configurations.

If we consider the first three devices I have created, the current was very small (about few pA), however, except from the value, the behaviour is overall the wanted one. Moving to the three newest devices, the obtained current is much greater (uA) and also in this case we can appreciate the wanted behaviour. In fact, with the configuration I we have a greater current respect to the configuration IV.

These results remark that the two position of the Gd atom lead to two different situations. The first thing to say is that the study of the structure of the C82 cage has been made in a proper way. This is verified by the fact that there is a true existence of (at least) two stable sites inside the selected cage. In addition to this, the atom of Gd has been positioned in a right position. This has been done thanks to the study of the C82 cage and its different faces.

The difference between the currents can be easily seen in fig. 5.1. I am not referring to the differences among "new" and "old" devices, but on the dissimilarity that characterizes the different configurations of each "old" and "new" system. In other words Gd@C82-I and -IV. It could be said that the variation is not as big as expected. However, if we consider for example the bias point 0.5 V, we have a difference of 5.55 uA, which is measurable.

Can these differences be employed to represent logic states 0 and 1? Can then a memory cell based on this device work? The first question finds an answer in another simple question: why not? These dissimilarities can be measured and considered as two different states. Practically, configuration I could be considered 1 and IV could be considered 0.

With the purpose to try to answer to the second question, I have performed a further study related to electronic properties of the devices: the prediction on the reaction mechanisms using the Nudged Elastic Band (NEB) method. The obtained results in this case are very interesting, in fact I have obtained that it is possible to move from a configuration to the other employing 4 eV. In more practical words, this means that we need 4eV to pass from configuration I to IV, so from state 0 to state 1 and viceversa. If we think more "electronically", in terms of memory, this can be considered as that we need 4V to write 0 or 1. Then in order to read the information, we have to consider V_{DS} , which can be obtained analysing where we have the greatest difference between the current in state 1 and state 0, in this case

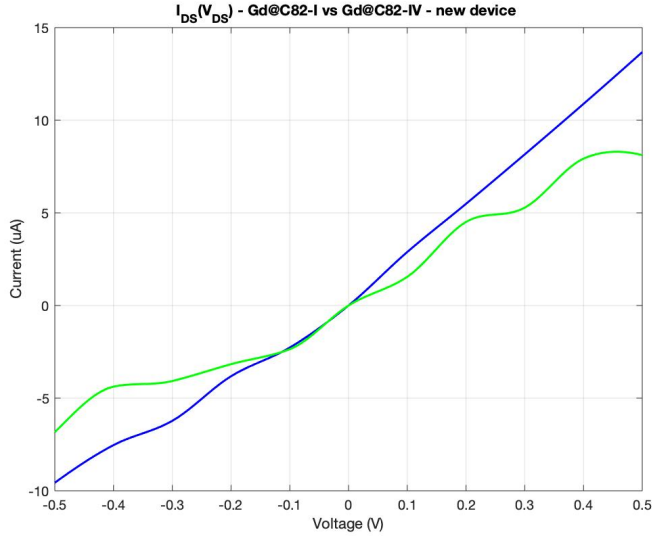


Figure 5.1. $I_{DS}(V_{DS})$ - Gd@C82-I vs Gd@C82-IV - new device. In blue Gd@C82-I and in green Gd@C82-IV.

0.5V.

Analysing, the behaviour obtained we can finally say that it works as a Flip-Flop of type Toggle. The toggle Flip-Flop is a type of bistable sequential logic circuit and it allows two functions:

- maintain the data in memory;
- complement the output, which is the negation of the previously stored value;

So, the toggle Flip-Flop can be used as a basic digital element for storing one bit of information. It has a single input and one or two complementary outputs.

In the present case, we need 4V in input to toggle (see 4.11.2), in the output we have the current which determines with its value the state "selected" (0 or 1). The data is maintained until we "toggle" again. It is important to know that in every electronic circuit, the internal voltage can not be greater than the supply voltage. So in this case we need V_{DS} at 4V. A further step on this work is for sure study the distinction on the behaviour using 4V for V_{DS} .

5.2 Future works

As announced before, it is very difficult to find in literature a lot of information on the Single-Molecule Electret. This is probably because it is a really new topic. This produces, not only difficulties in the study and learning of the subject, but also troubles if one wants to deepen some aspects.

However, at the same time, this is also one of the most fascinating aspects of this subject since it gives the true possibility to experiment. In fact, this such new and interesting topic allows to free our imagination and proceed in many different ways. As Walt Disney once said: "Fantasy and reality often overlap". This work is just a small crumb on all the infinite ways we could approach to this field.

It has to be said that the greatest amount of the decisions I made, was restricted to the time constraints I had (about 8 months). Without any type of limitations I would for sure chose another path, including for example the usage of a more accurate method for all the simulations. In fact, as I have anticipated during this work, one should always be prepared to move from a method to another and be aware that the ideas could change every second.

As anticipated in 2.5.3, there is an interesting question that one could ask: what about other SMEs? Again, there is not a lot of material available on this, just few mentions on the encapsulation of different species inside the C82 cage. However, at the end of this work, I had few ideas for possible future works that could be very interesting and useful for the growing of this new field.

A possible continuation of this report could be for sure to try to obtain a similar behaviour by changing the structure. This can be done in different ways:

- Choose another type of cluster, maintaining the same C82 cage. I have used the Gadolinium, but following the suggestions given in the paper [4], it would be interesting to analyze the behaviour obtained by using other species. For example: Lanthanum (La), Terbium (Tb), Dysprosium (Dy), Holmium (Ho) or the Erbium (Er).
- Change the C82 cage. This could be very useful, since maybe by choosing a smaller cage, the computational cost will reduce a lot. During this work, for all the simulations, the time was a non negligible aspects. In fact, to reach every result it took very long and I had to direct my decision in order to respect the time constraints I had. Moreover, reducing the computational cost, one could also be more free to choose the method of analysis reaching more precise results in lower time. Then it is remarkable that this change implies also the study of the different fullerene cage since all of them are characterized by different geometrical properties and, of course, in order to proceed in this way it is necessary to find a cage that exploits an asymmetry that could replicate at least two stable sites inside it.

- Finally, as a consequence, one could also change settings and so choose the best method that can give more accurate results. Another possible idea could be to redo this work, maintaining the same structures but changing method.

Chapter 6

Appendix

Matlab Code used for TS, DDOS and DDOS vs
MES - first device: C82 empty cage.

```
1  clc
2  clear all
3  %% Script for MES, DDOS, TS plot from QuantumWise ATK
4  %MES @ EQ of cage
5  fileID = fopen( 'MES_cage.txt' , 'r' );
6  formatSpec = '%f %f';
7  INData = textscan( fileID , formatSpec , 'HeaderLines' ,10);
8  fclose( fileID );
9  C82_EnergyLevels=INData{1,1};
10 C82_EnergyLevels=(C82_EnergyLevels) .';
11 occupancy=INData{1,2};
12
13 %DDOS @ EQ of device
14 fileID = fopen( 'DOS_cage_spdf.txt' , 'r' );
15 formatSpec = '%f %f';
16 INData = textscan( fileID , formatSpec , 'HeaderLines' ,6);
17 fclose( fileID );
18 C82_DDOS_E_mol=INData{1,2};
19 C82_DDOS_device=INData{1,1};
20 xx = -3.5:0.01:3.5;
21 yy_C82_DDOS_device=makima(C82_DDOS_E_mol, C82_DDOS_device ,
    xx);
22
```

```

23 fileID = fopen('DOS_cage_s.txt','r');
24 formatSpec = '%f %f';
25 INData = textscan(fileID,formatSpec,'HeaderLines',6);
26 fclose(fileID);
27 C82_DDOS_deviceS=INData{1,1};
28 yy_C82_DDOS_deviceS=makima(C82_DDOS_E_mol, C82_DDOS_deviceS
    ,xx);
29
30 fileID = fopen('DOS_cage_p.txt','r');
31 formatSpec = '%f %f';
32 INData = textscan(fileID,formatSpec,'HeaderLines',6);
33 fclose(fileID);
34 C82_DDOS_deviceP=INData{1,1};
35 yy_C82_DDOS_deviceP=makima(C82_DDOS_E_mol, C82_DDOS_deviceP
    ,xx);
36
37 %DDOS @ EQ of electrode dx
38 fileID = fopen('El_dx.txt','r');
39 formatSpec = '%f %f';
40 INData = textscan(fileID,formatSpec,'HeaderLines',6);
41 fclose(fileID);
42 C82_DDOS_E_mol=INData{1,2};
43 C82_DDOS_electrode_d=INData{1,1};
44 xx=-3.5:0.01:3.5;
45 yy_C82_DDOS_electrode_d=makima(C82_DDOS_E_mol,
    C82_DDOS_electrode_d ,xx);
46
47 fileID = fopen('El_dx_s.txt','r');
48 formatSpec = '%f %f';
49 INData = textscan(fileID,formatSpec,'HeaderLines',6);
50 fclose(fileID);
51 C82_DDOS_electrodeS_d=INData{1,1};
52 yy_C82_DDOS_electrodeS_d=makima(C82_DDOS_E_mol,
    C82_DDOS_electrodeS_d ,xx);
53
54 fileID = fopen('El_dx_p.txt','r');
55 formatSpec = '%f %f';
56 INData = textscan(fileID,formatSpec,'HeaderLines',6);
57 fclose(fileID);
58 C82_DDOS_electrodeP_d=INData{1,1};
59 yy_C82_DDOS_electrodeP_d=makima(C82_DDOS_E_mol,
    C82_DDOS_electrodeP_d ,xx);

```

```

60 fileID = fopen( 'El_dx_d.txt' , 'r' );
61 formatSpec = '%f %f' ;
62 INData = textscan( fileID , formatSpec , 'HeaderLines' ,6) ;
63 fclose( fileID );
64 C82_DDOS_electrodeD_dx=INData{1,1};
65 yy_C82_DDOS_electrodeD_dx=makima(C82_DDOS_E_mol,
66     C82_DDOS_electrodeD_dx, xx);
67
68 %DDOS @ EQ of electrode sx
69 fileID = fopen( 'El_sx.txt' , 'r' );
70 formatSpec = '%f %f' ;
71 INData = textscan( fileID , formatSpec , 'HeaderLines' ,6) ;
72 fclose( fileID );
73 C82_DDOS_E_sx=INData{1,2};
74 C82_DDOS_electrode_sx=INData{1,1};
75 xx = -3.5:0.01:3.5;
76 yy_C82_DDOS_electrode_sx=makima(C82_DDOS_E_sx,
77     C82_DDOS_electrode_sx ,xx);
78
79 fileID = fopen( 'El_sx_s.txt' , 'r' );
80 formatSpec = '%f %f' ;
81 INData = textscan( fileID , formatSpec , 'HeaderLines' ,6) ;
82 fclose( fileID );
83 C82_DDOS_electrodeS_sx=INData{1,1};
84 yy_C82_DDOS_electrodeS_sx=makima(C82_DDOS_E_sx,
85     C82_DDOS_electrodeS_sx ,xx);
86
87 fileID = fopen( 'El_sx_p.txt' , 'r' );
88 formatSpec = '%f %f' ;
89 INData = textscan( fileID , formatSpec , 'HeaderLines' ,6) ;
90 fclose( fileID );
91 C82_DDOS_electrodeP_sx=INData{1,1};
92 yy_C82_DDOS_electrodeP_sx=makima(C82_DDOS_E_sx,
93     C82_DDOS_electrodeP_sx ,xx);
94
95 fileID = fopen( 'El_sx_d.txt' , 'r' );
96 formatSpec = '%f %f' ;
97 INData = textscan( fileID , formatSpec , 'HeaderLines' ,6) ;
98 fclose( fileID );
99 C82_DDOS_electrodeD_sx=INData{1,1};

```

```
97 yy_C82_DDOS_electrodeD_sx=makima(C82_DDOS_E_sx,  
   C82_DDOS_electrodeD_sx ,xx);  
98  
99 %DDOS @ EQ of C82 molecule  
100 fileID = fopen('cage_dos_mol_sp.txt','r');  
101 formatSpec = '%f %f';  
102 INData = textscan(fileID ,formatSpec , 'HeaderLines' ,6);  
103 fclose(fileID);  
104 C82_DDOS_E_mol=INData{1,2};  
105 C82_DDOS_molecule=INData{1,1};  
106 xx_dos = -3.5:0.01:3.5;  
107 yy_C82_DDOS_molecule=makima(C82_DDOS_E_mol,  
   C82_DDOS_molecule , xx_dos);  
108  
109 fileID = fopen('cage_dos_mol_s.txt','r');  
110 formatSpec = '%f %f';  
111 INData = textscan(fileID ,formatSpec , 'HeaderLines' , 6);  
112 fclose(fileID);  
113 C82_DDOS_molecules=INData{1,1};  
114 yy_C82_DDOS_molecules=makima(C82_DDOS_E_mol,  
   C82_DDOS_molecules ,xx);  
115  
116 fileID = fopen('cage_dos_mol_p.txt','r');  
117 formatSpec = '%f %f';  
118 INData = textscan(fileID ,formatSpec , 'HeaderLines' ,6);  
119 fclose(fileID);  
120 C82_DDOS_moleculeP=INData{1,1};  
121 yy_C82_DDOS_moleculeP=makima(C82_DDOS_E_mol,  
   C82_DDOS_moleculeP , xx);  
122  
123  
124 %%%%%%%%%%%%%%%%%%%%%%%%%%%%%%%%%%%%%%%%%%%%%%%%%%%%%%%%%%  
125 %TS @ EQ of C882 empty cage  
126 fileID = fopen('TS_cage.txt','r');  
127 formatSpec = '%f %f';  
128 INData = textscan(fileID ,formatSpec , 'HeaderLines' ,2);  
129 fclose(fileID);  
130 C82_TS_E=INData{1,2};  
131 C82_TS=INData{1,1};  
132 xx_ts = -3.5:0.01:3.5;  
133 yy_C82_TS=makima(C82_TS_E, C82_TS, xx_ts);  
134 %%%%%%%%%%%%%%%%%%%%%%%%%%%%%%%%%%%%%%%%%%%%%%%%%%%%%%%%%%
```

```

135
136
137
138 %%plots
139 figure(1)
140 plot(xx_dos, yy_C82_DDOS_molecule, 'LineWidth', 2);
141 grid minor
142 box off
143 title_string = sprintf('DOS - case1: C82 cage');
144 title(title_string);
145 xlabel('Energy (eV)');
146 xlim([-3.5 3.55]);
147 ylim([0 100]);
148 for i = 1:length(C82_EnergyLevels)
149 xline(C82_EnergyLevels(i), '-', 'LineWidth', 0.5);
150 end
151 legend('Total', 's-type states', 'p-type states', 'Location
', 'Best');
152 ylabel('DOS (1/eV)');
153 set(gca, 'fontsize', 10);
154
155
156 figure(2)
157 plot(xx, yy_C82_DDOS_device, xx, yy_C82_DDOS_deviceS, xx,
yy_C82_DDOS_deviceP, 'LineWidth', 1.5);
158 grid minor
159 title_string = sprintf('Device Density of States (DDOS) -
case1: C82 cage ');
160 title(title_string);
161 xlabel('Energy (eV)');
162 xlim([-3.5 3.5]);
163 ylim([0 1000000000]);
164 legend('Total', 's-type states', 'p-type states', 'Location
', 'Best');
165 ylabel('DDOS (1/eV)');
166 set(gca, 'fontsize', 10);
167
168
169 figure(3)
170 plot(xx, yy_C82_DDOS_molecule, xx, yy_C82_DDOS_moleculeS,
xx, yy_C82_DDOS_moleculeP, 'LineWidth', 1.5);
171 grid minor

```

```

172 title_string = sprintf('Molecule Density of States (DOS) –
      case1: C82 cage ');
173 title(title_string);
174 xlabel('Energy (eV)');
175 xlim([-3.5 3.5])
176 ylim([0 100]);
177 legend('Total', 's-type states', 'p-type states', 'Location
      ', 'Best');
178 ylabel('DOS (1/eV)');
179 set(gca, 'fontsize', 10);
180
181
182 figure(4)
183 plot(xx, yy_C82_DDOS_electrode_d, xx,
      yy_C82_DDOS_electrodeS_d, xx, yy_C82_DDOS_electrodeP_d,
      xx, yy_C82_DDOS_electrodeD_dx, 'LineWidth', 1.5);
184 grid minor
185 title_string = sprintf('Right Electrode Density of States (
      DOS) – case1: C82 cage ');
186 title(title_string);
187 xlabel('Energy (eV)');
188 xlim([-3.5 3.5]);
189 ylim([0 1100000000]);
190 legend('Total', 's-type states', 'p-type states', 'd-type
      states', 'Location', 'Best');
191 ylabel('DOS (1/eV)');
192 set(gca, 'fontsize', 10);
193
194 figure(5)
195 plot(xx, yy_C82_DDOS_electrode_sx, xx,
      yy_C82_DDOS_electrodeS_sx, xx, yy_C82_DDOS_electrodeP_sx
      , xx, yy_C82_DDOS_electrodeD_sx, 'LineWidth', 1.5);
196 grid minor
197 title_string = sprintf('Left Electrode Density of States (
      DOS) – case1: C82 cage ');
198 title(title_string);
199 xlabel('Energy (eV)');
200 xlim([-3.5 3.5]);
201 ylim([0 11000000]);
202 legend('Total', 's-type states', 'p-type states', 'd-type
      states', 'Location', 'Best');
203 ylabel('DOS (1/eV)');

```

```

204 set(gca, 'fontsize', 10);
205
206
207
208 figure(6)
209 plot(xx_ts, yy_C82_TS, 'LineWidth', 2);
210 grid minor
211 box off
212 title_string = sprintf('Transmission Spectrum - case1: C82
    cage ');
213 title(title_string);
214 xlabel('Energy (eV)');
215 xlim([-3.5 3.5])
216 ylim([0 3]);
217 ylabel('Transmission');
218 set(gca, 'fontsize', 10);
219
220
221 figure(7)
222 semilogy(xx_ts, yy_C82_TS, 'LineWidth', 2);
223 grid minor
224 box off
225 title_string = sprintf('Transmission Spectrum - case1: C82
    cage ');
226 title(title_string);
227 xlabel('Energy (eV)');
228 xlim([-3.5 3.5])
229 ylim([0 8])
230 ylabel('Transmission');
231 set(gca, 'fontsize', 10);

```

Matlab Code used for IV curve: old device, new device and old vs new - first device: C82 empty cage.

```

1 %% Plot IV curve from QAIK
2 clc
3 clear all
4
5 % Old device
6 fileID = fopen('IV_cage_old.txt', 'r');

```

```
7 formatSpec = '%f %f';
8 INData = textscan(fileID ,formatSpec , 'HeaderLines' ,1);
9 fclose(fileID);
10
11 Vds_old=INData{1,1};
12 Ids_old=INData{1,2};
13
14 xx_Vds_old = -0.5:0.01:0.5;
15 yy_Ids_old=makima(Vds_old , Ids_old ,xx_Vds_old);
16
17
18 % New device
19 fileID = fopen('IV_cage_new.txt','r');
20 formatSpec = '%f %f';
21 INData = textscan(fileID ,formatSpec , 'HeaderLines' ,1);
22 fclose(fileID);
23
24 Vds_new=INData{1,1};
25 Ids_new=INData{1,2};
26
27 xx_Vds_new = -0.5:0.01:0.5;
28 yy_Ids_new=makima(Vds_new , Ids_new ,xx_Vds_new);
29
30
31
32 figure(1)
33 plot(xx_Vds_old , yy_Ids_old , 'LineWidth' , 1.5);
34 grid ON
35 title_string = sprintf('I_{DS}(V_{DS}) - case 1: empty C82
36 cage - old device ');
37 title(title_string);
38 xlabel('Voltage (V)');
39 xlim([-0.5 0.5])
40 ylabel('Current (A)');
41 set(gca , 'fontsize' , 10);
42
43
44 figure(2)
45 plot(xx_Vds_new , yy_Ids_new , 'LineWidth' , 1.5);
46 grid ON
```

```

47 title_string = sprintf('I_{DS}(V_{DS}) - case 1: empty C82
    cage - new device ');
48 title(title_string);
49 xlabel('Voltage (V)');
50 xlim([-0.5 0.5])
51 ylabel('Current (A)');
52 set(gca, 'fontsize', 10);
53
54
55
56 figure(3)
57 semilogy(xx_Vds_new, yy_Ids_new, xx_Vds_old, yy_Ids_old, '
    LineWidth', 1.5);
58 %plot(xx_Vds_new, yy_Ids_new, xx_Vds_old, yy_Ids_old, '
    LineWidth', 1.5);
59 grid ON
60 title_string = sprintf('I_{DS}(V_{DS}) - case 1: empty C82
    cage - old vs new device ');
61 title(title_string);
62 xlabel('Voltage (V)');
63 xlim([0 0.5])
64 ylabel('Current (A)');
65 set(gca, 'fontsize', 10);

```

Matlab Code used to compare the IV curves of the two different configurations: Gd@C82-I and Gd@C82-IV new.

```

1 %% Comparison of the plots IV curve from QATK: Gd@C82-I vs
    Gd@C82-IV
2 clc
3 clear all
4
5 % device Gd@C82-I
6 fileID = fopen('IV_I_new.txt', 'r');
7 formatSpec = '%f %f';
8 INData = textscan(fileID, formatSpec, 'HeaderLines', 1);
9 fclose(fileID);
10
11 Vds_I=INData{1,1};
12 Ids_I=INData{1,2}*10^6;

```

```
13
14 xx_Vds_I = -0.5:0.01:0.5;
15 yy_Ids_I = makima(Vds_I, Ids_I ,xx_Vds_I);
16
17
18 % device Gd@C82-IV
19 fileID = fopen('IV_IV_new.txt','r');
20 formatSpec = '%f %f';
21 INData = textscan(fileID ,formatSpec , 'HeaderLines' ,1);
22 fclose(fileID);
23
24 Vds_IV = INData{1,1};
25 Ids_IV = INData{1,2} * 10^6;
26
27 xx_Vds_IV = -0.5:0.01:0.5;
28 yy_Ids_IV = makima(Vds_IV, Ids_IV ,xx_Vds_IV);
29
30
31 figure
32 plot(xx_Vds_I, yy_Ids_I, '-b', xx_Vds_IV, yy_Ids_IV, '-g',
33      'LineWidth', 1.5);
34 %semilogy(xx_Vds_new, yy_Ids_new, xx_Vds_old, yy_Ids_old, '
35      LineWidth', 1.5);
36 grid ON
37 title_string = sprintf('I_{DS}(V_{DS}) - Gd@C82-I vs Gd@C82
38      -IV - new device ');
39 title(title_string);
40 xlabel('Voltage (V)');
41 xlim([-0.5 0.5])
42 ylabel('Current (uA)');
43 set(gca, 'fontsize', 10);
```

Bibliography

- [1] Microelectronic Circuit Design, 4Th Edition. Authors(s): Richard C Jaeger and Travis Blalock.
- [2] Medium, *Highlights from the Nanoelectronics for 2020 and Beyond (Nanoelectronics) NSI*. <https://www.nano.gov/node/1932>. Accessed 22/06/2021
- [3] Medium, *Tube versus solid state: The truth behind tube distortion*. <http://www.tonestack.net/articles/guitar-amps/tube-vs-solid-state.html> Accessed 27/06/2021
- [4] Gd@C82 single-molecule electret: Zhang, K., Wang, C., Zhang, M. et al. A Gd@C82 single molecule electret. *Nat. Nanotechnol.* 15, 1019 1024 (2020). <https://doi.org/10.1038/s41565-020-00778-z>.
- [5] Welcome to the single-molecule electret device, Nishihara, Sadafum.
- [6] Electronic structures and spectral properties of endohedral fullerenes. Suchi Guhaa, Kazuo Nakamoto - Department of Physics and Astronomy, University of Missouri, Columbia, MO 65211, USA and Department of Chemistry, Marquette University, P.O. Box 1881, Milwaukee, WI 53217, USA Received 29 September 2004; accepted 8 November 2004 - Available online 5 January 2005.
- [7] Article: Spin resolved electronic transport through N@C20 fullerene molecule between Au electrodes: A first principles study. Author links open overlay SerkanCaliskan - Department of Physics, Georgia Southern University, 30460, Statesboro, GA, USA Received 20 December 2017, Revised 14 January 2018, Accepted 20 January 2018, Available online 20 February 2018.
- [8] Endohedral fullerenes: the importance of electronic, size and shape complementarity between the carbon cages and the corresponding encapsulated clusters. Maira R. Ceron, Fang Fang Lia and Luis A. Echegoyena. Published online in Wiley Online Library: 9 January 2014 (wileyonlinelibrary.com) DOI: 10.1002/poc.3245
- [9] Medium, *Atomic and Molecular Endofullerenes: Spins in a box*.

- <https://gow.epsrc.ukri.org/NGBOViewGrant.aspx?GrantRef=EP/T004320/1> Accessed 23/09/2021
- [10] Medium, *1,2,4-triazines*. <https://www.sciencedirect.com/topics/chemistry/1-2-4-triazines> Accessed 24/09/2021
- [11] Chemistry of Nanocarbons - by Takeshi Akasaka, Fred Wudl and Shigeru Nagase - PUBLISHER: John Wiley Sons, DATE: 2010-07-26
- [12] Medium, *The dipolar endofullerene HF@C60*. <https://www-nature-com.ezproxy.biblio.polito.it/articles/nchem.2563.pdf> Accessed 24/09/2021
- [13] An Introduction to Fullerene Structures, Geometry and Symmetry - W. O. J. Boo The University of Mississippi, University, MS 38677
- [14] Gd@C 82 Fullerenol; by Huiming Zhang. In: Molecular Imaging and Contrast Agent Database (MICAD) [Internet]. Bethesda (MD): National Center for Biotechnology Information (US); 2004 2013. 2008 Oct 31 [updated 2008 Dec 1].
- [15] Supramolecular chemistry of fullerenes. Author: Harold W. Krotom, Publication: Tetrahedron, Publisher: Elsevier, Date: 27 February 2006
- [16] Medium, *Fullerene, chemical compound*. <https://www.britannica.com/science/fullerene> Accessed 28/06/2021
- [17] C60 Fullerene Derivatized Nanoparticles and their Application to Therapeutics. Author(s): Chun Mao Lin, Tan Yi Lu. Journal Name: Recent Patents on Nanotechnology - Volume 6, Issue 2, 2012.
- [18] What Are the Ground State Structures of C20 and C24? An Explicitly Correlated Ab Initio Approach. Debashree Manna and Jan M. L. Martin* <https://pubs.acs.org/doi/10.1021/acs.jpca.5b10266>
- [19] Medium, *Fullerene chemistry*. https://www.wikiwand.com/en/Fullerene_chemistry Accessed 28/06/2021
- [20] Medium, *Nonpolar compound*. <https://medical-dictionary.thefreedictionary.com/nonpolar+compound> Accessed 05/07/2021
- [21] Medium, *TYPES OF FULLERENES AND THEIR SPECIFIC USES (C60, C70, FULLERENOLS)*. <https://nanografi.com/blog/types-of-fullerenes-and-their-specific-uses-c60-c70-fullerenols/> Accessed 22/06/2021
- [22] Medium, *Highly energetic compositions based on functionalized carbon nanomaterials*. <https://pubs.rsc.org/en/content/articlehtml/2016/nr/c5nr07855e>. Accessed 30/06/2021
- [23] Medium, *Aromatic*. <http://www.ilpi.com/msds/ref/aromatic.html>. Accessed 28/06/2021

- [24] Medium, *Properties of Aromatic Compounds*. <https://courses.lumenlearning.com/introchem/chapter/properties-of-aromatic-compounds/>. Accessed 30/06/2021
- [25] Kwan Chi Kao, 5; Electrets, Editor(s): Kwan Chi Kao, Dielectric Phenomena in Solids, Academic Press, 2004, Pages 283-326, ISBN 9780123965615, <https://doi.org/10.1016/B978-012396561-5/50015-3>. <https://www.sciencedirect.com/science/article/pii/B9780123965615500153>
- [26] Medium, *THESIS Presented to the Faculty of the Division of Graduate Studies Georgia Institute of Technology*. https://smartech.gatech.edu/bitstream/handle/1853/13458/shalloway_arthur_m_195105_ms_108577.pdf Accessed 22/06/2021
- [27] Medium, *Which of the following is a crystalline allotrope of carbon?*. <https://www.toppr.com/ask/en-th/question/which-of-the-following-is-a-crystalline-allotrope-of-carbon/> Accessed 29/06/2021
- [28] R. K. Cavin, P. Lugli and V. V. Zhirnov, "Science and Engineering Beyond Moore's Law," in Proceedings of the IEEE, vol. 100, no. Special Centennial Issue, pp. 1720-1749, 13 May 2012, doi: 10.1109/JPROC.2012.2190155.
- [29] Medium, *Moore's Law*. <https://corporatefinanceinstitute.com/resources/knowledge/other/moores-law/> Accessed 29/06/2021
- [30] A. A. Chien and V. Karamcheti, "Moore's Law: The First Ending and a New Beginning," in Computer, vol. 46, no. 12, pp. 48-53, Dec. 2013, doi: 10.1109/MC.2013.431.
- [31] Single Molecule Electronic Devices - Authors: Hyunwook Song, Mark A. Reed, Takhee Lee
- [32] Medium, *The Non-Equilibrium Green's Function (NEGF) Formalism: An Elementary Introduction*. <https://ieeexplore-ieee-org.ezproxy.biblio.polito.it/stamp/stamp.jsp?tp=&arnumber=1175935> Accessed 14/07/2021
- [33] Medium, *Density Functional Theory*. <http://www.fisica.uniud.it/~giannozz/Didattica/MetNum/LectureNotes/metnum-cap2.pdf> Accessed 14/07/2021
- [34] Kurt Stokbro, Dan Erik Petersen, Søren Smidstrup, Anders Blom, and Mads Ipsen. «Semiempirical model for nanoscale device simulations». In: Physical review B 82.075420 (2010). doi: 10.1103/PhysRevB.82.075420.
- [35] Medium, *The stabilization of fused-pentagon fullerene molecules*. <https://pubmed.ncbi.nlm.nih.gov/21378913/> Accessed

- 15/07/2021
- [36] Medium, *Gadolinium - Gd*. <https://www.lenntech.com/periodic/elements/gd.htm> Accessed 15/07/2021
- [37] Medium, *Electret Energy Harvester*. <http://tikalon.com/blog/blog.php?article=2011/electret> Accessed 23/06/2021
- [38] Medium, *Why some reaction have no transition state?*. <https://chemistry.stackexchange.com/questions/98424/why-some-reaction-have-no-transition-state> Accessed 05/07/2021
- [39] Medium, *QuantumATK S-2021.06 Documentation*. <https://docs.quantumatk.com/index.html> Accessed 08/07/2021
- [40] Medium, *ELECTRONEGATIVITY*. <https://www.chemguide.co.uk/atoms/bonding/electroneg.html> Accessed 12/07/2021
- [41] Medium, *Mulliken Electronegativity*. [https://chem.libretexts.org/Bookshelves/Physical_and_Theoretical_Chemistry_Textbook_Maps/Supplemental_Modules_\(Physical_and_Theoretical_Chemistry\)/Physical_Properties_of_Matter/Atomic_and_Molecular_Properties/Electronegativity/Mulliken_Electronegativity](https://chem.libretexts.org/Bookshelves/Physical_and_Theoretical_Chemistry_Textbook_Maps/Supplemental_Modules_(Physical_and_Theoretical_Chemistry)/Physical_Properties_of_Matter/Atomic_and_Molecular_Properties/Electronegativity/Mulliken_Electronegativity) Accessed 12/07/2021
- [42] Medium, *Ionization Energy and Electron Affinity*. http://chemed.chem.purdue.edu/genchem/topicreview/bp/ch7/ie_ea.html Accessed 12/07/2021
- [43] Medium, *Electron Affinity*. [https://chem.libretexts.org/Bookshelves/Physical_and_Theoretical_Chemistry_Textbook_Maps/Supplemental_Modules_\(Physical_and_Theoretical_Chemistry\)/Physical_Properties_of_Matter/Atomic_and_Molecular_Properties/Electron_Affinity](https://chem.libretexts.org/Bookshelves/Physical_and_Theoretical_Chemistry_Textbook_Maps/Supplemental_Modules_(Physical_and_Theoretical_Chemistry)/Physical_Properties_of_Matter/Atomic_and_Molecular_Properties/Electron_Affinity) Accessed 12/07/2021
- [44] Medium, *Popolazioni di Mulliken*. <https://www.chimicamo.org/chimica-fisica/popolazioni-di-mulliken/> Accessed 12/07/2021
- [45] Medium, *Bonding and antibonding orbitals*. [https://chem.libretexts.org/Bookshelves/Physical_and_Theoretical_Chemistry_Textbook_Maps/Supplemental_Modules_\(Physical_and_Theoretical_Chemistry\)/Chemical_Bonding/Molecular_Orbital_Theory/Bonding_and_antibonding_orbitals](https://chem.libretexts.org/Bookshelves/Physical_and_Theoretical_Chemistry_Textbook_Maps/Supplemental_Modules_(Physical_and_Theoretical_Chemistry)/Chemical_Bonding/Molecular_Orbital_Theory/Bonding_and_antibonding_orbitals) Accessed 12/07/2021
- [46] Medium, *Chemisorption*. <https://www.corrosionpedia.com/definition/260/chemisorption> Accessed 13/07/2021
- [47] Frank Jensen. Introduction to computational chemistry. 2nd. John Wiley sons, 2007. isbn: 0-470-01187-4.

- [48] Mark Waller and Stefan Grimme. «Weak Intermolecular Interactions: A Supramolecular Approach». In: Handbook of Computational Chemistry. Ed. by Jerzy Leszczynski. Dordrecht: Springer Netherlands, 2016
- [49] Medium, *Dirichlet Boundary Condition*. <https://www.sciencedirect.com/topics/engineering/dirichlet-boundary-condition> Accessed 16/07/2021
- [50] Medium, *Adsorption and its Applications in Industry and Environmental Protection*. <https://www.sciencedirect.com/topics/chemical-engineering/chemisorption> Accessed 08/09/2021
- [51] Medium, *Application of Nanomaterials and Nanotechnology in the Reutilization of Metal Ion From Wastewater*. <https://www.sciencedirect.com/topics/engineering/physisorption> Accessed 08/09/2021
- [52] Medium, *Nudged Elastic Band* <https://theory.cm.utexas.edu/vtsttools/neb.html> Accessed 29/09/2021
- [53] Medium, *Nudged Elastic Band (NEB)* <https://www.scm.com/doc/AMS/Tasks/NEB.html> Accessed 29/09/2021
- [54] Medium, *Pt diffusion on Pt surfaces using NEB calculations* http://docs.quantumatk.com/tutorials/neb_pt/neb_pt.html#constructing-the-neb-paths Accessed 29/09/2021